The role of Topoisomerase II in replication in mammalian cells

Diana Muftic

Gray Institute for Radiation Oncology & Biology

and

Wolfson College

Trinity 2011

A thesis submitted in partial fulfilment of the requirements for the degree of

Doctor of Philosophy at the University of Oxford

Abstract

Topoisomerase 2α (Topo2α) is an essential protein with DNA decatenating enzymatic properties, indispensable for chromosome decatenation and segregation. It is a target for a plethora of antitumour drugs and Topo2α protein levels have been associated with the success of treatment, but also drug resistance and secondary malignancies. Although unique in its ability to resolve catenated chromosomes, the role of Topo2α in other steps of DNA metabolism, such as DNA replication elongation and termination have been elusive. A thorough understanding of the role of Topo2α in the cell will not only allow for increased insight into the mechanisms it is involved in, but it will also shed light on proteins and pathways that can act as back-up in its absence, and therefore hopefully expand the basis on which to improve treatment options.

Through a synthetic lethal interaction (SLI) screen with an siRNA library targeting 200 DNA repair and signalling genes, Topo2α emerged as being synthetic lethal to Werner protein (WRN), a RecQ helicase involved in maintaining genome integrity mainly in S phase, and the loss of which leads to Werner Syndrome (WS), a segmental progeroid syndrome. The screen was performed in WRN deficient cells, with the initial aim to find proteins that act to buffer against loss of viability, which is the central idea in the concept of synthetic lethality in the absence of WRN. The screen revealed an SLI between WRN and Topo2α and although we were unable to fully validate this, it spurred the question of Topo2α's role in DNA replication.

The findings in this thesis suggest that Topo2α is not required for DNA elongation and timely completion of S phase, and that simultaneous loss of the closely related isoform Topo2β does not affect replication, suggesting that these proteins do not act in parallel back-up pathways during replication. Interestingly, cells accumulate in the polyploid fraction after both depletion and inhibition of Topo2α, albeit with different kinetics. The mechanistic basis of this phenotype remains to be understood through further research, but it is highly interesting as aneuplidity and polyploidy are implicated in the initial stages of tumour development.

Table of Contents

List of figures

List of Tables

Abbreviations

4NQO	4-Nitroquinoline 1-oxide
ADP	Adenosine Diphosphate
APC/C	Anaphase-Promoting Complex
APEI	Apurinic/apyrimidinic Endonuclease 1
AT	Ataxia-Telangiectasia
ATM	Ataxia-Telangiectasia Mutated
ATP	Adenosine Triphosphate
ATR	ATM and Rad3 Related Protein
BER	Base Excision Repair
BLM	Bloom protein
bp	base pair
CldU	5-Chloro-2'-deoxyuridine
CPT	Camptothecin
C-terminal	Carboxy-terminal
DC	Decatenation Checkpoint
DDR	DNA Damage Response
DF	Dharmafect
DMSO	Dimethyl Sulfoxide
DNA	Deoxyribonucleic Acid
DNA-PK$_{CS}$	DNA-dependent Protein Kinase, Catalytic Subunit
Dox	Doxycycline
DSB	Double Strand Break
dsDNA	Double stranded DNA
dsRNA	Double stranded RNA
dsRNA	Double Stranded RNA
FACS	Fluorescence-Activated Cell Sorting
FUCCI	Flourescent Ubiquitination-based Cell Cycle Indicator
FUCCI	Flourescent Ubiquitination-based Cell Cycle Indicator
G1$_{tet}$	G1 Tetraploid Cells

G4	G-quadruplex DNA
G-segment	Gate segment
HJ	Holliday Junctions
HR	Homologous Recombination
HRDC	Helicase and RNase D C-terminal
HU	Hydroxyurea
ICRF-193	Imperial Cancer Research Fund-193
IdU	5-Iodo-2'-deoxyuridine
IF	Immunoflourescence
IR	Ionising Radiation
LP-BER	Long-patch Base Excision Repair
MC	Mitotic Catastrophe
MI	Mitotic Index
miRNA	micro-RNA
MMC	Mitomycin C
MMS	Methylmethane Sulfonate
MSC	Mitotic Spindle Checkpoint
NER	Nucleotide Excision Repair
NHEJ	Non-Homologous End Joining
NLS	Nuclear Localization Ssignal
NT	Non-Targeting
ORC	Origin Replication Complex
PARP	PolyADP Ribose Polymerase
PCNA	Proliferating Cell Nuclear Antigen
PFGE	Pulse Field Gel Electrophoresis
PI	Propidium Iodide
PIKK	Phosphatidylinositol 3-Kinase-like Kinase
PLK1	Polo-like kinase 1
Pol	DNA polymerase
pri-miRNA	primary RNA
PUVA	Psoralen + UVA

R51	Rad51
RC	Replication Complex
rDNA	Ribosomal DNA
RISC	RNA-induced silencing complex
RNAi	RNA interference
RPA	Replication Protein A
RQC	RecQ C-terminal
SDS	Sodium Dodecyl Sulfate
siRNA	Short Interfering RNA
SLI	Synthetic Lethal Interactions
SLIs	Synthetic Lethal Interactions
SP-BER	Short-patch Base Excision Repair
SSB	Single Strand Break
ssDNA	Single Stranded DNA
t-AML	Treatment Related Myelocytic Leukemia
Topo	Topoisomerase
T-segment	Transported segment
UTR	Untranslated Region
WRN	Werner protein
WS	Werner syndrome

Acknowledgments

Professor Thomas Helleday who in addition to being a supervisor has been a friend for a long time. I would especially like to thank you for giving me the opportunity to explore science in my own way and for providing me with the opportunity to come to Oxford.

The members of the Helleday lab in Oxford, especially Bastiaan, who livened up in the lab, but also took time for tea and talk, Tina for being a true sport during team meetings, Cissi for hosting me in my first week in Oxford and always being a rock, and also Annette, Ponnari, Nick, Nils, Guy, and Navita for providing a great atmosphere.

I would also like to thank Niki Sibson and Tim Humphrey whose help I truly appreciated and who stepped in and helped when it really mattered. Mick Woodcock for not only teaching me everything about FACS, but for being in great spirits, always, and a great lab colleague.

The members of the Helleday lab at GMT, Stockholm and also Richard O, Anne B, Björn, Mats, Ulf, Elisabeth and Dag. Of all the labs I have been to for my graduate studies in I have always come back to GMT. You have made me feel welcome even after leaving for UK -how could I not when my name is still on the staff list, even four years after I have left. I especially want to say thank you to Niklas, Fredrik, Daniel H., and Helge who all have been the best roommates to share an office and have lunch and "fika" with! Petra, Ingegerd, Ivo and Cecilia who were great lab colleges those times I worked at GMT, and who all finished their PhDs at the same time as me – rocky but also the best "disputationsfester" after!

Those who helped to proofread the thesis, Bastiaan, Anette, Cissi, Helge, and especially Esther who stepped in at the end and truly made a difference.

Events, places, and people that have made my DPhil time so much more than I could have hoped for (in no particular order): ML for getting me into bio in the first place; blue couch at GMT; Guest Nights; Oriel MCR; Sunday Hall; The champagne bowl; VM for "for protecting you from plagiarisms and allowing you to get into the mess of IB"; Brunnsviken; CPBS; AJ - neighbour, editor and friend; WCBC and especially KB and AMcL; TB and our tea breaks at work; yellow house and all the best housemates - CC, DH and LL; JMH; bop nights; BC dinners; Starbucks coffee; German brunches; Summertown bachelor pad with the three finest bachelors GF, JK and RP; punting; champagne; May morning; Summertown wine café; Cowley; Torpid blades; G&D's; Headington hill; some of the most fantastic Swedish people you can find: LS, Q, NH; and the Oriel legends – JW, ES-W, JC, CH, BA and Jochen and Becca.

Jonas och Nadine, ni är de bästa vännerna jag kan ha fått. Hur långt bort ni än är så är ni alltid nära.

Jonatan, för att skrivandet gick som en dans med ditt stöd, för alla fantastiska minnen vi har skapat och de äventyr som ligger framför oss.

Most importantly, Dejan and my parents whose support, love and help carried me higher than I would have ever made it myself. I am immensely grateful for your perseverance, continuous discussions, and endless effort and for being my best friends.

Chapter 1

Introduction

1 Introduction

Topoisomerases

1.1 Topology of DNA

The DNA thread inside one cell is dramatically longer than the nucleus it needs to fit into. The entire genome is $3*10^9$ base pairs, approximately 1.8 m long, and fits into the nucleus with an average diameter of 6 μm. This makes the circumference of an average mammalian nucleus about one million times smaller than the length of the genome it needs to pack inside it. To solve the problem of space, the DNA is tightly compacted and organized into higher order structures [1]. This property of the DNA strand is called supercoiling. The B-form of DNA (the Watson-Crick structure) is a double-helix, in which both strands of the DNA coil around an axis. Further coiling of the axis upon itself is described as supercoiling [2]. If the B-structure is equated to a phone cord, the supercoiling would be when the coiled cord coils around itself.

The folding mechanism must however not only pack the DNA, but also allow access to the information in the DNA. Processes such as DNA replication and transcription require unpacking of DNA and DNA strand separation. Because free rotation of the whole DNA thread is not possible, the opening of the double-helix introduces further topological stress of the DNA strand [3]. Other metabolic processes such as recombination and chromosome segregation also require alteration of DNA topology.

DNA topology and supercoiling are precisely regulated processes mediated by proteins called topoisomerases.

1.1.1 DNA supercoiling

Most work on DNA supercoiling and topology has been performed on circular DNA. As there are no free ends, opening up the double helix creates tangling and topological strain. The eukaryotic chromosomes are linear, but they can be treated as closed circles because DNA loops are firmly attached to the nuclear matrix. Therefore, every loop can be viewed as a circular topological domain [2].

In almost all instances in nature the DNA double helix is underwound [4, 5]. This means that the double-helix has fewer helical turns around the primary axis than expected of the B-structure. Instead of the expected 10.5 base pairs per every full turn in a relaxed DNA molecule, the DNA in the nucleus has 12.0 base pairs (Figure 1.1 A and B). This "stretching" of the helix is actively and ezymatically maintained and causes DNA to become thermodynamically strained. One energetically favourable way of reducing this strain is by strand separation, which causes tightening of the coils (Figure 1.1 C top). This is important in aiding DNA proteins that need to open the DNA, such as those involved in transcription or replication initiation. However, in most instances in the cell, the topological strain is relieved by negative supercoiling. It is important to note that a supercoiled DNA molecule is more condensed than a relaxed DNA molecule of the same length, thus this mechanism is essential for DNA condensation and fitting the whole thread in the nucleus.

The topological properties of the double-helix are described by the so called linking number, *Lk*. When the DNA is relaxed the *Lk* is equal to 0. In the case of underwinding, there are fewer coils than in the relaxed state and the *Lk* is negative. Supercoiling from underwound DNA is thus called negative supercoiling. Most naturally occurring DNA is negatively supercoiled [4, 5]. Strand separation initially relaxes negative supercoiling,

whereas further separation leads to positive supercoiling (Figure 1.1 C), an undesirable state that impedes further separation by the helicase.

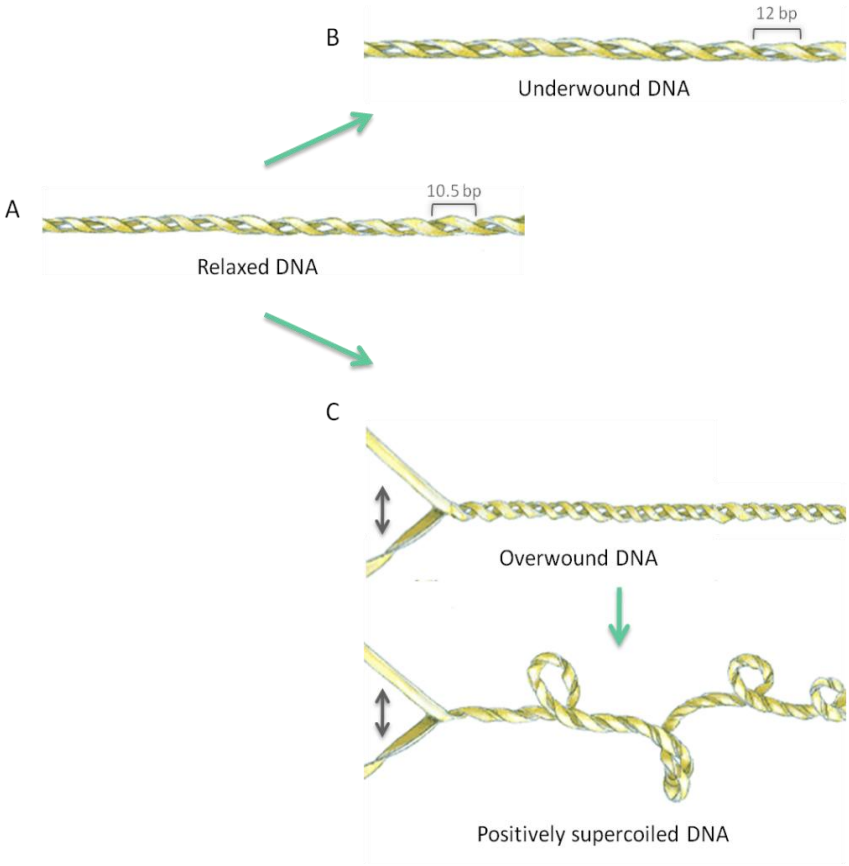

Figure 1.1 | DNA topology

A. Relaxed DNA has 10.5 base pairs per every turn.

B. Removing a turn underwinds DNA and induces a strain. This "stretching" of the DNA thread results in 12 bp per every turn. Underwound DNA is the most common state in the nucleus and is ezymatically maintained. Underwound DNA leads eventually to negative supercoiling.

C. Separation by helicases "tightens" the coil if it is not allowed to rotate. Overwinding leads to positive supercoiling. Adapted from [6].

1.1.2 Topological constrains of DNA replication

The process of DNA replication requires that the Lk of the two strands of the double-helix be reduced to zero. During the elongation step of replication, the unwinding by the helicase causes overwinding in front of the replication fork (Figure 1.2 A) [7]. This leads to accumulation of positive supercoiling, which becomes an obstacle for replication if it is not removed. This problem was first recognized by Champoux and Been, who suggested that if the replication machinery is allowed to rotate, it would distribute the topological stress behind the replication fork, creating precatenanes (Figure 1.2 B) [8]. Therefore, precatenanes are junctions of sister duplexes in the replicated part of the DNA. Existence of precatenanes has been confirmed in vitro using electron microscopy [9]. Once the whole DNA strand is replicated, the precatenanes turn into catenated chromosomes. For cell division to proceed the catenanes need to be unlinked. Although the theory of precatenanes it is widely accepted, rotation of the replication machinery might be constrained as the replication factories are anchored to nuclear structures. Further research will have to determine the exact topological events during replication.

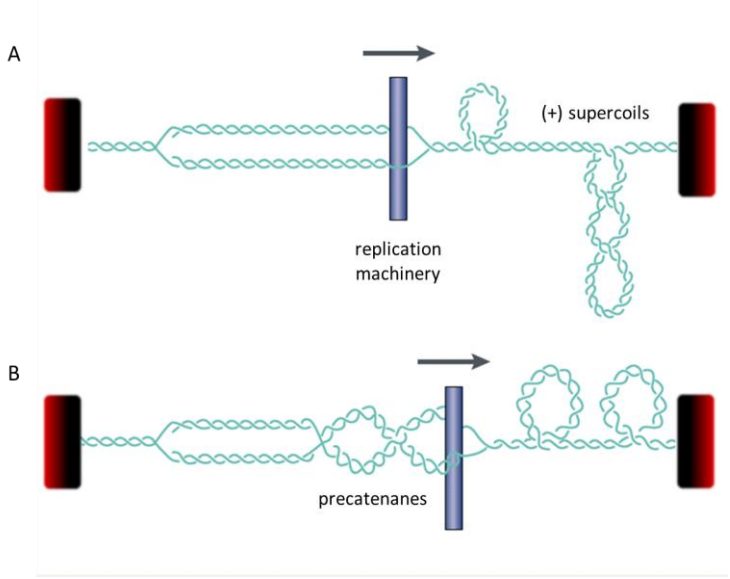

Figure 1.2 | Topological problems associated with progression of the DNA replication fork

Images represent a topological domain of DNA anchored to structures in the nucleus. These structures can be cell membrane or protein aggregates, and prevent free rotation of the domain. Replication machinery is represented as a rod.

A. Replication machinery separates the two DNA strands, causing "tightening" of the helix. Overwound, or supercoiled DNA accumulates in front of the replication machinery.

B. Supercoils can be removed by topoisomerases to release the torsional stress. Alternatively, if the replication machinery is allowed to rotate around its own axis precatenanes are formed.

Adapted from [10] and [11].

Additional topological problems arise when two bidirectional replication forks converge. To date, there are two suggested pathways to resolve the late replication intermediates. The first (Figure 1.3, left) was suggested by Sundin and Varshavsky and proposes that the remaining parental DNA is unwound, following which both strands of the double helix are replicated, leaving sister duplexes catenated [12-14]. These can then be resolved by the topoisomerase 2 (Topo2) enzyme. Minden and Marians proposed instead that the duplex is first separated into single stranded DNA by a RecQ helicase (Figure 1.3, right) [15]. Topoisomerase 3 (Topo3) enzyme, which binds to single stranded DNA (ssDNA), would follow behind, unlinking each turn as replication continues. Currently there is evidence for both pathways.

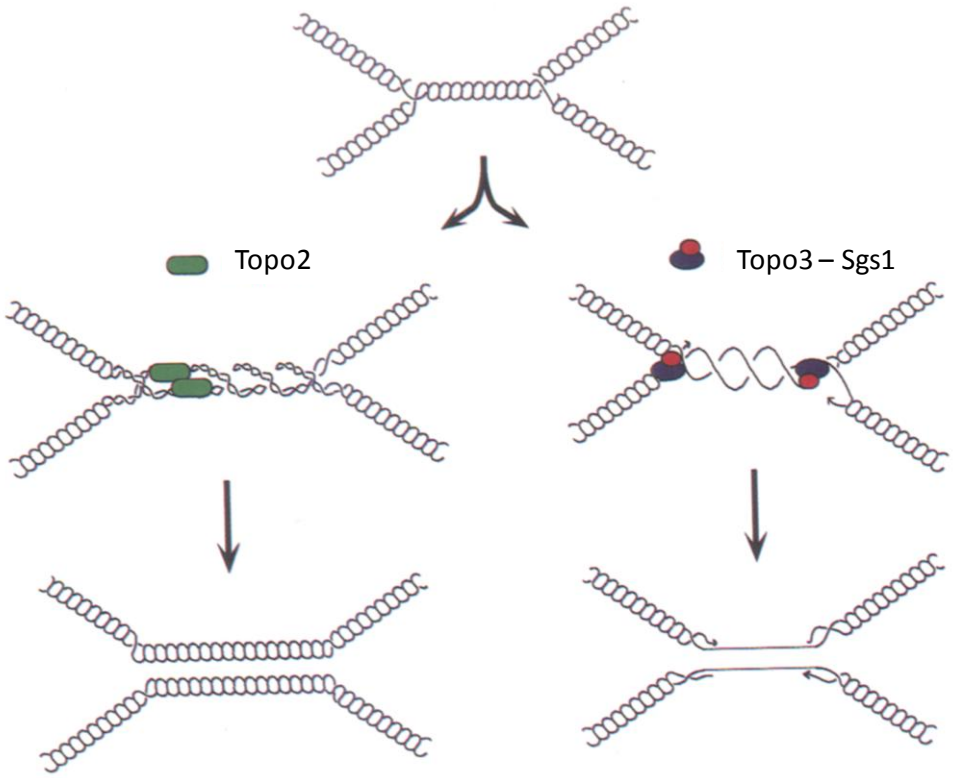

Figure 1.3 | Pathways for resolution of converging DNA replication forks

As two replication forks coverge, torsional stress accumulates in the short unreplicated region. Two pathways have been suggested for resolution of merging replicons. In the *left* pathway replication continues through the short region using leading strand synthesis and creating catenanes for each double-helix turn. Following replication completion catenanes are removed by Topo2. The *right* pathway suggests that the remaining helix turns are seperated into ssDNA by a RecQ helicase, depicted as *S. cerevisiae* Sgs1 here, and Topo3. Once Topo3 has unlinked the helix, DNA synthesis fills in the single stranded gaps.

Adapted from [16].

1.2 DNA topoisomerase

Topoisomerases are essential, ubiquitous enzymes that modulate the topology of DNA. They regulate DNA under- and overwinding, and remove catenanes, knots and tangles in different processes of DNA metabolism. Topoisomerases are divided into two classes distinguished by their catalytic mechanisms (Table 1.1). Type I enzymes nick one strand of the DNA backbone and allow for controlled rotation to alleviate torsional stress. They are

monomeric proteins, whilst type II are homo- or heterodimers. The mechanism of type II enzymes is to cleave both strands of the backbone, creating a double strand break (DSB), and letting another double stranded helix pass through. Notably, all topoisomerases cleave the phosphodiester backbone through a nucleophilic attack by a tyrosine residue. This reaction creates a transient and reversible covalent enzyme-DNA complex [17].

Subfamily	Representative member	Mammalian member
IA	Bacterial topoisomerase 1 and 3 Yeast topoisomerase 3 *D. melanogaster* topoisomerase 3α and 3β	Topoisomerase 3α and 3β
IB	Eucaryotic topoisomerase 1 Pox virus topoisomerase 1	Topoisomerase 1 Mitochondrial topoisomerase 1
IIA	Bacterial gyrase, topoisomerase 4 Phage T4 topoisomerase Yeast topoisomerase 2 *D. melanogaster* topoisomerase 2	Topoisomerase 2α and 2β
IIB	*Sulfolobus shibatae* topoisomerase 5	

Table 1.1 | Subgroups of topoisomerases and representative members

Type I topoisomerases are subdivided into type IA and IB subclasses. *Escherichia coli* (*E. coli*) type IA protein was the first topoisomerase 1 (Topo1) to be discovered [18, 19]. This subgroup of topoisomerase proteins binds double stranded DNA (dsDNA), causing base unpairing, upon which a transient nick is introduced in one ssDNA [20, 21]. As described above, strand separation is only energetically favourable in negatively supercoiled DNA. Therefore, type IA topoisomerases relax only underwound, or negatively supercoiled DNA. The subsequent strand passage is guided by the enzyme where the intact one strand passes through the nicked one, which is held firmly by the protein. This subgroup includes human Topo3α and 3β. Just like the *E.coli* Topo1, these only relax negative supercoiling and

have been shown to be involved in resolving DNA replication and recombination intermediates together with RecQ helicases [22].

The IB subclass, into which the human Topo1 falls, differs from subgroup IA by two major characteristics [18]. First, it relaxes both negative and positive supercoils. This is thought to be because the enzyme nicks dsDNA and lets the other end rotate freely before ligation [18]. Second, it cleaves the phosphodiester backbone at the 3'-end. Together with the mitochondrial Topo1 it is the only topoisomerase to form the covalent complex on the 3'-end of the backbone. All other topoisomerases form the covalent protein-DNA complex on the 5'-end of DNA.

Type II topoisomerases were all thought to belong to one subclass until the IIB subgroup was discovered in archea *Sulfolobus shibatae* [23]. The two subclasses have structural differences, but it is clear that they are both widely distributed in all organisms [23, 24]. Type II topoisomerases are the only enzymes that can separate replicated, catenated chromosomes, making them essential for survival [25].

DNA topoisomerases are highly conserved proteins [7] and genomic sequence searches indicate that all organisms have at least the type IA enzyme and one type II enzyme. The latter is usually a type IIA, except in archea that expresses type IIB. Therefore from current evidence, the minimal requirement for living organisms seems to be one type IA and one type II enzyme [7, 23, 26]. Additionally, all eukaryotes encode at least one type IB enzyme, and Topo1 is essential in both vertebrates and *Drosophila melanogaster* (*D. melanogaster)* [27, 28]. Yeasts have three topoisomerases, IA, IB and IIA, but in laboratory conditions *S. cerevisiae* expressing only type IIA topoisomerase was viable [29].

The human genome encodes six topoisomerases. Two from every subcategory are represented – IA (Topo3α and 3β), IB (Topo1, mitochondrial Topo1 (mt-Topo1)) and IIA

(Topo 2α and 2β). The human Topo1 is well studied because of its pivotal role in cancer treatment. It is the sole target for the camptothecin (CPT) group of drugs, which are used extensively in treatment of many types of cancers. The mechanism of cytotoxicity is believed to be conversion of the drug-stabilized covalent complex to DNA damage through collision with DNA replication and transcription machinery.

Mouse has six topoisomerases, all but two of which are essential. Topo1 mutants die before the eight-cell stage [30]. Topo2β knock out animals die just before birth making it possible to isolate embryonic cells [31] while Topo2α knock out is lethal after the first cell division [32]. Topo3α deletion leads to death shortly after implantation [33]. Inactivation of Topo3β leads to viable animals, albeit with shorter life spans, and mtTopo1 seems dispensable in mice [34, 35].

The genome of *E.coli* codes for four topoisomerases [1]. The bacterial gyrase, which falls into the IIA subclass, is unique in that it has the ability to introduce negative supercoils in addition to removing positive supercoils [36, 37]. Because the gyrase is present in prokaryotes and not in human cells, it makes an excellent target for antibiotics. Examples of these include chloroquine (used in malaria treatment) and ciprofloxacin (used to treat e.g. urinary tract infections and anthrax), both of which belong to quinolones group of drugs.

1.3 Topo2α catalytic cycle

The human Topo2α acts as a homodimeric enzyme [19]. There is no particular sequence specificity, but the enzyme does prefer DNA crossover regions, such as knots, catenanes and supercoils. Briefly, the overall reaction is to bind two segments of DNA, create a DSB in one, translocate the unbroken DNA strand and reseal the break.

The first step is the binding of the duplex DNA that is to be cleaved by the enzyme (Figure 1.4 A). This segment forms a gate (G-segment) through which the intact duplex is transported (T-segment). The binding of the G-segment is aided by magnesium ions in the

TOPRIM domain. In the presence of Mg^{2+}, the tyrosine residues from each monomer launch a nucleophilic attack on the phosphodiester bonds on opposite strands of the bound double-helix. This creates two single strand breaks, four bases apart (Figure 1.4 B) [5]. Topo2α becomes covalently attached to the cleaved 5'-ends, creating what is called the covalent complex. The covalently bound Topo2α ensures that the DNA ends are protected from exonuclease attack and that they do not elicit a DNA damage response. The energy of the phosphodiester bond is conserved in the phosphotyrosine bond, making the reaction easily reversible.

In the next step, each monomer binds an adenosine triphosphate (ATP) molecule, leading to a conformational change from an open to a closed clamp. This allows for the T-segment to pass through the cut G-segment. The hydrolysis of ATP to adenosine diphosphate (ADP) and an inorganic phosphate Pi promotes another conformational change in the carboxy-terminal (C-terminal) to release the T-segment from the clamp. After strand release, the G-segment is re-ligated within the homodimer complex before being released.

A

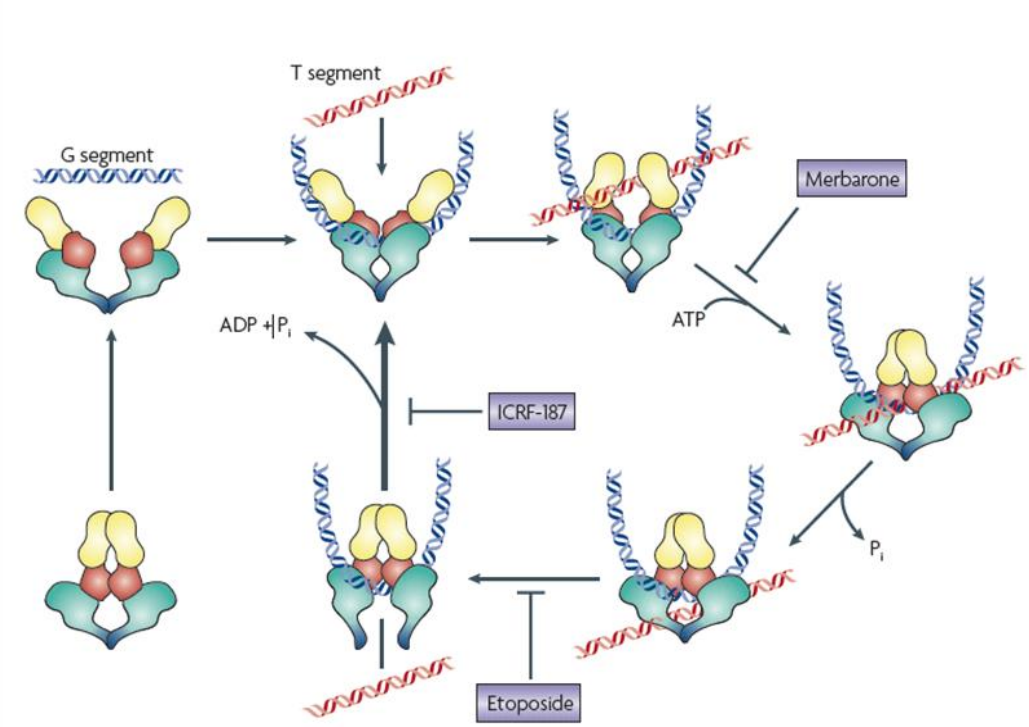
T segment
G segment
Merbarone
ATP
ADP +|P$_i$
ICRF-187
P$_i$
Etoposide

B

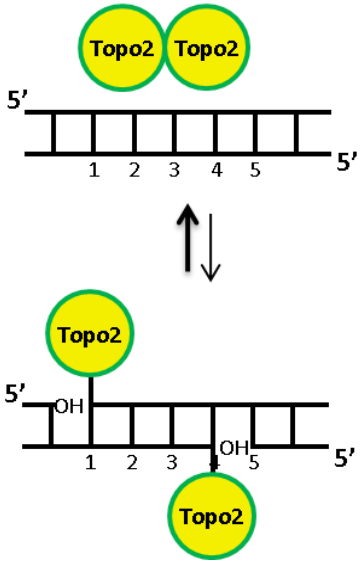
Topo2
Topo2
5'
1 2 3 4 5
5'
Topo2
5'
OH
OH
1 2 3 5
5'
Topo2

Figure 1.4 | Topo2α strand passage mechanism

A. Topo2 protein interacts with both dsDNA strands to catalyse the strand passage reaction. Starting from top left, the G-segment binds to Topo2α for cleavage. In the presence of Mg^{2+} the enzyme cleaves the DNA backbone, forming a covalent bond with DNA. After ATP binding the protein forms a closed clamp, sequestering the T-segment. The first ATP hydrolysis assists with strand passage of the T segment. The second allows the clamp to reopen and release the G segment. Yellow represents the N-terminal, red the central domain, and green the C-terminal.

Topo2 catalytic cycle can be inhibited by different drugs at every step. Most clinically active drugs stabilize the covalent complex (Figure 1.4 B bottom). This interferes with many DNA metabolic processes and results in the formation of lethal DSBs. These drugs, which include etoposide and doxorubicin, are termed topoisomerase poisons. Compounds that do not stabilise the covalent complex, but interfere with Topo2 function are termed topoisomerase inhibitors. An example of these is bisdioxopiperazines such as ICRF-193. It inhibits ATP hydrolysis and prevents protein turnover. Agents that prevent DNA cleavage, such as Merbarone, are also expected to act as catalytic inhibitors. From [17].

B. Schematic illustrations of covalent complex formation. Each Topo2α monomer forms a 5'-phosphodtyrosine bond on opposite strands, four base pairs apart. This creates 5´-overhangs. The arrows indicate a reversible reaction, which favours relegation under normal conditions. Adapted from [1].

1.4 Topo2α structure

Currently there is no complete crystal structure for mammalian Topo2α. Most structural data for Topo2 is derived from studies on bacterial gyrase and Topo IV [38], as well as yeast Topo2. However, eukaryotic topoisomerases type II are highly conserved in their primary sequence, thus the insights are likely to apply to the human Topo2α.

Each Topo2 monomer is divided into three functional domains [19]. The first approximately 670 amino acids constitute the highly conserved N-terminal and contains the site of ATP binding [39]. The N-terminal is responsible for homodimerization. ATP binding on each monomer contributes to homodimerization and the overall structure of the

homodimer. Similarly after ATP hydrolysis dimerisation is destabilised. The C-terminal end of the N-terminal domain has been termed the transducer domain. It undergoes a conformational change upon ATP binding that may trigger conformational change in the central domain of the protein. This change is required for DNA nicking and ligation to be more efficient [19].

The central domain of Topo2 contains the active tyrosine that is responsible for the nucleophilic attack that forms the covalent complex with DNA. The N-terminal of the central domain contains the TOPRIM domain where the Mg^{2+} ion binds, aiding cleavage of the backbone [40].

Unlike the two other domains, C-terminal is highly variable between species and also between the two human isoforms [5]. It contains the nuclear localisation sequence (NLS) and post-translational modification sites [41]. Recent work has indicated that the C-terminal plays a role in recognition of DNA geometry, directing the protein to its substrate. It also forms the gate that is the exit point for the un-nicked strand.

1.5 Biological functions of Topo2α

The protein levels of Topo2α are highly modulated in a cell cycle dependent manner. The levels increase steadily from S phase to reach the highest level at G2/M phase. In HeLa cells the change is mediated through a 15-fold increase in mRNA levels which is due to a 2-fold increase in transcription and an 8-fold increase in mRNA stability [42]. After the transition from M to G1, the protein is degraded within 4 hours. Topo2α is therefore highly associated with proliferating cells, and in agreement with this it is found in tissues such as thymus, spleen, bone marrow, intestine and testis and upregulation of Topo2α is also associated with cancerous cells.

1.5.1 DNA replication

The role of Topo2 has been implicated in many DNA metabolic pathways where modulation of topology is required. Supercoiling in front of the replication fork (Figure 1.2) is predicted to be removed by type IB or type II enzymes [7, 18], and recent evidence suggests that in mammalian cells Topo1 is responsible for propagating replication elongation [43]. In yeast however, simultaneous removal of Topo1 and Topo2 emphasises the S phase problems of Topo1 mutant [44] suggesting that Topo2 is either acting in front of the fork as well, or removing precatenanes behind replication machinery. In mammalian cells depleting Topo2α has failed to reveal a role in replication, although one report suggests it is required to underpin normal S phase progression [45].

In later stages of replication when two replication forks merge together there would be no room left for Topo1 to act in front of the replication forks (Figure 1.3) and instead Topo2 would be able to act at the replication termination substrate. Topo2 yeast mutants with a catalytically dead protein accumulated gapped, nicked and catenated DNA molecules suggesting replication termination was not completed. Topo2 was directly required for fork fusion around 71 termination regions identified which consisted of fork stalling elements such as high transcription regions and centromeres [46]. The mechanism in mammalian cells remains to be availed.

1.5.2 Chromosome decatenation and segregation

Type II topoisomerases are the only proteins able to remove precatenanes and to resolve catenated chromosomes. If left catenated, sister chromatids missegregated and this can further lead to aneuploidy and polyploidy [47]. In yeast Topo2 is indispensable for chromosome segregation in mitosis. When Topo2 was depleted in S. *cerevisiae* and *Schizosaccharomyces pombe* (*S. pombe*), the chromosomes were left completely catenated

[48]. Cells then entered mitosis showing minimal cell cycle delay, and instead accumulated missegregated and broken chromosomes during mitosis and G1 [49, 50].

Similarly to yeast, depletion of Topo2α in human cells led to the conclusion that it is responsible for the majority of the decatenatory activity [51, 52]. Interestingly, unlike in yeast, human cells were suggested to have a G2 checkpoint that was sensitive to the catenation state and prevented entry into mitosis [53, 54]. This checkpoint was termed decatenation checkpoint.

Topo2 localizes to specific chromosome regions, such as centromeres even prior to onset of G2/M, during S phase and it seems that failure to terminate replication results in decatenation problems at these sites [17, 46]. Furthermore depletion of Topo2 resulted in abnormal localisation of chromosome arms and failure to attach centromeres to opposite poles of the spindle [55, 56].

In addition to decatenation and segregation activity, Topo2 has been implicated in chromosome condensation although this function is debated given that condensation can occur in contexts where Topo2 is absent [17].

1.6 Catalytic inhibitors of Topo2α

Topo2α is a major target of anticancer drugs, and there are agents that are able to interfere with every step of the catalytic cycle (Figure 1.4 A). Different drugs targeting Topo2α are used in treatments of breast, lung, and prostate cancer, as well as haematological malignancies [57]. These drugs are highly effective, but tumours frequently become resistant. Recent work has shown that cellular levels of Topo2α can be correlated to drug sensitivity and that tumours refractory to treatment have low levels of Topo2α protein [17, 58]. Additionally, evidence shows that Topo2α poisons have the potential to generate translocations and secondary malignancies as negative side effects.

Topo2α targeting agents are divided into two classes [17]. The largest group includes most of the clinically active agents, such as etoposide, doxorubicin and mitoxantrone. They are able to stabilize the DNA Topo2α covalent complex, and consequently generate DNA breaks. The stabilized covalent complex blocks transcription and replication, and elicits DNA damage response, with a subsequent apoptotic response [59-61]. These agents have been termed Topo2α poisons.

A second group, Topo2α inhibitors, is a heterogeneous group that inhibits Topo2α, but does not increase levels of Topo2α covalent complex. In experiments, these agents antagonize the toxicity of Topo2α poisons, indicating that they sequester Topo2α and act by a separate mechanism [62]. Topo2α inhibitors are thought to be unspecific with regards to isoforms and other proteins. One Topo2α inhibitor is Merbarone. It is a thiobarbituric acid derivative that targets Topo2α isoform. It does not affect DNA binding, nor ATP hydrolysis, but it does block Topo2α mediated cleavage [63]. The cellular effect of Merbarone is an increase G2 population, which is typical of many Topo2α inhibitors. The drug was also tested clinically, but was discontinued due to nephrotoxicity and general lack of antitumor activity [57].

The most important class of Topo2α inhibitors is bisdioxopiperazines, which includes ICRF-193. They are considered to be the only inhibitors that are Topo2α specific [64, 65], hence they have been used extensively to elucidate the role of Topo2α. Topo2α is ten times more sensitive to ICFR-193 than Topo2β [66]. The initial compound, ICRF-154, was developed into ICRF-159, and eventually into ICRF-187. ICRF-187 (Dexrazoxane, Cardioxane, Zinecard, and ADR-529) is the (+)-enantiomer of ICRF-159 and is used clinically to reduce doxorubicin-induced cardiotoxicity. Eventually ICRF-193 was developed as a dimethyl derivative of ICRF-154, and is considered the most potent bisdioxopiperazine derivative targeting Topo2α.

ICRF-193 blocks Topo2 after strand passage, but before the hydrolysis of the second ATP. This stabilizes a non-covalent form of the enzyme, which encircles the DNA strands, and leaves Topo2 blocked by non-hydrolysable ATP analogues (Figure 1.4 A).

Bisdioxopiperazines do not provoke the DNA damage response (DDR) that Topo2α poisons do, as they do not cause enzyme-generated DNA damage [67, 68]. However, there is disputing evidence that they might cause damage following long-term exposure [69], or even during short-term exposure [70].

1.7 Topoisomerase 2β

Whereas lower eukaryotes code for only one Topo2, vertebrates express two isoforms, Topo2α and Topo2β. The human Topo2β was isolated six years after Topo2α from murine P388 cells [42]. Because the intron-exon arrangement is similar between the two isoforms, the gene is thought to have arisen by gene duplication. The Topo2β gene locates to chromosome 3 and codes for a 180 kDa protein, slightly larger than the 170 kDa Topo2α [42]. Topo2β shares significant amino acid homology with the α isoform, but the homology is mainly contained to the N-terminal. The C-terminal is the least conserved domain and is thought to distinguish the role of the two isoforms. In a conditional knock down Topo2β fails to compliment a Topo2α deficiency unless it is highly overexpressed (at least 10-fold) [71]. Meanwhile, fusion of the catalytic domain of Topo2β to the C-terminal of Topo2α complimented the deficiency, confirming that the enzymatic mechanism is similar, but the protein substrate differs.

Topo2β mRNA has been found in many different tissues, and unlike Topo2α, it is even found in low proliferating tissue such as brain. In proliferating cells, Topo2β constitutes 25% of total Topo2, while in the plateau phase the ratio increased to almost 50%.

Previous work has implicated Topo2β in neural development in mice [31, 72]. Homozygous deletions of *Topo2β* led to multiple neuronal defects, including failure to

innervate the diaphragm. Topo2β was required for viability, but it was possible to isolate cells as the embryos developed almost to term. In that study, Lyu *et al* were able to show that Topo2β localizes to developmentally regulated genes, and that 1 - 4% of those showed changes in gene expression when Topo2β was absent [73]. Recent work has strengthened the hypothesis that Topo2β is involved in transcription initiation and regulation. Topo2β was shown to localize to the promoter regions and was required for efficient transcription activation of genes whose expression is activated by nuclear hormone receptors [74, 75]. Another recently published study [76] showed that in breast cancer cells, exposure to 17β-estradiol, the major estrogen species in humans, leads to DSBs at the promoter for the estrogen responsive gene. The DSB was Topo2β dependent and co-localized with Rad51, suggesting homologous recombination (HR) was needed for repair.

Topo2β has also been implicated in secondary malignancies induced by Topo2 poisons. Etoposide treatment is known to induce treatment related myelocytic leukaemia (t-AML), which is characterized by chromosome translocations [77, 78]. Studies in mice suggest that these secondary malignancies involve Topo2β, thus highlighting the need for Topo2α specific drugs.

Werner protein

1.8 Werner Syndrome

Werner syndrome (WS) is an autosomal recessive progeria syndrome characterized by genomic instability and premature aging. Progeroid syndromes are heritable human disorders that show early onset of aging. Other progeroid syndromes include Hutchinson-Gilford progeria syndrome, Cockayne syndrome, Ataxia-Telangiectasia (AT), as well as disorders of Down, Klinefelter and Turner syndrome. Notably, none of the syndromes recapitulate all of the features associated with normal aging, and there is a varying degree of phenotypical overlap with the regular aging progression. Thus, the syndromes are termed segmental, as opposite to global progeroid syndrome. WS is considered to best recapitulate normal aging among the segmental progeroid syndromes.

WS was first identified in 1904 by Dr. Otto Werner at the Kiel University [79]. Patients develop normally until puberty, when the expected growth spurt is omitted and patients start to show symptoms of accelerated aging. The symptoms include osteoporosis, diabetes mellitus (type II diabetes), arteriosclerosis, ocular cataracts, early greying of the hair and cancers. However, WS patients also show phenotypical changes that are not typical for normal aging, such as short stature, “bird-like face”, high pitched voices, hyperkeratosis (thickening of the skin due to accumulation of keratins), telangiectasia (small dilated blood vessels near the surface of the skin), increased hyaluronic acid in the urine, and hypogonadism. Men with WS are generally infertile, but females have a varying degree of infertility. It has also been observed that the types of cancers presented in WS patients are rare in the general population. These are tumours of mesenchymal origin. Mesenchymal cells are derived from the mesodermal germ layer and include many cell types found in connective and other supporting or blood-forming tissues. The cancers in WS include

neoplasms such as sarcomas. The most common cause of death is either from cancer or cardiovascular disease and the average age of death is below 55 [80-82].

WS is rare in the Caucasian population (1 in 10^6), but is relatively common in Japan, estimated at around 1 in 20,000 to 1 in 40,000. The high incidence is thought to be contributed to consanguinity. In 1996 the gene responsible for WS was identified and subsequently named *WRN* gene [83]. It is located on chromosome 8p12 and encodes a 162-kDa protein that belongs to the RecQ helicase family. In addition to a 3´-5´ helicase activity, WRN also possesses 3´-5 exonuclease activity [80, 81, 84].

Mutations in *WRN* are responsible for 90% of WS cases and so far 58 different mutations throughout the gene have been reported (Figure. 1.5). Most mutations lead to gene truncation, thus prematurely terminating transcription and as the NLS is situated at the C-terminus, the truncated protein remains in the cytoplasm and is degraded. Therefore, most WS patients have a total absence of the WRN protein. There are no reports of patients with mutations in either the helicase or the exonuclease domain only, indicating that both biochemical activities must be lost to promote WS phenotype [84].

A cDNA microarray analysis shows that the gene expression patterns in WS cells resemble that of naturally aged controls. This supports the notion that WS is an ideal model to study normal aging .

It has been reported [84, 85] that epigenetic silencing of the *WRN* gene was found in tumour cell-lines. The inactivation of *WRN* was due to hypermethylation of CpG islands in the promoter region and showed loss of WRN protein. This is consistent with the increased cancer risk in WS .

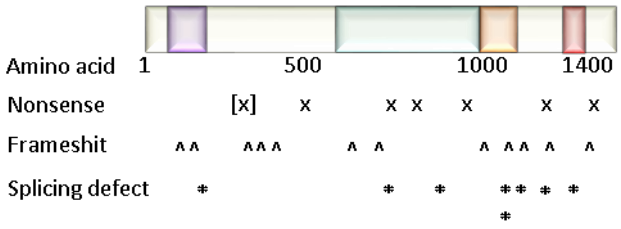

Figure 1.5 | Found mutations in WRN affected individuals

Purple box represents exonuclease domain, green box represents the helicase domain, orange box represents the RQC domain, and the NLS is represented by the red box. The R369Stop, which is the most common mutation in Caucasian patients, is marked by an [X]. Double star in splicing defects represents the most common mutation in Japanese WS patients (deletion of exon 26). Picture adapted from [81].

1.9 RecQ Helicase Family

Helicases are enzymes that separate complimentary strands while deriving energy from ATP hydrolysis. WRN protein is one of five human homologues in the human RecQ family, which is one of the most conserved groups of helicases and at least one orthologue is found in all eukaryotic organisms . The family is named after the first identified *recQ* gene in *E. coli* and it was discovered 20 years ago in a screen that identified mutations conferring resistance to thymine starvation [81, 86]. In humans, at least three out of the five homologues are connected to a genetic disease, namely, Bloom syndrome (mutations in *BLM*), Rothmund-Thomson (mutations in *RECQ4*), and WS. Even though they all have a distinct phenotype, there are several common abnormalities, such as chromosomal instability and predisposition to cancer .

RecQ helicases have several domains present in most homologues: the helicase, the RecQ C-terminal (RQC), and the Helicase and RNase D C-terminal (HRDC) domains. The conserved helicase domain is present in all homologues and has a 3´ - 5´ polarity, as defined by the movement of the protein on the bound strand. It comprises seven sequence motifs (I, Ia, II, III, IV, V and VI) considered the hallmark of superfamily-1 and -2 helicases, to which RecQ helicases belong. There is an additional conserved motif, motif 0, which is unique to RecQ helicases and is N-terminal to motif I. Motif I is critical for helicase activity and leads to a total loss of helicase activity if deleted in *WRN*. In most RecQ helicases, the preserved RQC domain and HRDC domains are located C-terminal to the helicase domain. These sequences are thought to mediate DNA binding and interactions with other proteins. Some RecQ isoforms, such as WRN, have an NLS proximal to the C-terminal [80, 84].

The RQC domain is conserved in three out of five human homologues and in all bacterial RecQ helicases found so far. This domain is made up of two elements: the Zn^{2+}-binding platform and the winged-helix subdomain. Both subdomains are implicated in DNA binding and stabilization of protein-protein binding . Missense mutations in *BLM* in the Zn^{2+}-binding domain result in the loss of ATPase and helicase activity and gives rise to Bloom's syndrome .

The HRDC domain is the least conserved domain, absent in many RecQ homologues. The WRN HRDC domain preferentially binds Holliday junctions (HJ) and forked substrates, although binding affinity increases with addition of the RQC domain and other C-terminal domains.

The processivity of RecQ helicases is surprisingly low, especially for WRN protein. Without auxiliary proteins it is unable to unwind duplexes longer than 40 base pairs (bp). Addition of single strand binding proteins SSBP or Replication protein A (RPA) significantly increases the unwinding to over 500 bp [81, 87, 88]. Even though there are some differences in the preferential substrates for RecQ helicase, there is a consensus that they process specialized DNA structures other than the standard B-form DNA. These include branched junctions, such as 4-way junctions that mimic the HJ. BLM and WRN are able to promote HJ migration over several thousand base pairs [84, 89]. G-quadruplex DNA (G4) is also processed by RecQ helicases. This is a highly stable non-Watson-Crick DNA secondary structure implicated in G-rich telomere sequences and around the replication fork, creating "roadblocks". In addition to the above-mentioned substrates, RecQ helicases show unwinding of a number of other substrates, including gapped DNA, D-loops, RNA-DNA hybrids and triplex DNA [90].

1.10 WRN Protein

WRN protein and its homologue in *Xenopus laevis* (*X. laevis*), FFA-1, are unique amongst RecQ helicases in that they also posses a 3´-5´ exonuclease domain in the N-terminus. This domain can operate independently of the helicase domain. There is, however, evidence indicating that the helicase and nuclease activity might function in coordination i*n vitro* .

The exonuclease domain of WRN belongs to the DnaQ family, which has a replicative proof reading activity and is activated in a Zn^{2+} dependent manner. Unlike proofreading exonucleases WRN does not process ssDNA, but prefers substrates such as dsDNA with a 5´-overhang. It will also digest blunt-ended DNA if the substrate contains a fork, Holliday junction or a D-loop. Poor substrates include ssDNA or blunt-ended dsDNA.

WRN binds many proteins, but it has been shown that it interacts functionally with only a limited number of them, many of which are involved in DNA replication and recombination.

1.11 The role WRN in DNA replication

WRN cells have been shown to have an extended S-phase [81, 91]. This has been attributed to a decreased rate of DNA replication and disruption in origin firing during unperturbed S phase. In *X. laevis* FFA-1 is needed for assembly of the functional replication foci [91]. However, the effects of WRN depletion are most evident when DNA replication is disturbed by DNA damage and WRN cells are sensitive to treatments with DNA damaging agents that interfere with replication and in particular cross-linking agents. WRN protein has structure-resolving activity and prefers substrates such as G4 DNA [90]. Therefore it could be postulated that WRN acts as a "plough" in front of the replication fork in order to resolve the "roadblocks" prior to the arrival of the replication machinery. In the absence of WRN, stalled replication forks are converted into DSBs suggesting that WRN functions to protect cells from DSB formation at impaired and stalled forks .

WRN has also been implicated in replication of the lagging strand. It was shown that WRN aids DNA polymerase δ (Polδ), the suggested lagging strand polymerase [92, 93], to traverse G4 structures and alleviates stalling at G4 DNA. At the same time WRN did not exert the same effect on Polε and Polα, the leading strand polymerase and the primase [94]. WRN and Polδ interact directly and it was shown that WRN recruits this polymerase to the nucleolus. In addition to Polδ interaction, there is further evidence for WRNs role in lagging strand replication. WRN interacts with FEN-1 and can stimulate its cleavage of very long 5' flaps. This suggests that WRN is involved in maturation of Okazaki fragments, but also restart of the replication forks, as this process may also require unwinding and cleavage of DNA flaps.

Interestingly, WS cells show shortening and deletions of telomeres specific to the lagging strand [95]. Telomeres are G-rich DNA repeats that cap the chromosome end to protect it from degradation and fusion. Replication of the telomeres is complicated by a 3´overhang that is proposed to loop back to form a so-called T-loop to cap the end as well as the high G content that is prone to forming secondary structures. WRN has been shown to localize at the telomeres and interact with many of the telomere binding proteins. Together with POT1, WRN was shown to resolve G4 telomeric structures and clear the way for the replication machinery, especially on the lagging strand through interaction with Polδ. Crabbe *et al.* showed that part of the genome instability in WS cells, such as deletions and translocations, can be explained by the telomere loss from individual sister chromatids [96]. They show that in WS cells this uncapping leads directly to chromosome fusions and chromosome aberrations in subsequent cell cycles [96].

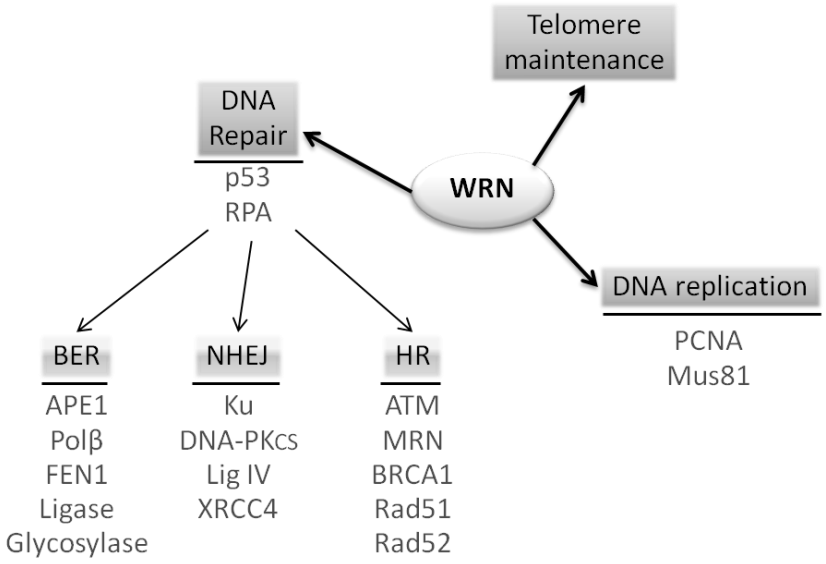

Figure 1.6 | Role of WRN in the cell

The figure shows some of the pathways WRN protein is involved in and the proteins it interacts with. Many pathways in the cell share common steps and therefore proteins can be involved in several pathways. Adapted from [97].

1.12 The role of WRN in repair

The DNA molecule is under constant attack from exogenous and endogenous sources, resulting in a many different kinds of lesions throughout the genome. If left unrepaired this damage can disrupt DNA metabolism and lead to mutations and cell death. The cell has developed a number of pathways to remove and repair different types of lesions and maintain genome stability. In short, the major pathways are base excision repair (BER), nucleotide excision repair (NER) and DSB repair, which includes HR and non-homologous end joining (NHEJ). Different types of DNA damage are repaired by different repair mechanisms. For example, oxidative DNA base modifications are removed by BER, while cross-links and bulky helix-distorting lesions are dealt with by NER.

WRN has been implicated in several repair pathways (Figure 1.6) including BER, HR, NHEJ and cross-link repair [98]. After certain damages that cause replication and transcription arrest, it re-localizes into foci in the nucleoplasm, most likely reflecting its appearance at the site of DNA damage. Regulation of the translocation is not understood, but it is dependent on the type of damage [99].

WRN cells are sensitive to oxidative damage and indeed, they show reduced BER activity and accumulation of oxidative damage after oxidative stress. The BER pathway can proceed via short patch BER (SP-BER), removing only a single nucleotide or long patch BER (LP-BER) which involves strand displacement of multiple nucleotides. The strand displacement activity of Polβ, involved mainly in SP-BER, is stimulated by WRN. *In vitro* data show that the exonuclease activity of WRN can act to proofread Polβ incorporation. Additionally there are other BER proteins in both BER pathways, which are either stimulated by or interact with WRN. These include NEIL1, a glycosylase; apurinic/apyrimidinic endonuclease 1 (APE1); OGG1, major glycosylase for the 8-

oxoguanine lesion, which is one of the most common lesions after oxidative damage and polyADP ribose polymerase (PARP-1), which ribosylates proteins during repair [98, 100].

WRNs implicated role in recombination is much the same as the one implied in replication: to resolve secondary structures. This ability is important from two aspects. Firstly, if secondary structures are removed, the replication fork can proceed smoothly and there will be no need to initiate HR, whose outcomes can lead to chromosome aberrations. Secondly, if HR has been initiated, WRN is required to resolve intermediates and complete the process. WS cells are known to be sensitive to damaging agents such as CPT, hydroxyurea (HU), and several cross-linking agents such as mitomycin C (MMC), psoralen plus UVA (PUVA) and *cis*-Platin, all of which require HR to be resolved [101, 102].

It has been shown that WRN is directly required for HR, in an experiment using recombination reporter plasmids p*NeoA* and p*Lrec* [103]. In this assay cells are cultured under antibiotic pressure and only the ones that are able to recombine to produce an intact antibiotic resistance gene successfully survive. From this it was concluded that the phenotype of WRN cells arises from a recombinational defect that can be rescued by suppressing HR through Rad51 knock down [89]. Similar results have been obtained in yeast [104]. WRN cells are able to initiate recombination, but cannot resolve HR intermediates created by Rad51, some of which are HJ. In accordance with this, the level of Rad51 foci was elevated in WS cells believed to be detention of Rad51 at unresolved structures [98]. Bacterial resolvase protein RusA can rescue survival and recombination in WS cells after treatments such as CPT and cis-Platin [105]. RusA, an endonuclease that recognizes the HJ and cuts two DNA strands at the crossover, also enhanced replication rate in unperturbed WS cells [103].

1.13 The role of WRN in S phase checkpoint

DNA damage activates DNA checkpoints to halt the cell cycle and initiate repair. The apical kinases that initiate signalling in S phase are ataxia telangiectasia mutated (ATM) and ATM and Rad3 related protein (ATR). Generally ATM is the main kinase at DSBs, while ATR is activated at stalled replication forks [106, 107].

WRN appears to be involved in recovering stalled DNA replication forks not only through repair, but seemingly through its involvement in checkpoint signalling. WRN interacts with both ATM and ATR during S phase. After PUVA treatment, ATM activation is impaired in WRN cells and the cell cycle delay is omitted, indicating that the checkpoint activation is abrogated [108]. Another cross-linker, MMC, also increases association with ATR [109]. Furthermore, WRN is phosphorylated in an ATM/ATR dependent manner after damage associated with replication forks .

Chapter 2

Material and Methods

2 Material and Methods

2.1 Cell culture

All cell lines were regularly mycoplasma tested and new vials were thawed every 8-12 weeks. To passage cell lines, media was removed and the cells were washed twice with phosphate buffer saline (PBS) (Oxoid) after which trypsin (Sigma) was added. After 5 - 10 minutes incubation at 37°C, 5% CO_2, cells were resuspended in 10 times more media to naturalise the trypsin and obtain a monocellular suspension.

2.1.1 AG03141 and GM01604 cell lines

AG03141 and GM01604 cell lines were a kind gift from V.A. Bohr (NIA, NIH, USA).

AG03141 hTERT-immortalized WS skin fibroblasts and GM01604 hTERT-immortalized lung fibroblasts from a healthy donor were cultured in 1 g/l D-glucose Dulbecco's Modified Eagle Medium (DMEM) (Gibco) supplemented with 10 % foetal calf serum (FBS) (Gibco), and 10 U/ml penicillin-0.1mg/ml streptomycin (Sigma). Cells were grown at 37°C, 5 % CO_2.

2.1.2 U2OS and variant cell lines

Human osteosarcoma U2OS cells were cultured in 1 g/l D-glucose DMEM supplemented with 10 % FBS, and 10 U/ml penicillin-0.1 mg/ml streptomycin (Sigma) at 37°C, 5 % CO_2.

U2OS cells supplemented with WRN short hairpin RNA (shRNA), and non-targeting control shRNA were obtained from V.A. Bohr (NIA, NIH, USA). They were cultured in the same media as untransfected U2OS cells, under 250 μM Hygromycin B (Calbiochem) selection. The shRNA targeted against WRN mRNA was cloned into the pSilencerTM 3.1-H1 hygro vector (Ambion Inc.) for a stable transfection. The WRN RNAi target sequence is:

TGAAGAGCAAGTTACTTGA. A pSilencer vector expressing a shRNA that is not homologous to any known human genes (Ambion) was used as a negative control.

2.1.3 HTETOP and variant cell lines

Human fibrosacroma HTETOP cell line and the cell line derivatives were a kind gift from A.C.G. Porter and are all published reagents [52, 101, 110]. In short, HT1080 cells were stably transfected with tTA expression plasmid (pUHC13.3, G418 selection) and Topo2α cDNA with tTA-responsive promoter (pUHC13.3hygTOP). The endogenous *Topo2α* genes were disrupted with a Zeocine and gpt cassette through gene targeting.

HTETOP cells were grown at 37°C, 5 % CO_2 in 4.5 g/l glucose and non-essential amio acids (NEAA) (sigma) containing DMEM supplemented with 10 % FBS, 100mM sodium pyruvate (Sigma), 200 mM L-glutamine (Sigma) and 5 U/ml penicillin-0.05 mg/ml streptomycin. Cells were regularly kept under 200 μg/ml hygromycin B (Calbiochem) selection, but checked for Zeocine (Invitrogen) and G418 (Calbiochem) resistance occasionally, by adding the drugs for 5-7 days.

To disrupt Topo2α expression in both cell lines, 1 μg/ml doxycycline (Sigma) was added for indicated times. When required, doxycycline media was renewed every 48 - 72 hours.

2.1.4 MO59 cell lines

These cell lines differ in their sensitivity towards ionizing radiation: the radiosensitive MO59J cells are deprived of a catalytic subunit of DNA-dependent protein kinase (DNA-PK_{cs}) and the radioresistant MO59K cells have a normal level of DNA-PK_{cs}. Cell lines were cultured in DMEM:F12 (1:1) medium, with 10 % FBS, and 10 U/ml penicillin-0.1 mg/ml streptomycin (Sigma) at 37°C, 5 % CO_2.

2.1.5 Mycoplasma testing

Cells were seeded in 96-well plates and grown in antibiotic free media for 48-72 hours. They were then rinsed with PBS and fixated in 4% paraformaldehyde (in PBS) for 10 minutes. DNA was counterstained with DAPI and the cells were visualised in the InCell Analyzer 1000 (GE Healthcare). Appearance of mycoplasma was score as appearance of small DAPI positive structures around the large nucleus.

2.1.6 Cell counting

Cells were counted on the electronic Beckman Coulter Particle Counter ZI (Coulter Particle Characterization, Hialeah, USA). 100 µl cell suspension was added to 9.9 ml sodium citrate solution (0.3% w/v tri-sodium citrate, 0.6% w/v sodium chloride (Fisher Scientific)) and cell concentration was determined automatically. Alternatively cells were counted manually in a Haemocytometer (Marienfeld).

2.1.7 Cryopreservation of cell lines

Cells were grown to 50-60% confluency in a 75 cm^2 flask and trypsinized as described above, with the exception of that the trypsin was removed before the 37°C incubation. The whole flask was resuspended in 4 ml medium containing 10% dimethyl sulfoxide (DMSO) (Sigma) and divided up into three cryo vials. Cells were initially transferred to -80°C and then liquid nitrogen for long-term storage.

2.2 Cell viability assay

Cell viability was measured in 96 -well plates, using the resazurin sodium salt (Sigma) dissolved in PBS at a stock concentration of 1 mg/ml. It was kept in the dark at 4°C. The reagent was used at a final concentration of 10 µg/ml, dissolved in media. Cells were incubated 60 minutes at 37°C and 5% CO2 and fluorescence was measured at Ex 530nm / Em 590 nm in Envision Multilabel Reader (PerkenElmer).

2.3 siRNA screen

SMARTpool siRNA library was purchased from Dharmacon, as were the deconvoluted individual siRNA species. 1 nmol siRNA was provided, which was diluted in 1x siRNA buffer (bought as 5x solution from Dharmacon, diluted to 1x with DEPC-water) to a stock of 20 μM. This stock was further diluted to working concentration of 2 μM in 96-well plates.

For the screen and the validation experiments cells were plated in 96 well plates. 6000 GM01604 cells and 3000 AG03141 cells were seeded 24 hours prior to transfection. Cells were rinsed with PBS and media was changed to antibiotic free media just before transfection.

For every transfection, 2.5 μl siRNA (final concentration of 50 nM) was diluted in 7.5 μl OptiMEM (Gibco) in 96 –well plates. Transfection in each well required 0.1 μl DharmaFECT 1 diluted in 9.9 μl OptiMEM. For logistic reasons, the total volume DharmaFECT solution required for the whole screen was made up in a tube and then dispensed onto the siRNA mixture in the individual wells after 5 minute incubation. Once mixed, the siRNA and DharmaFECT solution was left to incubate for at least 20 minutes. The whole mixture was transferred over to 80 μl antibiotic free media in each well. 150 μl complete media was added 24 hours post transfection to each well.

Cell viability was measured in 96-well plates, using the resazurin sodium salt (Sigma) dissolved in PBS at a stock concentration of 1 mg/ml. It was kept in the dark at 4°C. The reagent was used at a final concentration of 10 μg/ml, dissolved in media. Cells were incubated 60 minutes at 37°C and 5% CO2 and fluorescence was measured at Ex 530nm / Em 590 nm in Envision Multilabel Reader (PerkenElmer).

2.4 siRNA sequences

All siRNA was kept at a stock concentration of 2μM at -20°C in aliquots to avoid freeze-thaw cycles.

Non-targeting RNA (AllStars Neg. Control siRNA, Qiagen)

	Duplex Number	Target	Sequence
SMARTpool			
	#1	CCNA2	GCUGUGAACUACAUUGAUA
	#2	CCNA2	GAUGAUACCUACACCAAGA
	#3	CCNA2	AAGCUGGCCUGAAUCAUUA
	#4	CCNA2	GGAAAUGGAGGUUAAAUGU
	#1	CHEK1	GCAACAGUAUUUCGGUAUA
	#2	CHEK1	GGACUUCUCUCCAGUAAAC
	#3	CHEK1	AAAGAUAGAUGGUACAACA
	#4	CHEK1	CCACAUGUCCUGAUCAUAU
	#1	INCENP	CCACGAUGCUGACUAAGAA
	#2	INCENP	CAAGAAGACUGCCGAAGAG
	#3	INCENP	GCAAAGAGCCAGAGCUGAU
	#4	INCENP	UCUGCAACAUGGAUAAUAA
	#1	RAD21	GGAAGAAGCAUUUGCAUUG
	#2	RAD21	GAACAGAGCACCAGCAAUC
	#3	RAD21	GAGCCCAACUUAGUGAUUA
	#4	RAD21	GGGAGUAGUUCGAAUCUAU
	#1	Topo2α	CAAACUACAUUGGCAUUUA
	#2	Topo2α	AAACAGACAUGGAUGGAUA
	#3	Topo2α	CGAAAGGAAUGGUUAACUA
	#4	Topo2α	GAAAGAGUCCAUCAGAUUU
Others (Chapter 4)			
		Topo2α (Indicated as #2 in Chapter 4)	CGUAGGCUGUUUAAAGAAA
		TopoIIβ	GGGCUAGGAAAGAAGUAAA
		Chk1	UCGUGAGCGUUUGUUGAAC

2.5 Measuring transfection efficiency using BLOCK-iT Flouresecent Oligo assay

AG03141 and GM01604 cell were seeded at $0.1x10^6$ cells per well in 6-well plates and transfected with 50 nM BLOCK-iT Flouresecent Oligo (Invitrogen) one day later. siRNA was diluted in 200 µl OptiMEM and 5 µl of transfection agent, DharmaFECT 1 (Dharmacon), was diluted in 200 µl OptiMEM in a separate tube. Each tube was incubated for 5 minutes before they were combined, after which the mixture was incubated for another 20 minutes, then added to 2 ml plating volume of antibiotic free media.

24 hours post transfection cells were visualised in Biorad Radiance confocal microscope using a 10x lens, after which they were harvested and fixated in 70 % ethanol (Fisher Scientific) at –20°C over night. They were then centrifuged at 2000 rpm for 5 minutes and the cell pellets were resuspended in 500 µl PBS containing 10 µg/ml propidium iodide (Sigma-Aldrich) and 0.4 mg/ml PureLink RNAase (Invitrogen). The suspension was transferred to FACS tubes (Falcon) and incubated at 37°C for 30 minutes. Samples were run directly or stored at 4°C for no more than two days until they were analyzed using a FACScaliubur (Becton Dickinson). Analysis was performed using Flowjo (Tree Star Inc.). Cells were first gated according to their size (FSC) and granularity (SSC) to avoid doublets in the analysis. A second gating was done according to GFP incorporation (FL1 – Hight) and size (FSC).

2.6 Fluorescence Activated Cell Sorting (FACS)

2.6.1 IdU incorporation assay

U2OS cells were seeded at $0.1x10^6$ cells per well, and GM01604 and MRC5 cells were seeded at $0.075\ x10^6$ cells per well in 6-well plates. They were transfected one day after seeding with 1 nM siRNA Topo2α #2. The reaction was performed with 8 µl INTERFERin

(Polyplus transfection) in 200 µl antibody and serum free media. The reagents were all vortexed and incubated for 20 minutes. The transfection mix was added to 2 ml plating volume of antibiotic free media. 2 ml fresh media was added 24 hours post transfection and cells were prepared for FACS analysis 72 hours post transfection.

All cells were seeded in 6-well plates and transfected as described above. HTETOP cells ($0.1x10^6$) were plated in doxycycline containing media, where indicated. Cells were released into ICRF-193 containing media as necessary and were pulse labeled with 25 µM IdU (Sigma) for the last 20 minutes of incubation.

Cells were harvested and single cells were fixed overnight in 70% ethanol (Fisher Scientific) at –20°C. Cells were centrifuged at 2000 rpm for 5 minutes and the cell pellets were resuspended in 2 M hydrochloric acid (HCl) (Fisher Scientific) containing 0.1mg/ml pepsin (Sigma-Aldrich) for 20 minutes at room temperature. Samples were washed once in 10ml PBS, followed by a 5 ml wash with blocking solution (0.5 % FBS and 0.5 % Tween 20 in PBS). Cell were incubated with primary mouse antibody anti-IdU/BrdU (BD Biosciences) . It was diluted 1:50 in blocking solution and the cells were incubated in 100 µl for 1.5 hours at room temperature, mixing every 30 minutes. Samples were washed with 5ml PBS and spun at 2000rpm for 5 minutes. The pellets were resuspend in 100 µl α-Mouse AlexaFluor 488 (Invitrogen, gG (H+L) 2 mg/mL) diluted in blocking solution and incubated for 1 hour at room temperature in the dark, mixing every 30 minutes. Samples were washed in 10 ml PBS and resuspend in 500 µl PBS containing 10 µg/ml propidium iodide (Sigma-Aldrich) and 0.4 mg/ml PureLink RNAase (Invitrogen), transferred to FACS tubes (Falcon) and incubated at 37°C for 30 minutes. Samples were run directly or stored at 4°C for no more than two days until they were analyzed using a FACScaliubur (Becton Dickinson). Cell cycle analysis was performed using CellQuest (Becton Dickinson). A total of 10,000 cells were collected per sample and cells were gated according to their size (FSC) and granularity

(SSC) to avoid doublets in the analysis. Samples were assessed for DNA content (FLA3-Area) and IdU incorporation (FL1-Hight).

2.6.2 ICRF-193 G2 arrest

$0.3x10^6$ cells were seeded in 6- well plates and treated 24 hours later. After 24 hours of ICRF-193 treatment, cells were harvested fixated in 70 % ethanol (Fisher Scientific) at –20°C overnight. Cells were centrifuged at 2000 rpm for 5 minutes and the cell pellets were resuspended in 500 µl PBS containing 10 µg/ml propidium iodide (Sigma-Aldrich) and 0.4 mg/ml PureLink RNAase (Invitrogen). The suspension was transferred to FACS tubes (Falcon) and incubated at 37°C for 30 minutes. Samples were run directly or stored at 4°C for no more than two days until they were analyzed using a FACScaliubur (Becton Dickinson). Cell cycle analysis was performed using CellQuest (Becton Dickinson). A total of 10,000 cells were collected per sample and cells were gated according to their size (FSC) and granularity (SSC) to avoid doublets in the analysis. Samples were assessed for DNA content (FLA3-Area).

2.6.3 pSer-H3 staining

Between 0.1 and $0.3x10^6$ cells were seeded in 6 – well plates and treated as indicated. Cells were harvested fixated overnight in 70% ethanol (Fisher Scientific) at –20°C. Cells were centrifuged at 2000 rpm for 5 minutes. The pellets were resuspend in 100 µl Rabbit Histone H3 (phospho S28) (Abcam (ab 10543)) diluted in blocking solution and incubated for 1 hour at room temperature, mixing every 30 minutes. Samples were washed with PBS, respun and the pellets were resuspend in 100 µl α-Rabbit AlexaFluor 488 (Invitrogen, gG (H+L) 2 mg/mL) diluted in blocking solution and incubated for 1 hour at room temperature in the dark, mixing every 30 minutes. Samples were washed in 10 ml PBS and resuspend in 500 µl PBS containing 10 µg/ml propidium iodide (Sigma-Aldrich) and 0.4 mg/ml PureLink

RNAase (Invitrogen), transferred to FACS tubes (Falcon) and incubated at 37°C for 30 minutes. Samples were run directly or stored at 4°C for no more than two days until they were analyzed using a FACScaliubur (Becton Dickinson). Cell cycle analysis was performed using CellQuest (Becton Dickinson). A total of 10,000 cells were collected per sample and cells were gated according to their size (FSC) and granularity (SSC) to avoid doublets in the analysis. Samples were assessed for DNA content (FLA3-Area) and pSer-H3 staining (FL1-Hight).

2.7 DNA fibre analysis

2.7.1 Transfection

0.03 x10^6 cells were seeded in 24-well plates 24 hours prior to transfection.They were transfected with 10 nM siRNA as indicated. The reaction was performed with 3 µl INTERFERin (Polyplus transfection) in 100 µl antibiotic and serum free media. The reagents were all vortexed and incubated for 20 minutes. The transfection mix was added to 2 ml plating volume of antibiotic free media. 2 ml fresh media was added 24 hours post transfection and cells were prepared for FACS analysis 72 hours post transfection.

2.7.2 DNA fibre labelling

Halogenated nucleotides were dissolved in media at concentrations of 2.5 mM. Prior to experiment CldU (Sigma) was diluted 1:100 and IdU at 1:10 in temperature and CO_2 equilibrated media. Exponentially growing cells were pulse labelled with the analogues 20 minutes each. Cells were harvested, spun down, and diluted to 0.8 × 10^6 cells/ml in PBS. Cells were kept on ice until fibre spreading.

2.7.3 DNA fibre spreads

2 µl of cell solution was pipetted on a slide (Thermo Ficher) and air dried for 5 minutes. Each sample was spread on four separate slides. 7 µl spreading buffer (200 mM

Tris-HCl pH 7.4, 50 mM EDTA, 0.5 % SDS) was mixed with the cells and further dried for 2-3 minutes. Slides were then tipped to approximately 10° and the droplet was allowed to run to the bottom of the slide over 1-3 minutes. The slides were fixated in methanol/ acetic acid 3:1 for 10 minutes. After air drying, the slides were stored in 4°C.

2.7.4 DNA fibre staining and confocal microscopy

Fixed DNA fibres were rehydrated by two 5 minutes washes in dH_2O. Slides were rinsed once in 2.5 M HCl and then denatured for 1 hour 25 minutes in 2.5 M HCl. Slides were thoroughly rinsed twice with PBS and then incubated in blocking solution (PBS + 1 % BSA + 0. % Tween20) 2x5 minutes and then an additional 30 minutes.

Staining of CldU and IdU labels was done simultaneously. Antibodies were diluted in blocking solution. Rat anti-BrdU monoclonal antibody (Oxford Biotechnology, Oxon, United Kingdom), directed at CldU tracks was diluted at 1:1000 and mouse anti-BrdU (Clone B44, Becton Dickinson) directed at IdU tracks at 1:1500 and slides were incubated for 1h at 37°C. Slides were washed 3 times in PBS and then fixed with 4% paraformaldehyde (in PBS) and incubated with AlexaFluor secondary antibodies, αMouse AlexaFluor 555 and αRat AlexaFluor 488 (Invitrogen, gG (H+L) 2 mg/mL), for 30 - 60 minutes in 37°C. After, slides were washed 2 times with PBS, three times with blocking solution and 2 -3 times with PBS again. Slides were sealed with Vectashield and analysed on confocal microscope within 24 hours. They were kept at 4°C when not under microscope. Fibre images were collected using Biorad Radiance confocal microscope using a 60× (1.3NA) lens. The lengths of labelled fibres and replication structures were analysed using the ImageJ software, and micrometer values were converted into kilobase using the conversion factor 1 μm = 2.59 kb.

2.8 Pulse-field gel electrophoresis

U2OS cells were treated with the indicated doses and times. After trypsinization, $1x10^6$ cells were set into agarose plug (75 µl, 1% InCert Agarose, BMA). Positive control plugs were kept in cold media and radiated with γ -irradiation (^{137}Cs) in Gamma Service Medical (type GSR D1). The dose rate was 1.81 Gy/min. All Inserts were incubated in 0.5 M EDTA, 1% *N*-laurylsarcosyl and proteinase K (1 mg/ml) at 50°C for 48 hours, and thereafter washed four times in TE-buffer (10 mM Tris-HCl and 1 mM EDTA) prior to loading onto an agarose separation gel (1% Chromosomal grade agarose, Bio-Rad). Separation was performed on a CHEF DR III equipment (BioRad; 120° field angle, 240 seconds switch time, 4 V/cm, 14°C) for 24 hours. The gel was stained with ethidium bromide (Sigma) overnight and subsequently analysed by a scanning fluorescence reader (BioRad Molecular Imager FX).

2.9 Immunoflourescence

2.9.1 53BP1 foci

HTETOP cells ($0.1x10^6$) were plated were plated onto coverslips in 6-well plates in doxycycline containing media or treated with Zeocine or ICRF-193 as indicated. Following treatment, the medium was removed and the coverslips were rinsed once in PBS (37 °C) and fixed in 3% paraformaldehyde in PBS-T (PBS, 0.1% Triton X-100 and 0.15% bovine serum albumin) for 20 min. The coverslips were rinsed twice in PBS-T prior to incubation with a rabbit anti-53BP1 (Bethyl Laboratories Inc., 1:500) for 1 h at room temperature. The coverslips were rinsed 4 × 15 min in PBS-T followed by 1 hour incubation at room temperature with a α-rabbit AlexaFluor 488 (Invitrogen, gG (H+L) 2 mg/mL) at a concentration of 1:500 and then rinsed 4 × 15 min in PBS-T. Antibodies were diluted in PBS containing 3% bovine serum albumin. DNA was stained with 1 µg/ml To Pro (Molecular

Probes). Coverslips were mounted with SlowFade Antifade Kit (Molecular Probes). Images were obtained with a Zeiss LSM 510 inverted confocal microscope using planapochromat 63×/NA 1.4 oil immersion objective and excitation wavelengths 546 and 630 nm. Through focus, maximum projection images were acquired from optical sections 0.50 μm apart and with a section thickness of 1.0 μm. The frequencies of cells containing 53BP1 foci were determined by counting at least 200 nuclei in each slide in each experiment. Nuclei containing more than 4 foci were classified as 53BP1 positive.

2.10 Western blotting analysis and antibodies

Cells were washed in ice-cold PBS and lysed in a lysis buffer (50 mM Tris-HCl [pH 7.4], 150 mM NaCl, 0.5% NP-40, 0.5% Triton-X, 0.25 mM NaPPi, 1 mM DTT, 1 μM EDTA) containing complete Protease Inhibitor Cocktail Tablets (Roche) and tyrosine phosphatase inhibitors (cocktail II, 1:100 Sigma) for 30 minutes on ice. The suspension was sonicated and centrifuged at 20,000 x g for 20 minutes at 4°C. Lysates were separated on Invitrogen NuPAGE Novex 4-12% Bis-Tris Gels with manufacturer's buffers and blotted on to Hybond ECL Nitrocellulose Membrane (GE Healthcare). Antibodies used were: Chk1 (Cell Signaling), γH2Ax (Upstate), rabbit TopoIIα (Affinity Bioreagents), mouse TopoIIβ (BD Biosciences), mouse tubulin (Abcam), WRN (Santa Cruz H-90), Rad51 (Santa Cruz H-92), PLK1 (Upstate).

Chapter 3

Results

3 siRNA screen for synthetic lethality in WRN deficient background

3.1 Introduction

WS is a premature aging disorder that also predisposes patients to cancer. It recapitulates the natural aging phenotype to a high extent, making it an excellent model system for understanding the molecular basis behind aging. The WRN protein is a RecQ helicase and is mutated in individuals suffering from WS.

Because fundamental steps in different cellular processes often share common features, WRN has been implicated in several different DNA metabolic pathways - DNA replication, recombination and repair as well as telomere maintenance and checkpoint signalling [111].

The biochemical properties of WRN are reflected in the cellular phenotype of the WS cells. In culture these cells display limited replication potential and delayed S phase. They have increased numbers of non-clonal chromosomal aberrations, such as reciprocal translocations, deletions and inversions. As a reflection of the role of WRN in DNA repair, WS cells show sensitivity to a number of DNA damaging agents such as topoisomerase I poisons, replication stalling agents, as well as hydrogen peroxide (H_2O_2), methane methanosulphate (MMS), and cross-linking agents [111]. Consistent with this genomically instable phenotype, epigenetic silencing of *WRN* was previously found in tumour cell lines [85].

Despite significant investigation of the WRN protein and its functions, the WS phenotype is not fully understood. The main approach for elucidating its function and identifying new protein interactions has been by *in vitro* investigations. However, biochemical findings are strengthened by context of cell based assays.

3.1.1 RNA interference

The discovery and development of the RNA interference (RNAi) has provided scientists with a powerful tool to evaluate function of a gene by silencing its expression and assessing the phenotype. The technique relies on introducing a synthetic short-interfering RNA (siRNA) into the cell, which binds to the endogenous messenger RNA (mRNA) of the targeted protein and degrades it, hence reducing the total protein level. In the initial step, one of the strands of the siRNA, the guiding strand, is incorporated into the RNA-induced silencing complex (RISC), which facilitates the binding of the protein-coding mRNA with the complimentary nucleotides by guiding the complex to the 3´ untranslated region (UTR) of the mRNA. The siRNA binds to the 3´ UTR through the so called seed region, which involves its first eight nucleotides at the 5´ end. The passenger strand of the siRNA, which has not been bound, may be degraded following this step. Once the target mRNA has been recognised and bound, it is cleaved by the endonuclease Agonaute 2, therefore reducing the total amount of mRNA available to translate into protein.

RNAi was first discovered in plants and fungi when introduction of RNA paradoxically reduced the levels of the intended protein [111]. Eventually Fire and Mello showed that double stranded RNA (dsRNA) was the trigger of gene silencing [111]. In the endogenous setting dsRNA is modified into the appropriate and required 21-25 long nucleotide dsRNA with 3’ overhangs by the RNase III enzyme, Dicer. Introduction of long dsRNA into human cells induces an interferone response and subsequent shutdown of all protein synthesis and is therefore not a useful tool in the laboratory. Conversely dsRNA shorter than 30 bp such as synthetic siRNA does not elicit this response. Because it is already in the right format that fits into RISC the preparation by Dicer is bypassed but,

Dicer seems to be required to load siRNA into RISC as siRNA does not induce protein silencing in human cells that lack Dicer [112].

RNAi is thought to have evolved as a defence mechanism against viruses, whereby viral dsRNA is degraded by the Dicer and used to target viral transcript to reduce the viral load [113]. The endogenous synthetic RNAi pathway is also a pivotal regulatory mechanism for post-translational control of gene expression [114]. Endogenously expressed micro-RNAs (miRNA) regulate the expression of mRNA translation for 1000s of genes identified so far, and differ from siRNA only in the biogenesis. Namely cellular miRNA is derived from long primary RNA (pri-miRNA) transcribed by the RNA polymerase II into a hairpin structure, that is further cleaved by the RNase III endonuclease Drosha to yield pre-miRNA. pre-miRNA is exported into the cytoplasm to be cut by Dicer and produce mature miRNA [114].

Identifying the RNAi pathway has propelled science, especially for performing functional studies in mammalian cells. Nevertheless, a large series of synthetic siRNAs showed that only one out of three siRNAs reduced levels of the targeted protein by >90% [115]. With these odds, using four different siRNA sequences to target a protein leaves a 25% chance that none of them will be effective [115]. Development of this technique has been focused on understanding how to increase efficacy of synthetic siRNA and predict if a sequence is going to achieve a high knock-down. Research on which siRNA strand enters the RISC complex has yielded the insights that sequence and structure of siRNA is important for a successful uptake by the complex and therefore an effective knock-down [114, 116].

The exogenous synthetic siRNA needs to be designed in such a way to most efficiently target the desired protein, but equally important reduce off-target effects. Unspecific behaviour by siRNA can lead to bewildering results and complicated interpretation, therefore strategies to mitigate off-target effects have increased the usefulness

of RNAi technique. One valuable discovery was that a chemical modification of 2´-O-methyl in position 2 of the guide strand lead to complete silencing of the intended protein, but reduced off-target silencing by 80% [117]. Although it is not quite understood why this modification is so effective, it is suggested that the bulky nucleotide interferes with cleavage by Argonaute if the sequence between siRNA and mRNA is only partially complimentary but the modification is negligible if the two RNAs are well matched. Equally, pooling of multiple siRNA species targeting the same protein is a widely used and effective method for reducing off-target effects. One study showed that pooling 10 different siRNA species, while not reducing the individual concentration of each, significantly reduced off-target effect [118]. This experiment indicated that competition amongst the siRNAs, rather than reduced concentration is responsible for reduction in undesirable silencing. However, lowering the siRNA concentration is an established method of significantly reducing off-target effects, and improvement of siRNA technique at this parameter has progressed significantly in only few years. Yet another discovery that matches in the 5´ seed region of the siRNA can lead to promiscuous binding of 3´UTR of the target mRNA have helped build better algorithms and also contributed to producing siRNA species that can be effective at lower concentrations [116, 119].

3.1.2 Synthetic lethality and high throughput screens

The term synthetic lethality was first described and coined in the early 20th century in studies using *D. melanogaster* and *D. pseudoobscura* [120]. It is used to define a relationship between two genes where knock-down of each gene is compatible with viability, but simultaneous removal of both causes cell death. Equally the concept has been extended to combinations that do not yield loss of viability but only reduce growth and cellular fitness, termed synthetic sick. The synthetic lethal interactions (SLI) between genes exist because of systems in the cell that are set up to buffer for each other and ensure that the cell is not

dependent on any single component, which could easily be lost through a mutation or an environmental assault. The relationship between two synthetic lethal genes can thus be explained by pivotal function of their protein products in two separate pathways, which compensate for each other [121]. Although this is the is the most straight forward concept of synthetic lethality, there are other imaginable scenarios such as that the two proteins might be part of the same pathway or multiprotein complex, and each gene loss further decreases the efficiency. Most SLIs have been described for loss-of-function mutations, but can also involve gain-of-function SLIs, where overexpression of one gene renders a second gene essential [122].

SLI have extensively been studied by geneticists because they reveal information about functional relationships and dissect cellular processes. Most potential has been derived in yeast genetics where mutants have been relatively easy to generate and today large scale screens have mapped comprehensive genetic interaction networks [123]. Recent progresses in RNAi technique and automatisation of the experimental processes by robots have made it feasible to perform such screens in mammalian cells. These advances have particularly been adapted and employed for cancer treatment research and identification of new drug targets [124]. The underlying idea is to find new drug targets that can selectively kill cancer cells by identifying druggable proteins which are synthetic lethal to a cancer-causing mutation.

siRNA libraries, which are becoming available from a number of commercial sources, offer the possibility of screening large numbers of genes and their biological function in an *in vivo* setting. I have utilized a library of 200 siRNAs targeting genes involved in DNA repair and damage signalling to better understand the function of WRN in a cellular setting and to try to find new genetic interactions. Similar synthetic lethal screens for the Sgs1 gene (*S. cerevisiae* homologue of WRN) have been done in the past and have generated a great deal of new information about Sgs1 function [125].

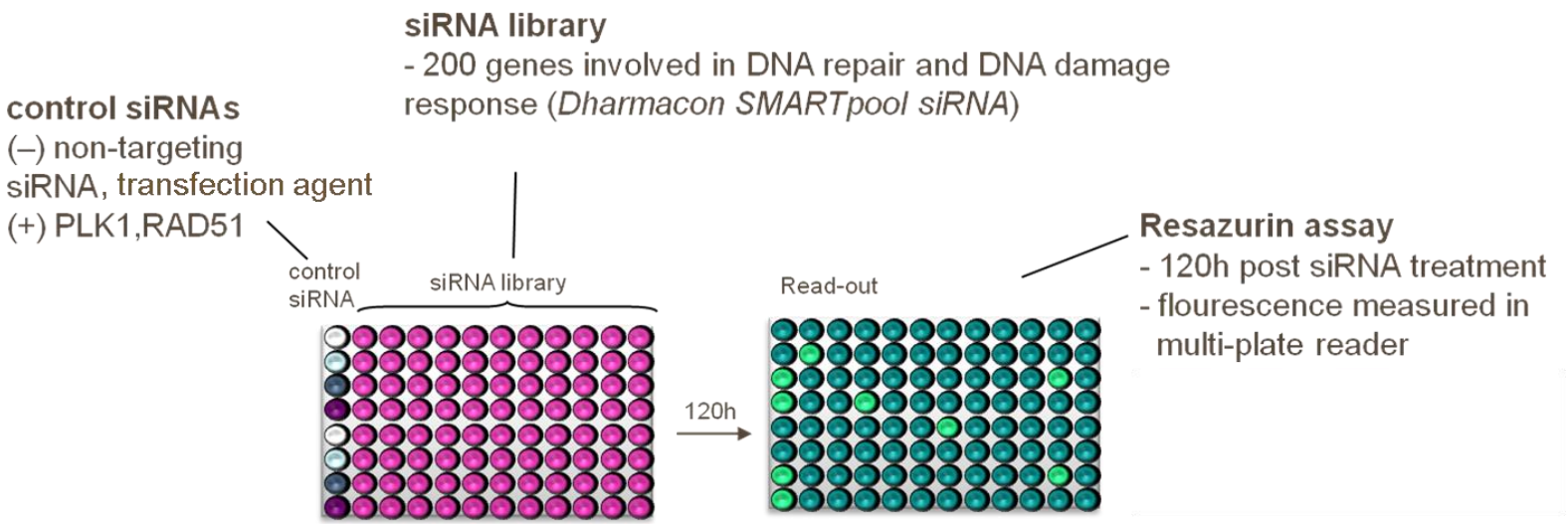

Figure 3.1 | Synthetic lethality screen in GM01604 and AG03141 cells with siRNA library of DNA damage response genes

The layout of the experiment. Cells were seeded in 96-well plates and transfected with 50 nM siRNA. The whole library of 200 genes required 2.5 plates. Positive and negative controls for transfection were included on each plate as depicted. After 120 hours cell viability was assessed by incubating cells in 10 µg/ml resazurin dissolved in medium. Fluorescence was measured at Ex 530nm / Em 590 nm after one hour. The screen was done manually and run in duplicate.

3.2 Aim

The aim is to identify synthetic lethal interactions with the WRN protein by utilizing an siRNA screen, with the goal to facilitate a more physiological characterization of WRN and further the understanding of its role *in vivo*.

3.3 Results

3.3.1 Optimization

Several parameters needed to be investigated and optimised prior to performing the siRNA screen on a full scale. These optimisation steps are described in the section below.

3.3.1.1 siRNA library

The screen was performed using a custom-made siGenome SMARTpool siRNA library from Dharmacon. The library targets 200 DNA repair genes representing all the known DNA repair and DNA damage signalling pathways. The library was obtained in 96-well plates, each well containing a pool of four different sequences targeting one gene. The dilution to working concentration is described in Material and Methods.

We chose to limit the investigation to only repair related genes for both practical and scientific reasons. Performing the experiment in duplicate, in two different cell lines is laborious and time-consuming. Anything more extensive would require automated handling to avoid errors and to complete the transfection within a reasonable time limit. Nevertheless, choosing a DNA repair gene library is still very valuable and scientifically valid – WRN is mainly, if not solely implicated in DNA metabolism. However, WS patients show perturbations of the physiological homeostasis that are not associated with DNA repair and replication defects [126]. Thus, it would be informative to extend the library in the future when the screen can be done on an automated system. The screen was repeated two times,

and each run was done in duplicate. Setting up a screen in duplicate helps compensate for errors in cell seeding, siRNA transfection and end-point read-out.

3.3.1.2 Cell lines

The cell lines used for the screen were non-isogenic AG03141, hTERT-immortalized WS skin fibroblasts and GM01604, hTERT-immortalized lung fibroblasts from a healthy donor [127]. These cell lines were selected because they come from a non-tumorous background and have previously been used in matching experiments [128]. The rationale for choosing non-transformed cells is that isogenic pairs that can be obtained by using cancer cells have numerous underlying mutations that would bias the total results more than when using a non-mutated background, albeit from different individuals. Figure 3.2 shows WRN status in the two cell lines with absence of WRN in AG03141 cells.

The amount of cells to be seeded was optimised first (Figure 3.3). The screen involved transfecting cells in 96-well plates and measuring viability 120 hours later. Cells had to be around 60% confluent at the time of transfection 24 hours post seeding, as suggested by the manufacturer's protocol, and could not reach confluency at the time of the read out. To determine the right concentration, varying amounts of cells were seeded in 96-wells and viability was measured each day using the resazurin assay (optimized simultaneously and described below) (Figure 3.4).

GM01604 cells grew best at a seeding density between 4,000-10,000 cells per well, where exponential growth was reached at the time of transfection, as reflected in the readout. However, 4,000 cells per well was less than 60% confluency, which was required for transfection while 8,000 and 10,000 cells per well, although still metabolizing the resazurin salt after 120 hours, were overgrown and close to detaching. Therefore, 6,000 cells per well was used in the screen.

AG03141 cells grew slower, as expected, but concentrations between 3,000 and 6,000 cells per well still showed the expected exponential growth. Because AG03141 cells are slightly larger, 3,000 cells per well was used for the screen as this number gave 60% confluency at the time of transfection.

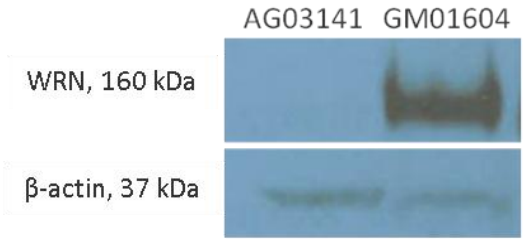

Figure 3.2 | WRN status in GM01604 and AG03141 cell line

30 µg whole cell extracts was loaded as indicated. The Western blot was probed with WRN and β-actin antibody. β-actin was used as loading control.

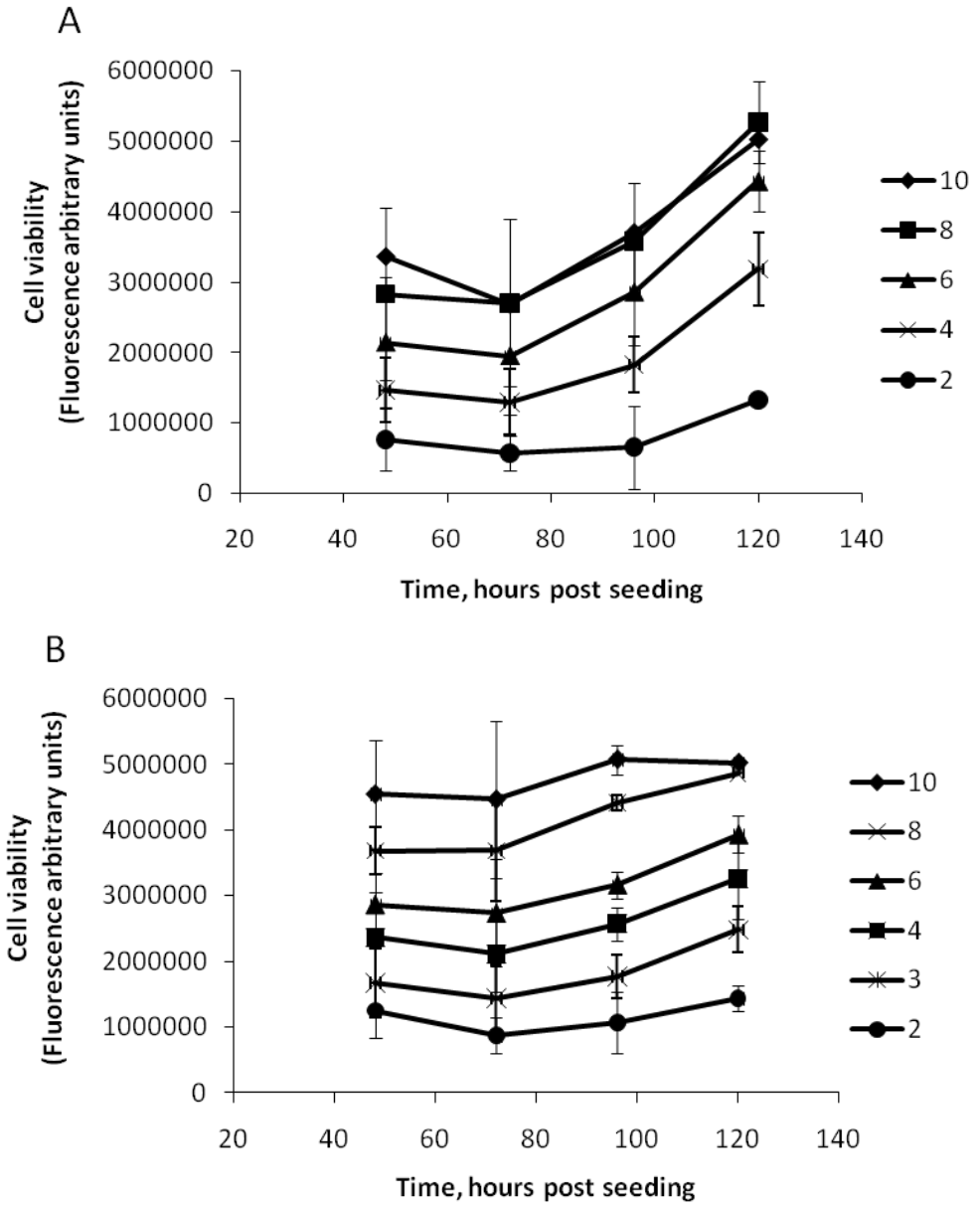

Figure 3.3 | Optimization of cell number seeded in each well

Cells were seeded in 96-well plates and viability was measured every 24 hours for 120 hours. The legend indicates the initial number of cells seeded, in thousands. Error bars represent standard deviation from the mean of two repeats. **A.** GM01604 cells **B.** AG03141 cells.

3.3.1.3 Resazurin assay

The aim of the screen was to identify proteins that are synthetic lethal to WRN, thus the cell viability was used as an end-point to measure the effect of siRNA knock-down in WS cells. To this end the resazurin colorimetric assay was chosen to measure viability. Resazurin is a salt, reduced by mitochondrial and cytosolic oxidoreductases [129] in viable cells to resorufin and dihydroresorufin. Resorufin is a fluorescent dye with an emission wavelength at 590-620 nm [130]. Resazurin is non-toxic and stable in medium [131] and has been shown to yield similar results as the MTT assay and the more conventional colony forming assay [132].

Resazurin salt was used at the recommended concentration of 10 μg/ml dissolved in media. The first parameter to be determined was the length of resazurin solution co-incubation time with the cells. The plate was read at several time points for up to two hours and fluorescence signal was measured. Figure 3.4 shows that the signal increased for up to one hour for both cell lines, and that the difference between one and two hours was modest. Therefore, one hour incubation with resazurin solution was chosen and used in the screen.

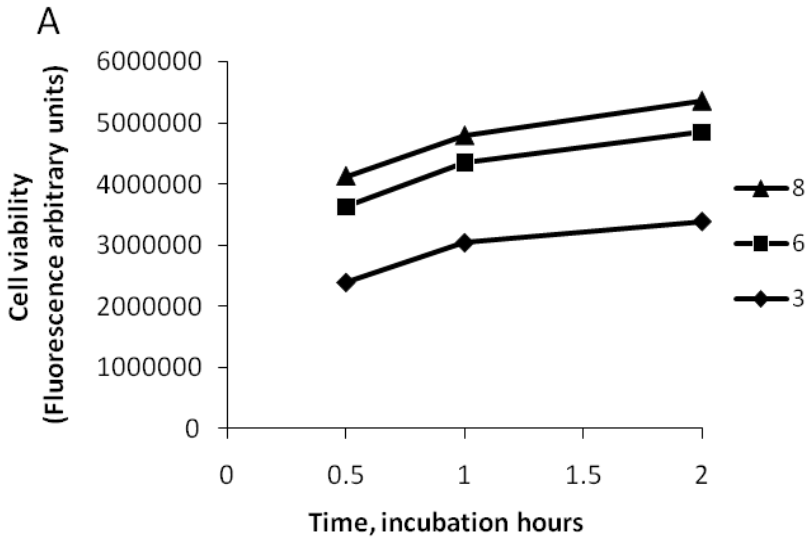

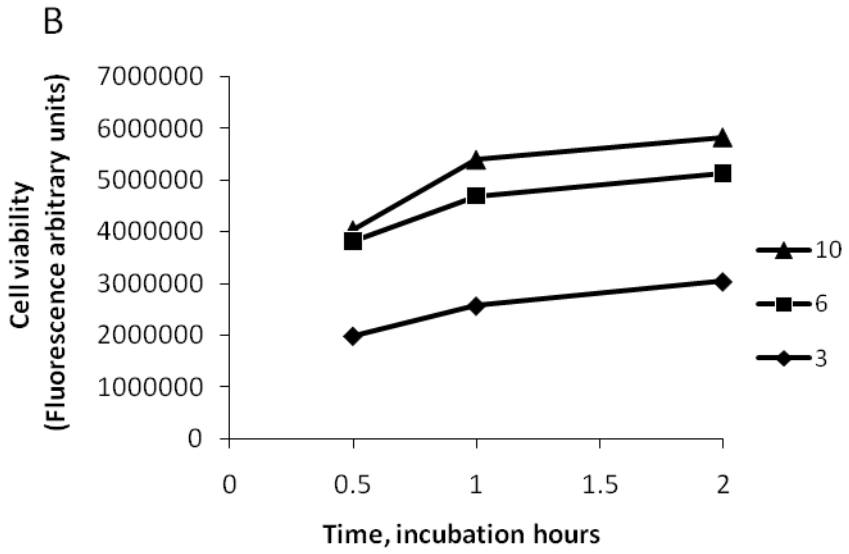

Figure 3.4 | Resazurin incubation times

Cells were seeded in 96-well plate incubated for 24 hours before addition of resazurin. Plates were then read at indicated times. The legend indicates the initial number of cells seeded, in thousands. **A.** GM01604 cells **B.** AG03141 cells.

To check that the strength of the fluorescence signal correlated to cellular metabolism of the cells and that it was directly correlated to the number of cells, the signal from increasing cell number was plotted (Figure 3.5). The correlation between cell density and the signal intensity was close to perfect in the used range between 2,000 and 6,000 cells per well, with R^2 value for GM01604 cell of 0.994 and 0.990 for AG 03141 cells.

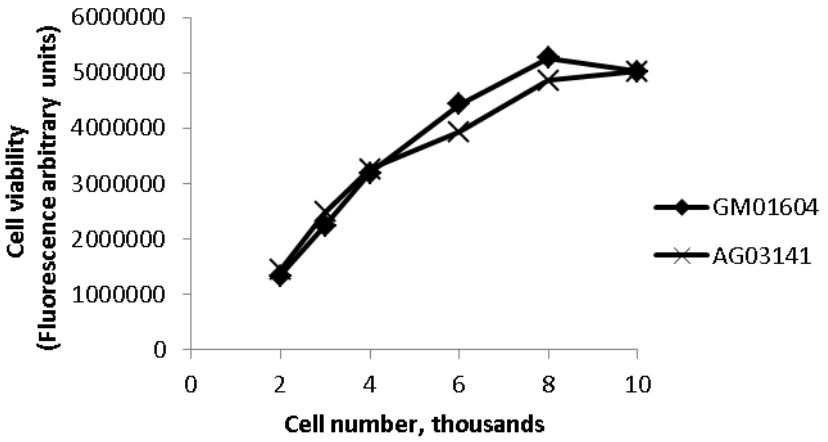

Figure 3.5 | Fluorescence signal is proportional to number of cells in the lower range

Fluorescence signal 120 hours post seeding in GM01604 and AG03141 cells. In the range between 2,000 and 6,000 cells the correlation between cell number and fluorescence was strong as indicated by R^2 value for GM01604 cell of 0.994 and 0.990 for AG 03141 cells.

3.3.1.4 Transfection efficiency

Because the cell lines are not isogenic, it was important to investigate transfection efficiency in order to verify that both cell lines would have equal knock-down and that results could be compared between them. Cell lines were transfected with 50 nM BLOCK-iT Fluorescent Oligo in 6-well plates and transfection efficiency was measured after 24 hours. The BLOCK-iT Fluorescent Oligo is a fluorescein-labelled dsRNA oligomer with the same length as an siRNA but does not target any gene. Uptake of the oligo was visualised in a microscope (Figure 3.6 A) after which cells were harvested and processed for fluorescence-activated cell sorting (FACS) analysis. This allowed for quantification of the uptake. Close to 100% of AG03141 cells took up the oligo, while that figure was 90% in GM01604 cells (Figure 3.6 B). These results were supported by the visual images.

To measure transfection response in a functional assay, cells were transfected with siRNA against Rad51 or PLK1 protein. These are both essential proteins and knock-down of

either leads to rapid apoptotic response [133]. To measure if the siRNA had an effect and how comparable it was between the two cell lines, cells were transfected with 50 nM siRNA in a 96-well plate and viability was measured by resazurin assay. Transfection reagent and non-targeting (NT) siRNA were used as negative controls.

Figure 3.7 shows viability, measured 72 hours post transfection. Cells transfected with siRNA against PLK1 were close to non-viable and Rad51 knock-down/depletion reduced cell survival to 30 – 40%. Importantly, both cell lines had an equally good response to the knock-down, suggesting that the slight difference in transfection efficiency as measured by FACS would not interfere with the screen readout.

To validate that viability status was correlated to loss of protein a Western blot was performed on cell lysates 48 and 72 hours post transfection, from cells that were treated in same conditions as those for viability measurements (Figure 3.8). PLK1 is potent inducer of apoptosis and a knock-down of this kinase kills most cancer cells [134]. Therefore there were no cells to harvest 72 hours post transfection, and only 48 hour time point was analysed (Figure 3.8). The blot shows that Rad51 levels are also reduced after PLK1 transfection, which can be explained by early apoptotic breakdown of DNA repair genes, presumably to prevent repair of apoptosis induced DNA fragmentation [133]. The reduced protein levels of PLK1 in siRNA Rad51 in GM01604 cells treated samples are harder to explain and could be due to an off-target effect. These positive and the negative controls, which included transfection agent DharmaFECT1 and siRNA NT were included on each plate to monitor the transfection efficiency (Figure 3.1).

A

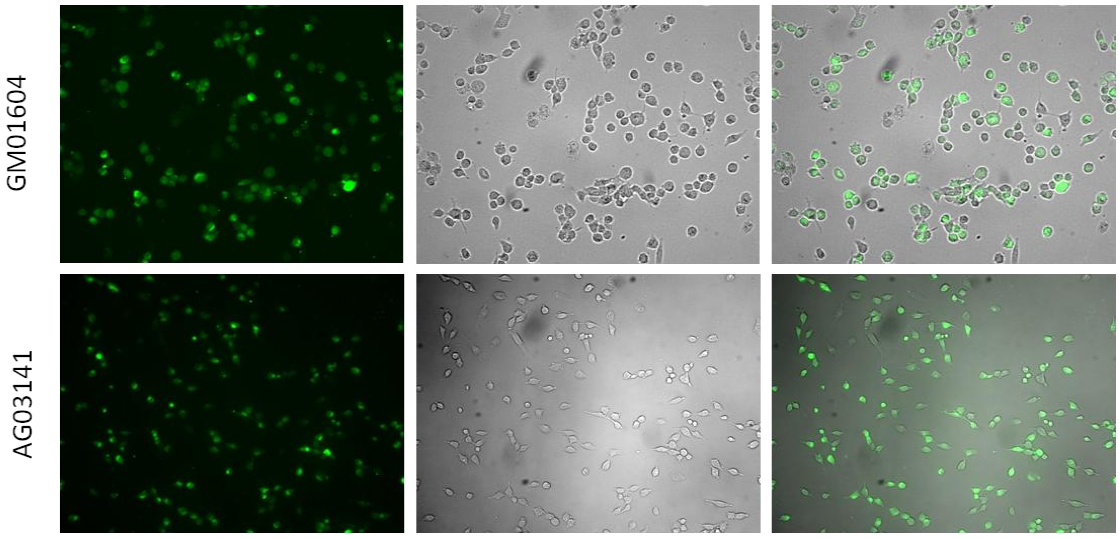
Invitrogen BLOCK-iT
Flouresecent Oligo, 50nM
Bright Field
Merge
GM01604
AG03141

B

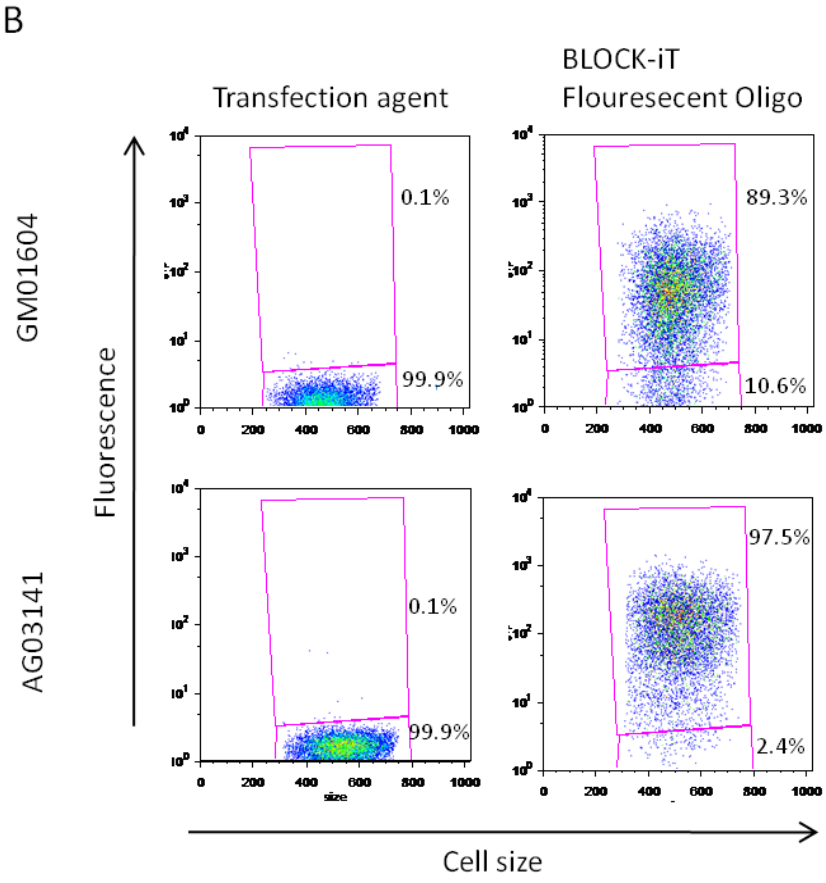
Transfection agent
BLOCK-iT
Flouresecent Oligo
GM01604
AG03141
Fluorescence
Cell size
0.1%
99.9%
89.3%
10.6%
0.1%
99.9%
97.5%
2.4%

Figure 3.6 | Transfection efficiency of GM01604 and AG03141 cells

A. Representative images of cells transfected with Invitrogen BLOCK-iT Fluorescent Oligo, 50 nM, 24 hours post transfection. 10 x objective.

B. Representative FACS plots of cells treated as in A. The proportion of transfected cells was calculated by gating as shown. Percentage of cells in each quadrant is indicated.

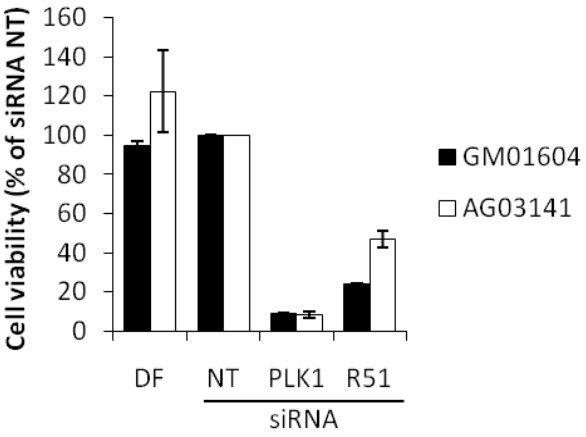

Figure 3.7 | Positive control siRNA Rad51 and siRNA PLK1 reduce viability in GM01604 and AG03141 cells

Cells were seeded in 96-well plate and transfected with 50 nM siRNA. Survival was measured by resazurin assay 120 hours post transfection. DharmaFECT (DF), non-targeting (NT), Rad51 (R51). Data bars are the means of at least three independent experiments. Error bars represent standard deviation from the mean.

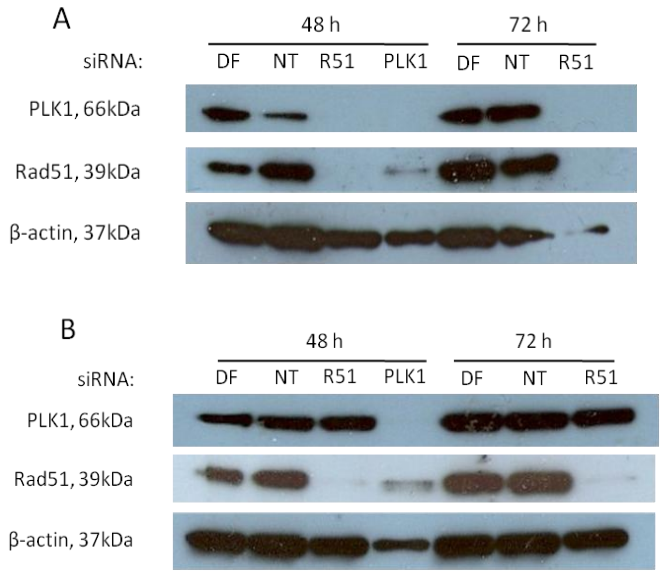

Figure 3.8 | Positive control siRNA Rad51 and siRNA PLK1 reduce the levels of protein in GM01604 and AG03141 cells

Western blot showing knock-down of PLK1 and Rad51. Cells were seeded in 96-well plates and transfected with 50 nM siRNA. Whole cell lysate was prepared 48 or 72 hours post transfection as indicated in Material and Methods. **A.** GM01604 cells **B.** AG03141 cells.

3.3.1.5 Quality of the screen

The Z-factor is a measure of the quality or power of a high-throughput screen. It measures the strength of the end point assay and its dynamic range. If the readout between the positive and the negative control is well separated, it allows for a large resolution of the screen data points. The formula for the Z- factor is:

$$Z\ factor = 1 - \frac{3 \times (\sigma_p + \sigma_n)}{|\mu_p - \mu_n|}$$

where μ_p and μ_n are the average readouts of the positive and the negative controls respectively and the σ_p and σ_n are the standard deviations of the same. A score of 1 is ideal and anything above 0.5 is considered excellent [135]. The Z-factor was calculated from the experiment shown in Figure 3.7. The Z-factor for AG03141 cells was 0.63 and for GM01604 cells 0.94, confirming that the resazurin assay was sensitive enough for the screen.

3.3.2 Screen results

The aim of the screen was identify genes that are synthetic lethal to WRN by determining whether an siRNA SMARTpool targeting a gene has greater effect on reducing viability in WRN deficient AG03141 cells compared to GM01604 control cells. Transfection reagent was prepared in 96-well plates for all 200 genes and dispensed onto the two replicates for each cell line. In the first repeat viability was measured after 72, 96, and 120 hours. The three tested time points resulted in a similar survival rate in both cell lines, but the difference between the negative and positive control increased in a time dependent

manner. A larger span between the controls is desirable because it results in a higher Z-factor, i.e. the read-out span widens. For those reasons 120 hours was used for the readout (Figure 3.1 and 3.6).

3.3.3 Statistical analysis

The raw data was processed in the following way to score the genes and identify hits. First, viability of each siRNA SMARTpool treatment was normalised to the siRNA NT sample for each plate. As an internal control, Rad51 and PLK1 demonstrated lowest survival in both cell lines. The screen was repeated twice. In order to investigate the reproducibility of the screen, the Spearman correlation coefficient was calculated for each cell line. For GM01604 cells it was 0.59, and for AG03141 0.62 (Figure 3.9), where r = 1 is perfect reproducibility.

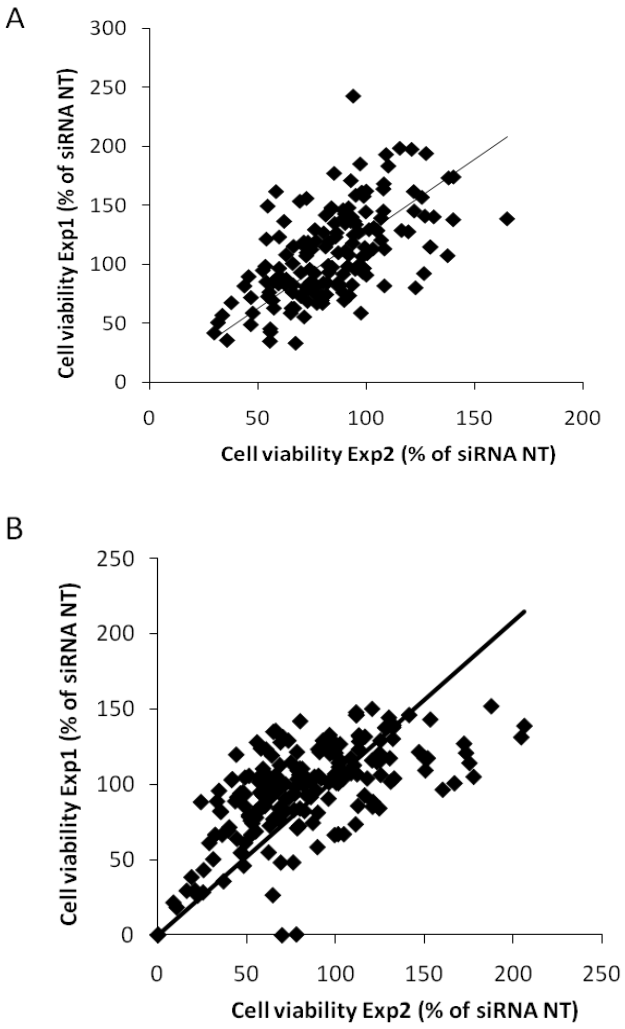

Figure 3.9 | Reproducibility of the screen

Cell viability for each siRNA SMARTpool gene, as percentage of siRNA NT. The line indicates X = Y, a perfect correlation. Spearman correlation coefficient for **A.** GM01604 is r = 0.59, and for **B.** AG03141 is r = 0.62.

Subsequently, the relative viability of each siRNA SMARTpool in AG03141 cells compared to GM01604 was calculated and data for the two runs was averaged. The Z-score is a measurement used for normally distributed data to show how many standard deviations from the mean a value is. After doing a normality test, the screen data revealed a Gaussian distribution with $r^2 = 0.98$, which meant that a Z-score could be assigned to each value

(Figure 3.10). Genes were classified as hits if the corresponding siRNA SMARTpool reduced the relative viability of AG03141 by three standard deviations. 99,7% of genes had Z-scores between -3 and +3 and those with outside of this were considered true hits (Table 3.1). Genes which when knocked down increase survival of WRN deficient cells as compared to WT were not in the scope of this thesis and have, thus, not been investigated further (Table 3.2). Instead, genes that produced a Z-score of -3 or below are listed in Table 3.1 and Figure 3.11. Complete dataset is shown in Appendix 1.

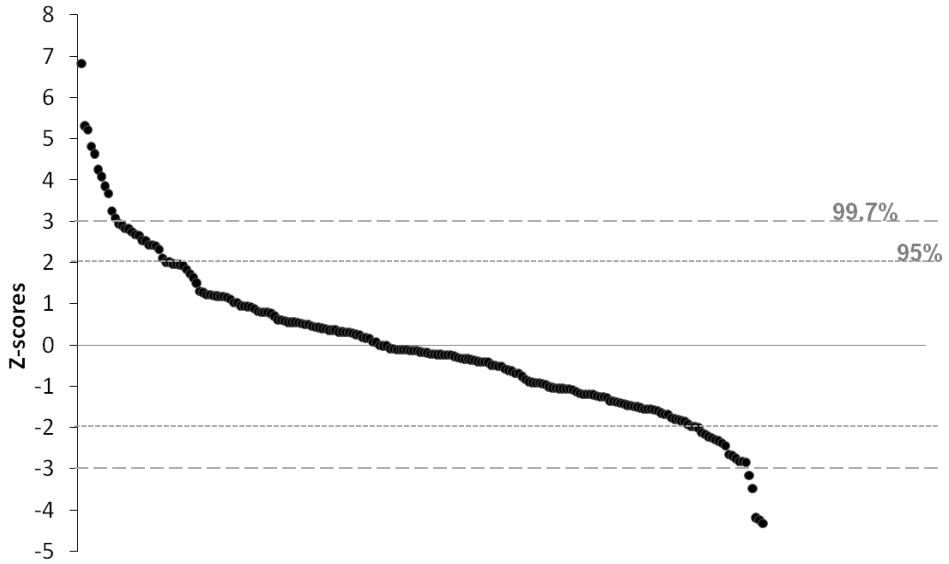

Figure 3.10 | The Z-score for each of the 200 siRNA SMARTpool targeted genes

99.7% of the genes lie between Z-score +3 and -3. Normal Gaussian distribution is evident from an almost symmetrical distribution of data around the mean at 0. SMARTpool sequences that reduced viability of AG03141 cells as compared to GM01604 cells are assigned negative values.

siRNA SMARTpool	Viability, % of GM01604	Z-score
CDC2	50%	-2.68
POLE4	49%	-2.75
FBXO18	48%	-2.82
CCNE1	48%	-2.82
IGF2	47%	-2.84
CCNA2	**42%**	**-3.16**
TOP2A	**37%**	**-3.48**
RAD21	**25%**	**-4.18**
CHEK1	**24%**	**-4.24**
INCENP	**22%**	**-4.33**

Table 3.1 | siRNA SMARTpool targeted genes which reduced relative AG03141 viability

The siRNA targeted genes with most negative Z-scores. The siRNAs are displayed in a Z-score order. Genes that have a score below -3 are considered hits. The middle column indicates percentage viability of AG03141 cells as compared to GM01604 treated cells.

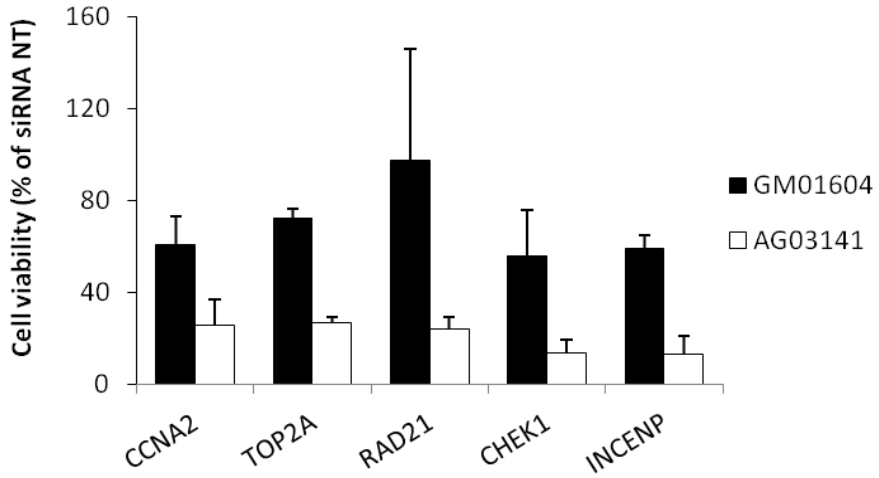

Figure 3.11 | Viability of individual cell lines transfected with siRNA targeting genes considered hits

Raw data showing cell viability for individual cell lines after 120 hours treatment with siRNA SMARTpool targeting genes which were considered hits in the negative Z-score range. Data bars are the means of at least three independent experiments. Error bars represent standard deviation from the mean.

siRNA SMARTpool	Viability, % of GM01604	Zscore
POLB	212%	6.82
ERCC5	186%	5.31
REV1L	185%	5.22
PRKDC	178%	4.82
CLSPN	175%	4.63
DCLRE1B	168%	4.26
TREX2	165%	4.08
MSH3	162%	3.85
RAD51	158%	3.67
MNAT1	151%	3.25
SMARCA4	148%	3.08
ERCC2	146%	2.94

Table 3.2 | siRNA SMARTpool targeted genes which increase relative AG03141 viability

siRNA SMARTpool targeted genes which reduced viability in GM01604 cells compared to AG03141 cells.

3.3.4 Validation

One of the risks associated with siRNA is that it can potentially suppress genes other than the intended target, so called off-target effect. Therefore, the SMARTpools were deconvoluted into four individual siRNAs and individually screened. The hits were considered "on-target" if two or more individual siRNA sequences produced the same or lower sensitivity in AG03141 cells as the SMARTpool [136]. After normalising the data for both cell lines and calculating the relative viability of AG03141 compared of GM01604 for the same genes**,** two out of the five initial hits fulfilled this criterion: Chk1 and Topo2α (Figure 3.12).

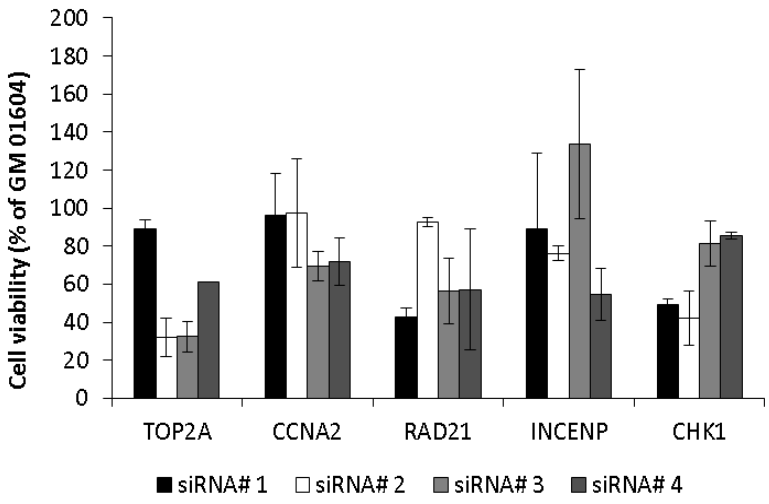

Figure 3.12 | Chk1 and Topo2α siRNA are true hits

The four individual siRNAs from the siRNA SMARTpool were deconvoluted. The graph shows the relative viability of AG03141 cells as compared to GM01604 cells. Viability was measured 120 hours post transfection using resazurin assay in 96-well plates. Data bars are the means of at least three independent experiments. Error bars represent standard deviation from the mean.

Among the two potential hits, Topo2α seemed like an interesting candidate. Studies in yeast have shown that Topo2 may interact with RecQ helicase during decatenation [137] further supported by a publication, showing that WRN is required for activation of the decatenation checkpoint and that WRN and Topo2α co-immunopercipitate in mammalian cells [93]. In this study, the authors show that ICRF-189, a Topo2 inhibitor, induces apoptosis in WRN deficient cells. To investigate if these results were reproducible, GM01604 and AG03141 cells were continuously treated with ICRF-193, a more potent ICRF inhibitor, and survival was measured with the resazurin assay. Figure 3.13 shows that AG03141 cells are indeed more sensitive to Topo2 inhibition.

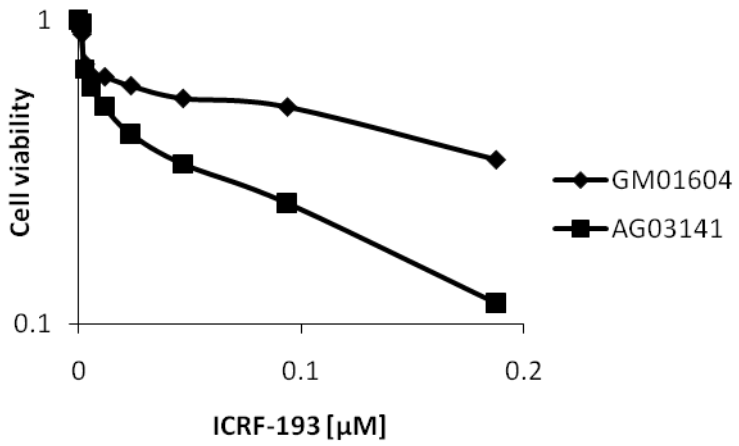

Figure 3.13 | AG03141 cells are more sensitive to the Topo2α inhibitor ICRF-193

Cells were seeded in 96-well plates and continuously treated with ICRF-193. Viability was determined in a resazurin assay and presented as relative survival to untreated cells. Experiment was performed one time.

To further validate the result, protein levels post transfection were measured by Western blot (Figure 3.14). In GM01604 cells all four oligos reduce protein levels of Topo2α. WRN siRNA was used as a transfection control. The results are not as clear in AG03141 cells. None of the siRNAs seem to reduce Topo2α levels. This Western blot was hard to produce and the film shown in Figure 3.14 B has been overexposed. Hence, it is hard to conclude anything from the Western blot, but the experiment suggests that the results might be due to off-target effects of the siRNA in AG03141 cells.

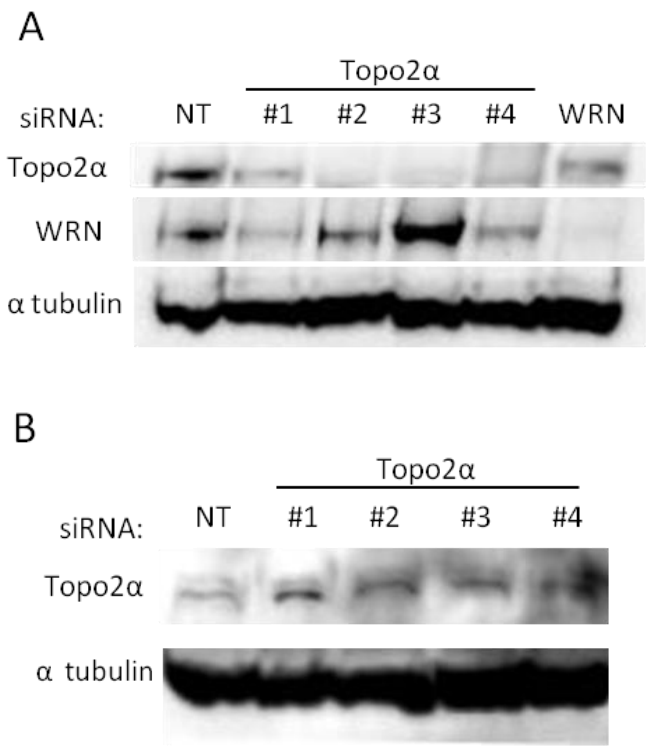

Figure 3.14 | Knock-down of the four individual siRNA SMARTpool sequences targeting Topo2α in GM01604 and AG03141 cells

Cells were transfected with 50 nM siRNA NT, WRN or the four individual siRNA Topo2α sequences from the deconvoluted siRNA SMARTpool. Whole cell extracts were made 72 hours post transfection. **A.** GM01604 cells **B.** AG03141 cells.

To investigate whether Topo2α was synthetic lethal to WRN in other cell lines, I utilised two other cell systems that were available to us. The first was a pair of osteosarcoma U2OS derived cell lines, stably transfected with a shWRN (U2OS WRN) or a non-targeting shRNA (U2OS Ctrl). The two cell lines were transfected with the four Topo2α siRNA oligos. Figure 3.15 shows that although siRNAs #2-3 did reduce viability in WRN deficient cells, the effect is not statistically significant. The second was the HTETOP cell line, described in further detail in the next chapter, which has a doxycycline regulated Topo2α

expression. Addition of doxycycline depletes the cell of Topo2α after 120 hours viability of these cells was reduced to 59%. Further depleting WRN with siRNA, reduced viability slightly, but not enough to be statistically significant (Figure 3.15 B).

In conclusion, although deconvolution of the siRNA smart pool oligos did indicate that Topo2α was a true hit, replicating the results in other cell lines was problematic. Meanwhile, the Western blot produced inconclusive results in AG03141 cells. These results are insufficient to conclude that WRN and Topo2α are synthetic lethal.

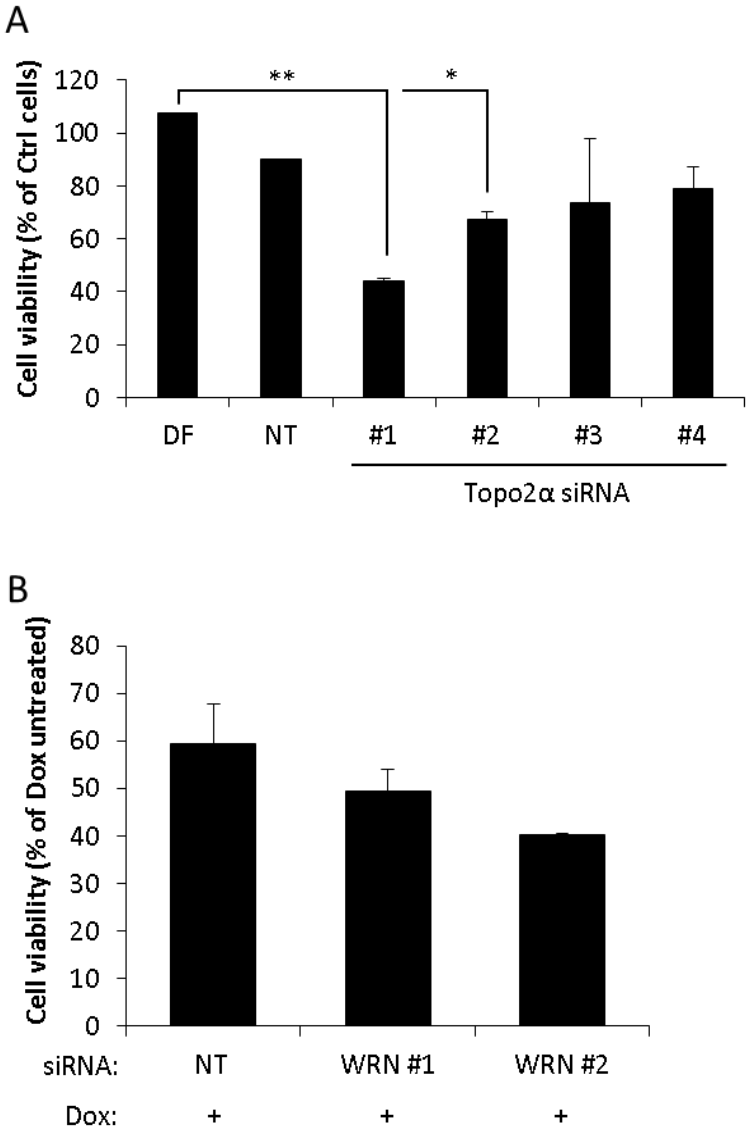

Figure 3.15 | Simultaneous removal of WRN and Topo2α in U2OS and HTETOP cells is not synthetic lethal

A. U2OS WRN and Ctrl were transfected with the four individual siRNAs from the siRNA SMARTpool targeting Topo2α. The graph shows the relative viability of U2OS WRN cells as compared to U2OS Ctrl cells. Viability was measured 120 hours post transfection using the resazurin assay in 96-well plates. Data bars are the means of at least three independent experiments. Error bars represent standard deviation from the mean. Statistical significance is indicated by one star (p-value < 0.05) or two starts (p-value < 0.01) in the Student's *t*-test.

B. HTETOP cells were treated with doxycycline and two siRNA WRN. Viability was measured 120 hours post transfection using resazurin assay in 96-well plates. Data bars are the means of at least three independent experiments. Error bars represent standard deviation from the mean.

3.4 Discussion

The aim of this chapter was to identify SLIs that occur with the WRN protein in order to expand the understanding of the protein's function, the pathways it is involved in and functional interaction with other proteins. For this purpose a SMARTpool siRNA library targeting 200 DNA repair and signalling genes was applied to wild type, GM01604, and WRN deficient cells AG03141 and the synthetic lethality was assessed by a cell viability assay.

There are several putative scenarios where SLI between two proteins can arise, but the underlying principal of synthetic lethality involves buffering of the effect by gene A when gene B is lost and vice-versa. When proteins of both genes are absent simultaneously this back-up mechanism is lost leading to reduction in viability or cell death. Identifying SLIs is, however, only the initial step in furthering the understanding of a protein's function. To fully grasp and exploit the SLI, it is important to conduct further work on the mechanistic basis behind the synthetic lethality. Functional understanding of an SLI not only elucidates

the function of a protein, but expands the knowledge of cellular processes and how they are interconnected. Moreover, it reveals not only synthetic interactions between the two proteins, but also the pathways they are involved in and therefore suggests additional SLIs between other members in those pathways. This potential of synthetic lethality has truly been realized in yeast where mapping of SLIs from large genome-wide screens has yielded comprehensive genetic interaction maps. These can be used to infer and further explore gene functions and pathways, as genes that act in similar processes often buffer for each other [138].

To find SLIs with WRN, a synthetic siRNA library was utilized. The availability and choices of RNAi libraries has greatly expanded in only a few years time, but essentially there are two parameters that need to be decided on, namely library size and format. The size of an RNAi library can be as large as to include genome-wide targets, or alternatively include only a smaller subset of genes. Although a large amount of data can be obtained from a genome-wide library, a more defined library can be relevant if it reflects and focuses on the biological question at hand. The drawback of larger libraries is also expense and time management, as a smaller library can be managed manually while large libraries require automated handling. The second parameter that needs to be evaluated before starting is the type of library format. Fundamentally, RNAi libraries can be divided into two types: collections of vector based short hair pinned RNAs (shRNAs) or synthetic siRNAs. The shRNA libraries are further subdivided depending on the type of vehicle used, such as non-viral, retroviral, adenoviral or lentiviral. These all have individual pros and cons, and should be used for specific purposes. For example the lentiviral vector is able to replicate in non-dividing cells and is therefore appropriate to use in these [139]. siRNA libraries are used for short term knock-down purposes and the knock-down is limited by the rate of cell division as the mammalian cell does not have a mechanism to amplify and propagate RNA (unlike *Caenorhabditis elegans*) [140]. Despite this drawback, transfection of siRNA libraries is

probably the easiest and fastest way to generate a knock-down and transfection efficiency is normally higher as compared to shRNA. One additional consideration is the choice of pooled RNAi libraries. Multiple siRNAs targeting different sequences in the same gene can be combined to reduce off-target effects and increase the possibility that the gene is knocked-down. One such library, SMARTpool from Dharmacon, was used in this chapter.

An siRNA library screen is powerful but there are also limitations, some of which can be moderated by careful optimization and good practice and others that are harder to control. The nature of RNAi mediated depletion is that it is rarely complete and varies between proteins and siRNA sequences. This should be considered when interpreting data from a large screen such as the one presented in this chapter. The result after siRNA treatment depends on many parameters such as specificity and efficacy of the siRNA sequence, kinetics of depletion, abundance of the protein and subsequent re-expression. Further complications ensue as a result of a large spread between protein dose requirements, i.e. incomplete knock-downs can in certain cases be sufficient to generate a detectable phenotype, and yet some proteins require a total removal to reveal a defect. There are also examples of multiple threshold levels for protein dose whereupon depending on the concentration the protein is involved in different mechanisms. Many of these variables are hard to control across a large screen since they are not only determined by experimental setup but innate biological factors. Therefore it is even more crucial to optimize factors which can be controlled to minimize fluctuation and misinterpretation. The optimization steps to control the experimental setting that were performed and those that needed more attention are discussed below.

3.4.1 Potential sources of error and improvements to the current data

There has been much technical advancement in the field of siRNA technology in recent years that could improve the experiments performed in this chapter. One such

example is the concentration of siRNA, which because of improvement has been lowered by a as much as ten fold in today's experiments. Simultaneous increase in awareness about off-target effects has expedited these advancements. Equally there are other areas for improvement in the execution of this screen that are not associated with technological advancements.

3.4.1.1 siRNA library

The choice of library was made on the premise that the WRN protein is required for genome stability and is involved in DNA repair and replication processes. The choice of a limited, custom-made library represents a cost-effective way to potentially generate a hit that is easily interpreted as compared to a large unspecific library that could results in hits which are hard to interpret and to put into a biological context. However, it is arguable that a very specific library will not extend the knowledge outside the already defined borders, and that a genome-wide screen would perhaps shed light on unknown functions of WRN protein. This would be especially appealing when trying to understand the systematic problems of WS, some of which do not seem to have an obvious connection to DNA metabolism. The small scale of the library in this project allowed it to be performed manually, but any larger library would require automated handling, which would involve a large set of new optimization experiments.

One of the essential parts to include in an siRNA library is controls, both positive and negative. Rad51 and PLK1 were chosen as positive controls for this experiment as they are essential for viability and accordingly survival was drastically reduced in their absence. The positive controls, siRNA Rad51 and siRNA PLK1, and the negative controls, siRNA NT and transfection agent DharmaFECT 1, were used on every 96-well plate in the screen to ensure that the transfection on those plates was successful. Reassuringly, controls on all plates worked each time, which meant that data from every plate was included in the statistical

analysis. In addition positive and negative controls provide a biologically relevant span to identify hits, which is described by the Z-factor.

Equally, an internal positive control, such as an already known gene that confers synthetic lethality in a WRN deficient background, is useful in verifying that the screen is returning valid results. Previously, a SL screen in *S. cerevisiae* with Sgs1 background was performed and yielded MMS4 as a result, of which Eme1 is the human homologue. MMS4 in a complex together with Mus81 is an endonuclease that preserves genetic integrity by resolving replication structures that arise in conjunction with damaged, stalled and collapsed replication forks [125]. Eme1 is included in the screen, however normalized viability after its knock-down in GM01604 cells is 71% and in AG03141 it is 78%. This difference is not statistically significant, possibly indicating that the transfection did not work. One caveat in this instance is that yeast produces the one RecQ helicase in yeast, Sgs1, while human cells have five. BLM helicase is most often equated to Sgs1 as they seem to prefer similar functions and substrates [141], and therefore there is a possibility that this SLI is not the same in mammalian cells. The knock-down of Mus81, the protein in the same complex as Eme1 was however shown to sensitise WS human cells to HU, as it was required for restart of forks, which in the absence of WRN had collapsed after stalling [142]. Viability after Mus81 knock-down in AG03141 was also unaffected as compared to GM01604 cells. In conclusion, whilst Eme1 was the only internal gene that could serve as a functionally relevant control and the absence of survival difference between the cell lines indicates that the screen is not returning relevant biological data, it is still possible that it was not the most relevant control. Alternatively the siRNA for Eme1 might not have been on-target, and a possible way to circumvent this problem would have been to evaluate the protein levels and ensure that they are truly reduced.

3.4.1.2 Transfection conditions

The first place to start when optimizing a screen is with the transfection conditions to assure that knock-down efficiency is increased while unspecific effects are minimised. One such is to work with as low concentrations of siRNA as possible. The RISC enzyme, alike many other enzymes, will lose its specificity with a high substrate to enzyme ratio and this potentiates off-target effects. Establishing what the lowest possible concentration of siRNA is can be accomplished by titration of siRNA, potentially on the siRNA species positive control, and correlating the phenotype to the degree of suppression. An example of this is if 1 nM supresses protein levels, but the phenotype is only observed at 10 nM, off-target effects must be suspected.

The siRNA library was applied at concentrations of a total of 50 nM, constituting of a pool of four different siRNA sequences at equal molarity. At the time the library was obtained the manufacturer's protocol suggested to use 100 nM for a 96-well transfection. 50 nM concentration had been tested in the lab previous to the start of the screen and shown to work for siRNA PLK1 and Rad51, therefore this concentration was used for the screen. For today's standard 50 nM is a very high concentration. The siRNA technology has developed rapidly in the past few years and several of the siRNA sequences from the library have been used in other parts of this thesis at concentrations as low as 1 nM, with excellent suppression. Therefore this is a very high dose and may potentiate off-target effects. However, titration of siRNA in the GM01604 and AG03141 should have been performed as described before starting the screen.

Another aspect of transfection that should be optimized is the transfection reagents. These are potentially toxic at too high doses and might affect cell viability, and therefore the readout. In general, all chemicals should be used at as low doses as possible to reduce undesirable effects. The dose of siRNA can be decreased if the transfection agent is efficient

and suitable for the specific cell type. Therefore, transfection agent should be tested for every cell type to find the one with the highest delivering ability at the lowest dose. For the screen 2,5 µl DharmaFECT1 per well was used as suggested by the manufacturer. Although it did not seem to cause toxicity, this step should have been optimized prior to start.

3.4.1.3 Validation

With the high probability of false positives the hits from the primary screen need to be validated before they can be explored any further. Established methods in the literature to validate screen results include redundancy and rescue [119]. Redundancy validation refers to demonstrating that the phenotype is obtained using multiple RNAi reagents that target different regions of the mRNA, but cause the same phenotype. This method will also uncover and separate target-specific effects from non-specific events. Deconvolution, which is a redundancy strategy, is one common way to validate the pooled siRNA, whereupon the individual siRNA oligos from the pooled sample are used at the same final concentration as the pool to investigate if they individually can reproduce the same phenotype. From previous studies hits have been classified as on-target if 50% of the individual sequences recapitulate the same phenotype. By this method, only Chk1 and Topo2α were considered true hits. A more extensive way of testing different siRNA species is to not only change sequences, but also the source, such as different commercial companies. The idea is that different companies will use their own algorithms, which alters the targeting sequence but also take into account attributes such as oligo length, 5´ sequence, and the way the oligos are handled such as the solution it is delivered in.

Rescue involves reversing the phenotype by re-expressing an siRNA resistant cDNA, thereby showing that it is the depletion of the specific protein that is responsible for the phenotype. Vectors are generated through site-directed mutagenesis to express cDNA which has a mismatch in the siRNA targeted sequence and can therefore not be targeted for

degradation. Alternatively, it is possible to construct siRNAs that target the UTR part of the mRNA, and then construct a rescue sequence that only contains the coding sequence, without the UTR. Although rescue experiments might be the ultimate way to show specificity of an effect, problems with exogenous expression might limit the possibility to use this method. It is also a very time consuming and laboratory intense experiment, however it would have been a useful method to employ.

Validating individual hits can be as time and cost consuming as performing the screen. Therefore persuing something that has some prior shown basis can help instil confidence that the effect is real. Prior to performing the screen there was one published report that showed that WRN and Topo2α coimmunopreciptate after treatment with ICRF-187 and the authors suggested that both proteins together are involved in activation of the G2 decatenation checkpoint . Therefore, I focused my efforts on Topo2α rather than Chk1, and pursued to test if it is an on-target hit. A good way to test if the phenotype is a result of protein suppression is to measure protein levels by Western blot. It is possible to confirm the knock-down by measuring levels of mRNA by quantitative real-time PCR, but numerous reports in the literature have shown suppression of the protein production without change in mRNA levels [93, 140]. The discovery that siRNAs, like miRNAs, can direct cleavage of mRNA when the sequences are extensively complementary, but only repress the expression of protein without cleaving mRNA when they are not offers a possible explanation to this phenomenon [114]. Protein levels after depletion with all four deconvoluted siRNA Topo2α sequences were therefore tested by Western blot in both cell lines to assess the protein repression. Unfortunately the blot with AG03141 samples was unsuccessful even after several attempts and it was therefore not possible to confirm if the reduced viability is truly a result of lowered Topo2α levels. An additional problem with the setup of this experiment is the transfection control. siRNA directed against WRN was used to asses if transfection was

successful, but since AG03141 cells are already negative for WRN this control was not able to clarify if the transfection was successful in these cells.

Next, the same four deconvoluted siRNA Topo2α sequences were used in a different WRN cell line, a derivative of U2OS cells with vectors expressing shWRN or shControl (a non-targeting sequence) sequence. Unfortunately none of the four siRNAs reduced viability in shWRN cells as compared to shControl cells. This could imply that the effect of Topo2α SLI with WRN is AG03141 cell specific, but there was a possibility that these cells were harbouring a mycoplasma infection at the time the experiment was performed, which could have resulted in altered behaviour and phenotype. As a result of this suspicion, all cell lines were continuously monitored for mycoplasma infections thereafter. The SLI could not be repeated in HTETOP cells either where Topo2α levels were repressed with doxycycline and WRN was targeted by two separate siRNA sequences. A Western blot is needed to complement this experiment and assure that WRN levels are reduced. This experiment was performed and did show depletion of WRN by both sequences, but it was not able to be displayed.

Although none of the experiments are a direct way of showing SLI observed between that Topo2α and WRN was due to an off-target result, and more experiments described in this discussion, should be performed to directly establish an off-target result, further investigation on this SLI was considered fruitless. However, interaction between Topo2 and Sgs1 helicases was established early on in yeast two-hybrid assays [137] and suggested that the two proteins interact during chromosomal segregation, which was further supported by the finding that WRN is required for decatenation in mammalian cells . There are also predictions that a RecQ helicase in concert with a Topoisomerase is required for replication termination [7, 93], and WRN and Topo2 are possible candidates in this pathway. At the time as the screen was performed it was not firmly established which topoisomerase is

required for replication propagation and therefore it was still highly possible that the SLI between WRN and Topo2α was true and that the two somehow interacted in the same pathway, either at some step during replication or chromosome segregation. Therefore instead of continuing our work to understand the SLI between WRN and Topo2α, research focus was directed towards investigating the possible role of Topo2α in replication, after which it could have been possible to revisit WRN results.

Chapter 4

Results

4 Role of Topo2 in replication

4.1 Introduction

Prompted by the results from previous chapter and biochemical evidence that Topo2 is capable of resolving substrates in front of the replication fork, I sought to investigate the role of Topo2 in replication.

The unwinding by the replicative helicases results in localized topological stress ahead of the replication fork, so called positive supercoiling. The supercoils can be transferred behind the fork, to release some of the torsional stress in the pre-replicated DNA, creating precatenanes. Topo2 is the only protein that can resolve these structures, and it might represent a plausible mechanism for its involvement in replication elongation [143].

Alternatively, there are several pieces of evidence that Topo2α can act ahead of the replication fork. First, yeast Topo2 is found at regions undergoing replication and yeast cells are able to replicate in absence of Topo1, but not when both Topo1 and Topo2 are attenuated simultaneously [44, 144, 145]. Second, *in vitro*, human Topo2α relaxes positive supercoils 10-fold faster than negative supercoils [146]. Additionally, models for anticancer drug action assume Topo2α ahead of the replication fork [147]. One such example is etoposide, where the replication fork is assumed to collide with the covalent complex and collapse the forks [17].

4.1.1 DNA replication

In each cell cycle the cell has to duplicate all of its DNA content in an orchestrated and tightly regulated manner. Eukaryotic cells initiate replication at multiple origins throughout the chromosome. Once initiated, the replication process is a bidirectional event that proceeds in a 5´-3´direction. The replication fork established at the origins has an asymmetrical

structure with the continuously synthesized leading strand and a lagging strand that is fragmented. The synchronization and coordination of initiation, elongation and also segregation of the daughter strands is achieved through complex interplay of proteins involved in replication machinery and cell cycle control. Mistakes in any of the steps can lead to loss or duplication of the genetic material and can be detrimental to the cell and the organism.

The initiation of DNA replication starts already in G1 phase when the origins are licensed for a single round of replication. In addition, origins are characterized by spatial and temporal regulation. Replication seems to happen in clustered "factories" in the cell and there is a timing difference between origins, as some fire early and others later. The mechanism that regulates timing of firing seems to depend on cyclin dependent kinases (Cdk) in the S-phase and chromatin structures [148].

After licensing, the pre-replication complex (pre-RC) is loaded onto the origins. This involves loading of the origin replication complex (ORC), Cdt1 and Cdc6 proteins to further recruit minichromosome maintenance protein (MCM) 2-7 to the site. At G1/S transition MCM 10, Cdc45 and some additional proteins are recruited. The only proteins from the initial conglomeration that travel with the replication machinery throughout elongation are Cdt1, Cdc45, and MCM 2-7, which are the replicative helicases [149].

Cdc45 is an essential gene in yeast and it associates not only with the MCM complex, but also with RPA and the replicative polymerases. Thus, it is implicated in both initiation and elongation. Cdc45 association with the replication machinery is regulated by checkpoint proteins such as Cdks [149, 150]. Following Cdc45 loading, unwinding of DNA starts and RPA is recruited, followed by the Polα addition [151]. Subsequently, Polε, the leading strand polymerase, is recruited, and this is also dependent on Cdc45, as well as some other components of the pre-RC. Finally, loading of Polδ by proliferating cell nuclear antigen

(PCNA) occurs. PCNA seems to be loaded on by RFC at the end of primer synthesis by Polα, and this loading displaces the primase polymerase and engages Polδ, the lagging strand DNA polymerase.

The three polymerases responsible for DNA propagation all belong to the B class of DNA polymerases. The main difference between the B group and the A group, where the *E. coli* Klenow fragment is the prototype, is the structural orientation of the exonuclease domain. Polε is a highly processive polymerase and PCNA interaction does not significantly increase its incorporation rate. Polα, the first polymerase recruited to the origin, incorporates a primase and polymerase activity in the four of its subunits. The primase inserts an RNA primer that is 8-12 nucleotides in eukaryotes and the polymerase unit extends this primer by approximately 20 nucleotides from which the lagging strand synthesis is continued by Polδ. The switch between the two polymerases seems to be dependent on the PCNA-RFC complex that loads PCNA onto the DNA strand. PCNA that has encircled DNA interacts with Polδ and promotes Okazaki fragment synthesis and maturation. There is evidence that the PCNA-Polδ complex already recruits flap endonuclease-1 at the synthesis step and travels together until it reaches the next RNA primer. Polα has not retained the proofreading exonuclease ability and as a result, the short DNA stretch, which it synthesizes after the RNA primer, is also removed by Polδ to insure that no misincorporated bases are retained. The 5´ flap is coated with RPA and cleaved by FEN-1. The nick is sealed by DNA ligase I. Studies in yeast and *X. laevis* show that in the absence of Polδ, lagging strand synthesis is defective as well as telomere maintenance on the lagging strand. In addition, where Polδ interacts tightly with FEN-1 to generate ligatable nicks, Polε completely lacks this ability [149].

4.2 Aim

The first aim was to determine if Topo2α is involved in replication elongation. Additionally, it was to investigate if Topo2β is able to compensate for loss of Topo2α, or alternatively, play a role in replication itself. The second aim was to investigate if depletion of Topo2α or drug inhibition exhibit different effects on DNA replication.

4.3 Topo2 knock-down on replication progression

To investigate if Topo2α and Topoβ underpin DNA replication, the first step was to determine the overall kinetics of the S phase. In the instance of DNA replication being disrupted, it would be expected for cells to progress slower and accumulate in the S phase. To determine if this was the case cell cycle analysis was performed by FACS. FACS analysis measures bulk DNA synthesis and the progression rate of the cell population through S phase. However, disruption of DNA replication can be due to any combination of parameters which include reduced fork rates, occurrence of stalled forks, and altered initiation of origin firing. These factors can be masked by taking the average of a cell population. Additionally, they can work in compensatory ways in order for the cell to complete the S phase in a timely manner. To make a more detailed analysis of the different parameters of DNA replication, cells were also prepared for a single DNA molecule analysis by fibre labelling technique, described in more detail below.

4.3.1 Measurement of Topo2 protein levels

To study the role of Topo2α and Topoβ in replication elongation two different immortalised human cancer cell lines were utilised. The first one is the well-characterized osteosarcoma U2OS cell line, which is p53 proficient [152]. The other cell line, HTETOP, is a derivative of the human fibrosarcoma HT1080 cell line, also with a functional p53 [52]. It was constructed by Carpenter and Porter to express Topo2α cDNA from an exogenous

plasmid with a tTA-responsive promoter, whilst the endogenous *Topo2α* genes were disrupted through gene targeting [52].

To reduce the levels of Topo2α and Topo2β protein in U2OS cells, 10 nm siRNA targeting the respective protein was used. Transfection conditions were optimized in the laboratory previous to the start of this thesis. Cells were transfected as described in Material and Methods and protein levels were determined by Western blotting 72 hours post transfection. Equal amounts of protein were loaded on the gel and α-tubulin served as the loading control. To avoid non-specific results due to off-target effects of siRNA, two different siRNA oligos directed towards Topo2α were assessed for future experimental use. Unless otherwise stated, siRNA #1 was used throughout this thesis.

A Western blot analysis confirmed that the knock-down for all siRNA oligos was efficient and isoform specific (Figure 4.1 A).

To remove Topo2α in HTETOP cells 1 μg/ml doxycycline was added to the media and the protein levels were assessed by Western blot after 72 hours of incubation (Figure 4.1B and C). As an additional control, Topo2α levels were also reduced with siRNA knock-down in separate samples. Addition of doxycycline or Topo2α siRNA did not affect levels of Topo2β, but reduced levels of Topo2α. Meanwhile, addition of doxycycline in conjunction with Topo2β siRNA successfully reduced the levels of both Topo2 isoforms.

In addition to determining the protein levels, removal of Topo2α in HTETOP by doxycycline was assessed phenotypically. As previously published for the HTETOP cell line, addition of doxycycline inhibits the cell expansion [52]. This was confirmed by counting the cells each day and determining the amount of doubling passages (Figure 4.1 D). Cells treated with DMSO commenced to increase in number after 2 to 3 days and at day 4 had started to double approximately every 24 hours. Addition of doxycycline prevented expansion, and after 4 days the number of cells was close to the amount seeded. The reason

for lack of increased amount of cells could be explained by cell cycle arrest in G2/M (see Chapter 5).

With these results, there were two established model systems available to study the effect of Topo2α and Topo2β depletion on replication elongation.

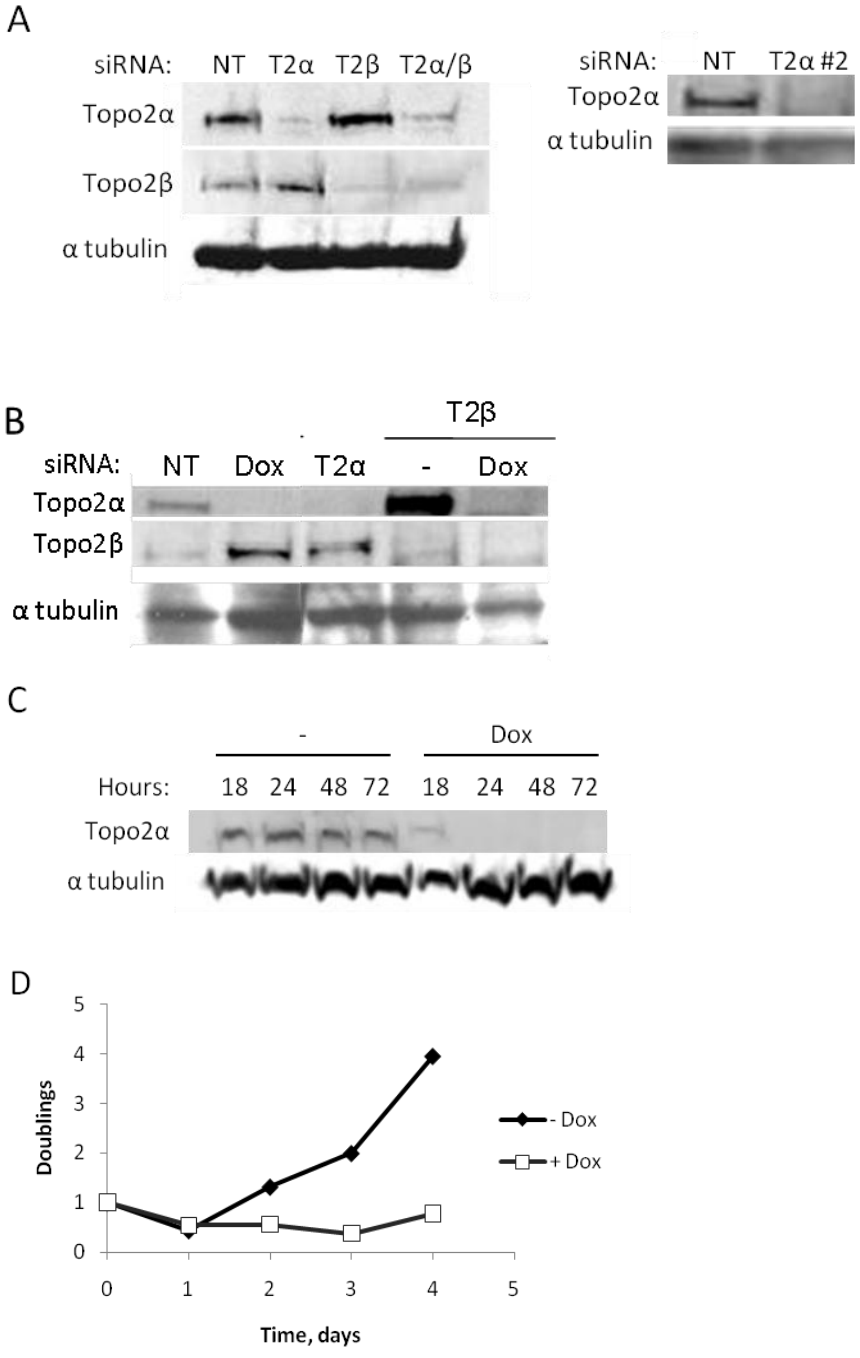

Figure 4.1 | siRNA and doxycycline knock-down Topo2α and Topo2β in U2OS and HTETOP cells

A. Western blot showing knock-down of Topo2α, Topo2β or both with 10 nM of siRNA in U2OS cells. Whole cell lysate was prepared 72 hours post transfection. Right panel shows the knock-down efficiency of a second Topo2α siRNA sequence, also 72 hours post transfection.

B. Western blot showing knock-down of Topo2α and Topo2β and in HTETOP cells. Topo2α levels were reduced with either 1 µg/ml doxycycline or 10 nM siRNA. Topo2β was removed with 10 nM siRNA. Protein levels were measured after 72 hours.

C. Western blot of time dependent Topo2α knock-down after addition of 1 µg/ml doxycycline in HTETOP cells.

D. Amount of cell doubling after addition of 1 µg/ml doxycycline in HTETOP cells. Cells were trypsinized and counted each day.

4.3.2 Cell cycle analysis in absence of Topo2α

To identify the effects of Topo2α down-regulation on the overall S phase progression, cells depleted of Topo2α were pulse-labelled with 5-Iodo-2'-deoxyuridine (IdU), a thymidine analogue that incorporates into DNA of dividing cells during replication. Asynchronous populations were used for this experiment to avoid possible artefacts caused by synchronizing agents. HTETOP cells were treated with doxycycline and U2OS cells were depleted of Topo2α with one siRNA sequence. After 72 hours of depletion IdU was incorporated for 20 min (Figure 4.2 A) and cells were released into the media to be harvested between 0 and 9 hours. After fixation, samples were analysed by FACS and the 2D analysis of IdU incorporation and propidium iodide (PI) revealed proportion of cells in S phase and the kinetics of replicating cells throughout the cell cycle (Figure 4.2).

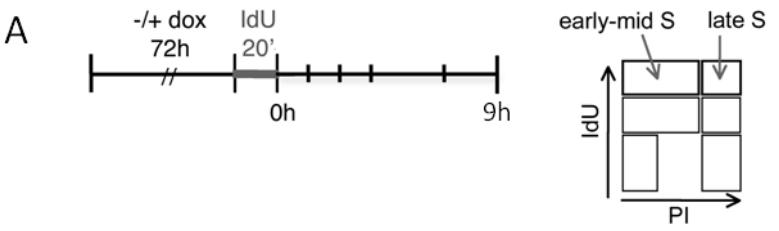
A
-/+ dox
72h
IdU
20'
0h
9h
early-mid S
late S
IdU
PI

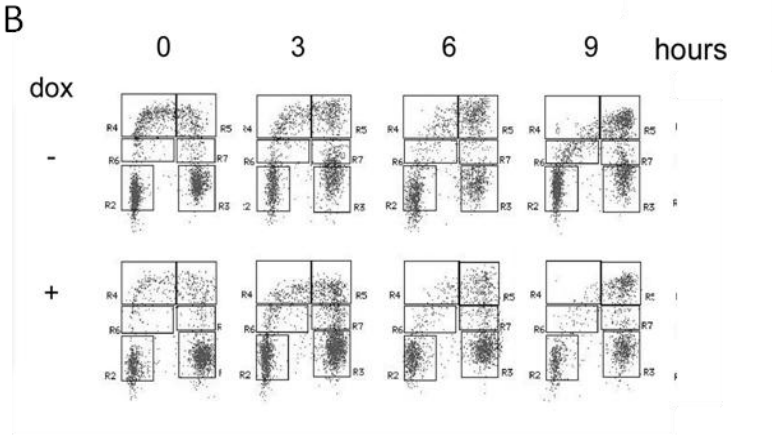
B
0
3
6
9
hours
dox
-
+

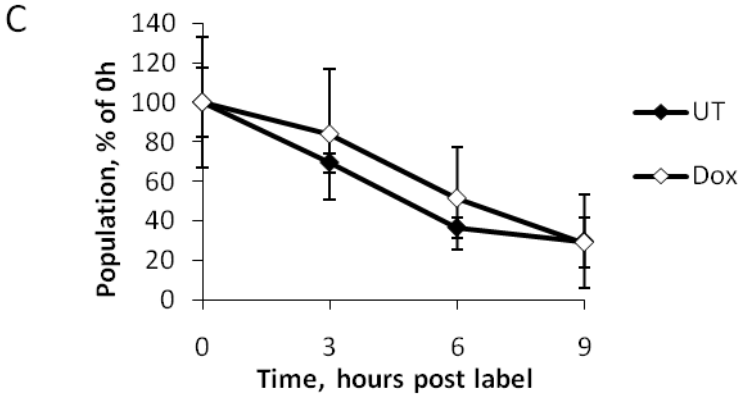
C
Population, % of 0h
140
120
100
80
60
40
20
0
0
3
6
9
Time, hours post label
UT
Dox

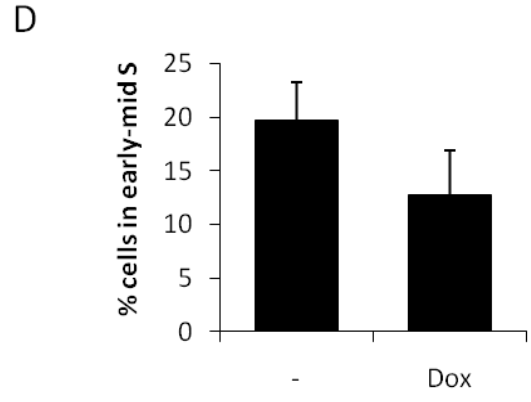
D
% cells in early-mid S
25
20
15
10
5
0
-
Dox

Figure 4.2 | S phase progression is unaffected by the absence of Topo2α in HTETOP cells

A. Experimental design. IdU was added to the last 20 minutes of the 72 hours doxycycline treatment. Cells were washed and released into fresh media to be harvested at indicated time points.

B. Representative FACS plots of cell samples collected at 0, 3, 6, and 9 hours after 72 hours treatment with 1 μg/ml doxycycline or DMSO. Cells were fixated with ethanol and processed and stained for DNA content (PI) and IdU incorporation. The proportion of cells in early-mid S phase was calculated by gating, as illustrated.

C. Quantification of data represented in B. Data are plotted as percentage of time point 0 hours. Data bars are the means of at least three independent experiments. Error bars represent standard deviation from the mean.

D. Proportion of cells in early-mid S phase at 0 hours quantified from B. Data bars are the means of at least three independent experiments. Error bars represent standard deviation from the mean.

Figure 4.2 B shows a series of representative images of HTETOP cells. After 72 hours of depletion, at 0 hours, there is a slight reduction of total amount of cells in the early and mid S phase in samples depleted of Topo2α (Figure 4.2 D) which is likely explained by Topo2α depletion arresting some cells in the G2/M phase of the cell cycle. To analyse and compare the progression rate through the early and mid S phase, the percentage of cells for each time point was related to 0 hours. Samples treated with doxycycline advanced through the early and mid S phase at the same rate as the untreated samples (Figure 4.2). This would suggest that Topo2α does not contribute to overall S phase progression in HTETOP cells.

In agreement with these observations, U2OS cells treated with Topo2α siRNA (Figure 4.3 A) also displayed a reduced proportion of cells in early and mid S phase compared to samples treated with siRNA NT (Figure 4.3 B). Meanwhile, the kinetics of S phase were left unaltered by the change in Topo2α status.

As a positive control for the S phase progression, U2OS cells were released into media with 2 mM HU, an agent that stalls replication forks by depleting the dNTP pool. This eventually results in checkpoint activation and accumulation of cells in S phase [153].

During the time course between 0 and 9 hours, which was enough for untreated cells to transverse early and mid S phase, cells treated with HU were accumulating in the early S phase, as shown in Figure 4.4 A and B.

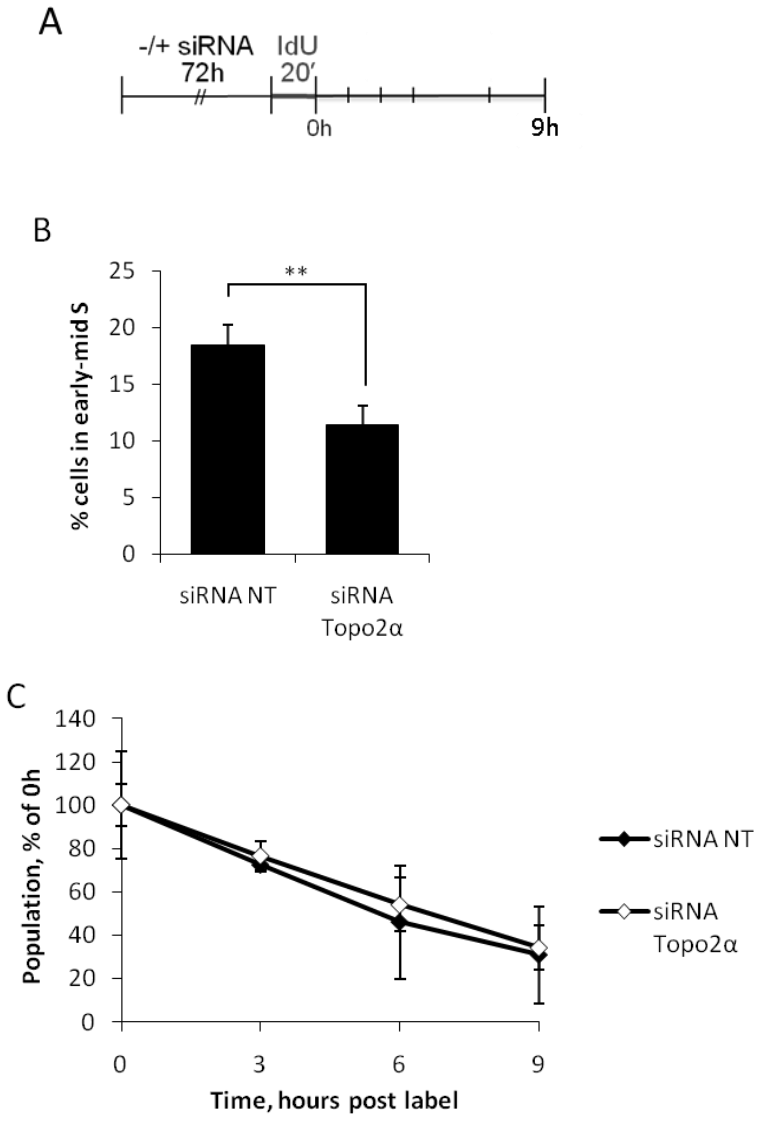

Figure 4.3 | S phase progression is unaffected by the absence of Topo2α in U2OS cells

A. Experimental design. IdU was added to the final 20 minutes of the 72 hours siRNA Topo2α treatment. Cells were washed and released into fresh media to be harvested at indicated time points.

B. Proportion of cells in early-mid S phase at 0 hours quantified as in Figure 4.2 B. Data bars are the means of at least three independent experiments. Error bars represent standard deviation from the mean. Statistical significance (p-value < 0.01) in Student's *t*-test is indicated by two stars.

C. Cell progression though early-mid S phase after release from IdU. Data was quantified as previously described in Figure 4.2 and is plotted as percentage of time point 0 hours. Data bars are the means of at least three independent experiments. Error bars represent standard deviation from the mean.

Both U2OS and HTETOP cells are p53 positive, but because they are derived from a tumour source it renders them susceptible to genetic instability. To establish that the results are not artefacts of their genetic background, the effect of Topo2α depletion was investigated in cells derived from normal tissue. The proportion of cells in S phase after siRNA Topo2α treatment in was measured in MRC5 and GM01604 cells to investigate if a S phase cell cycle arrest was induced. MRC5 cells are primary cells isolated from lung tissue (passage 17). GM01604 are SV40 immortalised cells, also derived from normal lung tissue. Both cell lines had about 13% of cells in S phase in siRNA NT treated samples, which was left unaltered by Topo2α depletion (Figure 4.5). ICRF-193 was used as a positive control, as it blocks cells in G2/M, hence depleting the cell population of S phase cells.

In conclusion, these results suggest that Topo2α is dispensable for timely progression through S phase independent of cell source.

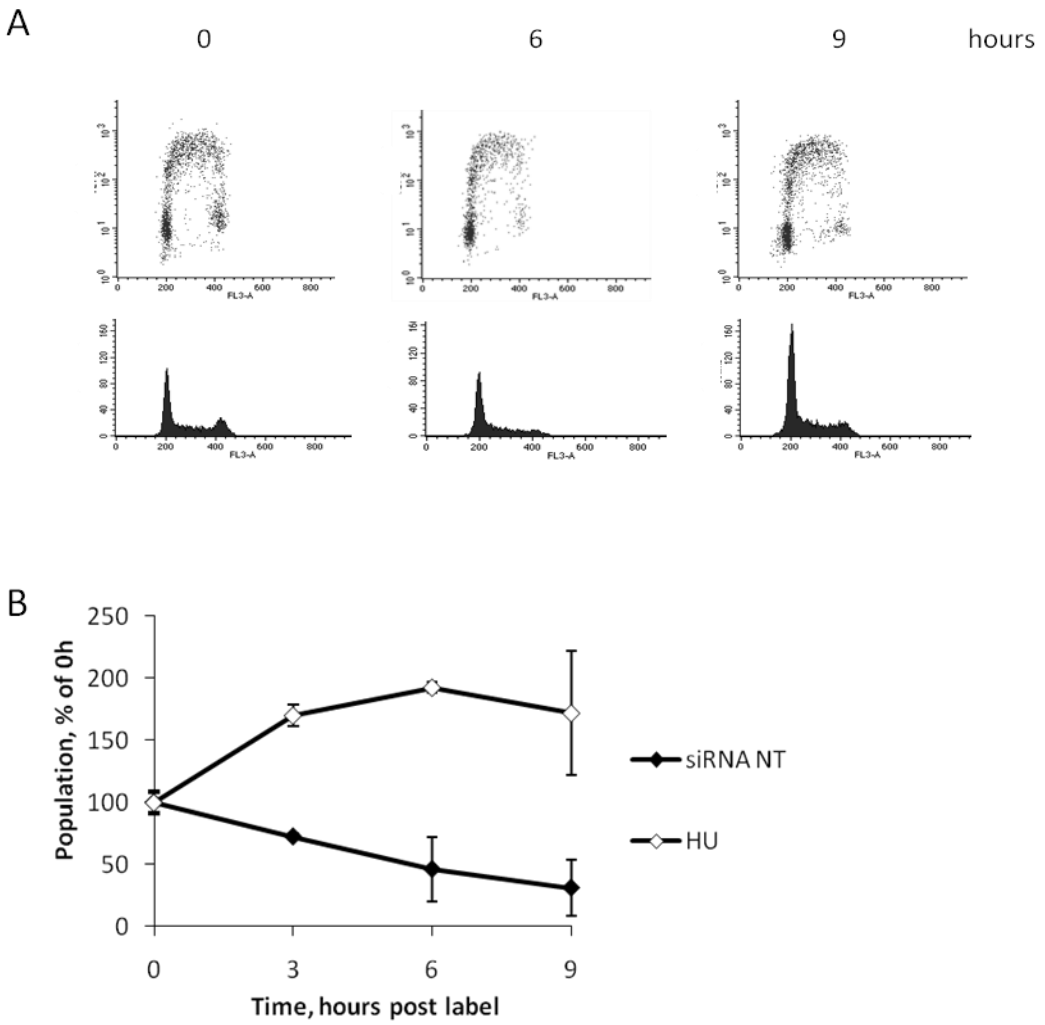

Figure 4.4 | U2OS cells accumulate in S phase after HU treatment

A. Representative FACS plots. Cells were labelled with IdU for 20 minutes and then released in medium containing 2 mM HU . Samples were collected after 0, 6, and 9 hours of HU treatment. Upper panels represents PI and IdU incorporation. Lower panels are complimentary DNA content plots.

B. Quantification of cells in early-mid S phase from data represented in upper panel in A. Data is plotted as percentage of time point 0 hours. Data points are the means of at least three independent experiments. Error bars represent standard deviation from the mean.

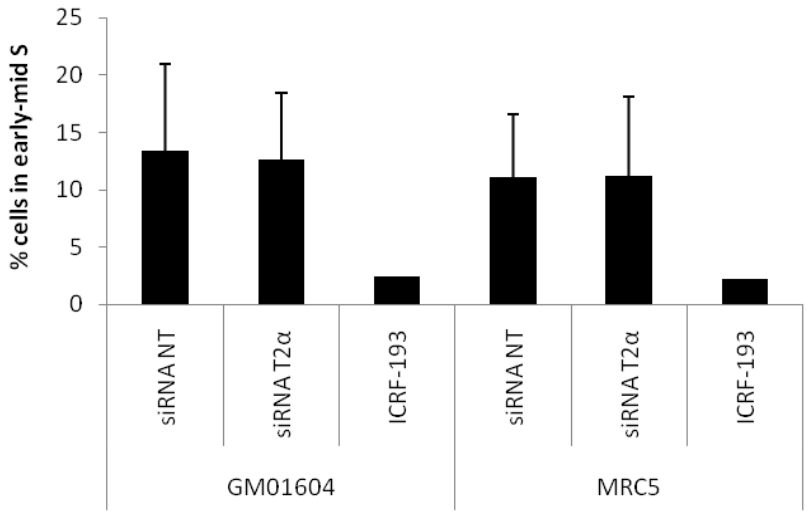

Figure 4.5 | Proportion of cells in early-mid S phase is unaffected by absence of Topo2α in GM01604 and MRC5 cells

Both cell lines were transfected with 10 nM siRNA Topo2α for 72 hours. IdU was incorporated during the last 20 minutes of treatment. ICRF-193 samples were treated with 5 µM ICRF-193 for duration of 9 hours, of which last 20 minutes included IdU. Cells were harvested, processed for FACS analysis and the results were quantified as previously described in Figure 4.2. Data is an average of two independent experiments. Error bars represent standard deviation from the mean.

4.3.3 DNA fibre labelling technique

The DNA fibre labelling technique allows for assessment of all the various parameters that determine the overall DNA synthesis rate. It provides detection and evaluation of individual replication forks and measurement of small effects that otherwise would have been elusive. It measures DNA synthesis across the genome, independent of chromatin structure and sequence.

Briefly, halogenated nucleotides are incorporated into DNA, after which cells are lysed on a glass cover slide and the DNA is spread by letting the sample run down. The

DNA is immunolabelled to detect the halogenated nucleotides and visualised using a confocal microscope.

This technique allows for quantification of several parameters. The rate of the replication fork progression is proportional to the length of the labelled track. The tracks are measured in micrometres and, with a known labelling time, converted to rate of nucleotide incorporation. The DNA extension factor was determined to be 2.59 kb/µm by Jackson and Pombo [154]. They determined it by measuring BrdU-labelled adenovirus tracks of known base pair amount and the extension factor is now used for all metazoan cells.

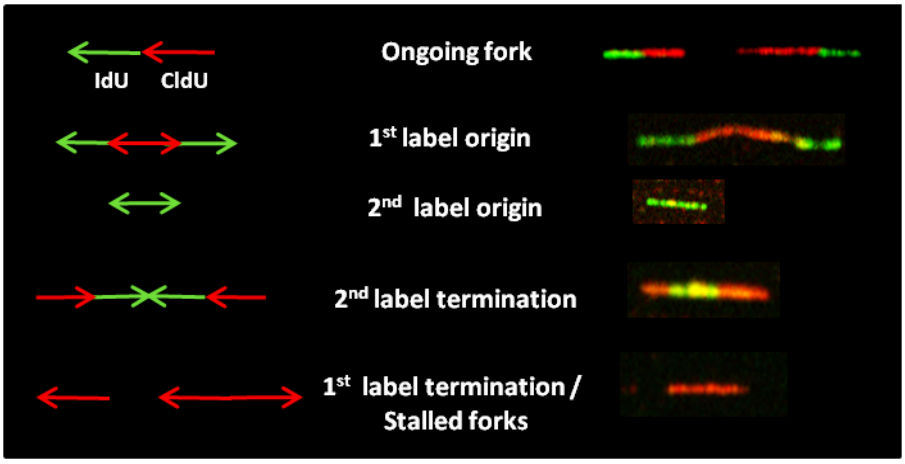

Figure 4.6 | DNA fibre labelling

Example of DNA fibres. Schematic representation on the left. Individual DNA molecules are labelled by incubating cells with 25 µM CldU and 250 µM IdU for 20 minutes respectively. The dual incorporation allows for direction of fork progression to be established, such that ongoing forks, newly fired origins, converging forks (terminations) and stalled forks can be identified.

By sequential labelling, firstly with 5-Chloro-2'-deoxyuridine (CldU) followed by IdU, it is possible to determine the directionality of the replication fork. Additionally, dual-

labelling allows for determination of DNA structures, such as newly fired origins, terminations, and stalled forks (Figure 4.6 [155]).

For the purpose of the project in this chapter, the fibre technique was predominantly used to determine the replication fork rate. Both CldU and IdU tracks were quantified to determine the rate, although no difference between the two labels was expected as they were incorporated during equivalent conditions. If removal of a protein or treatment effected replication in any way, the fibre length in both labels would be affected.

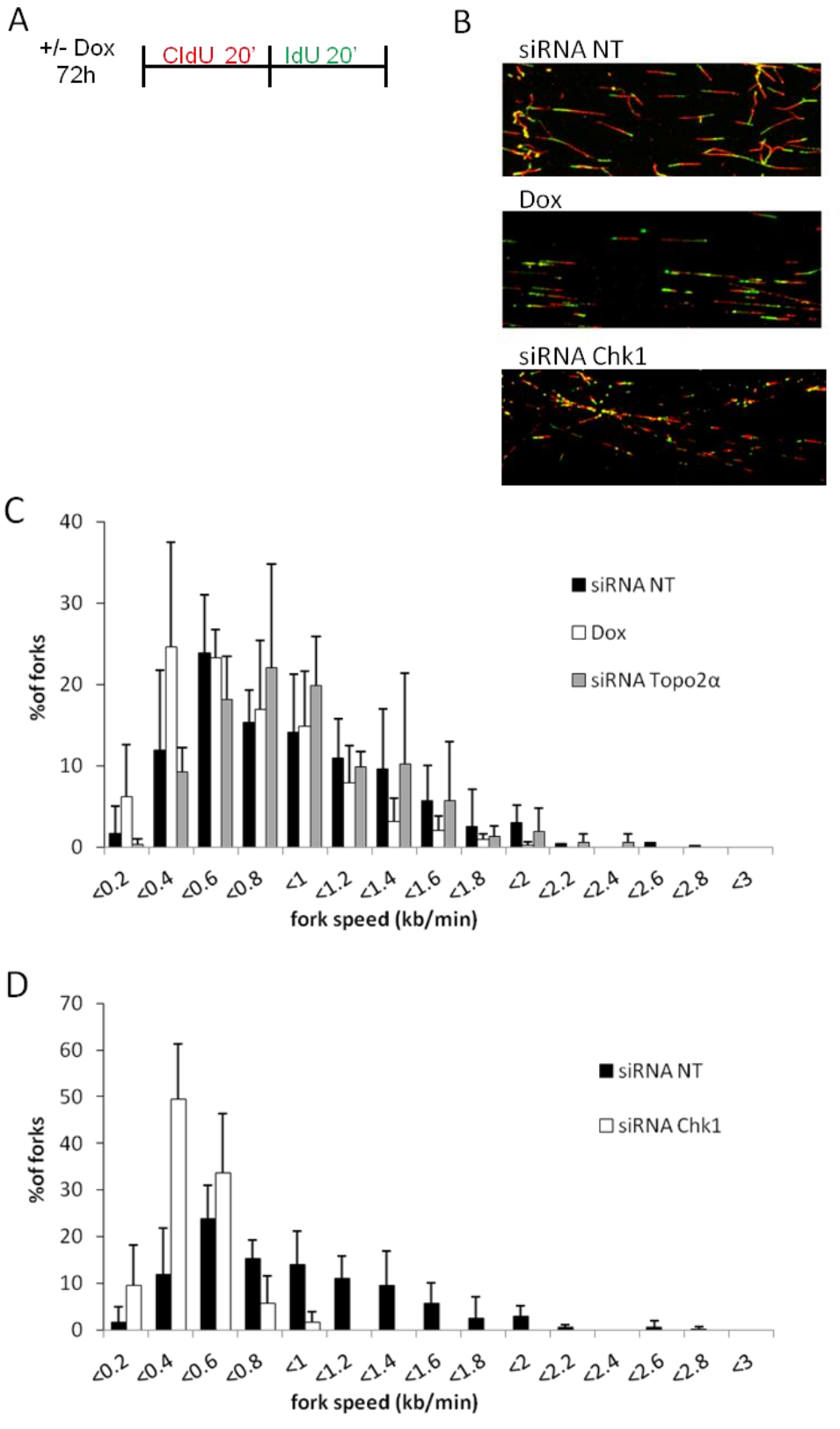
A
+/- Dox
72h
CldU 20'
IdU 20'
B
siRNA NT
Dox
siRNA Chk1
C
%of forks
fork speed (kb/min)
siRNA NT
Dox
siRNA Topo2α
D
%of forks
fork speed (kb/min)
siRNA NT
siRNA Chk1

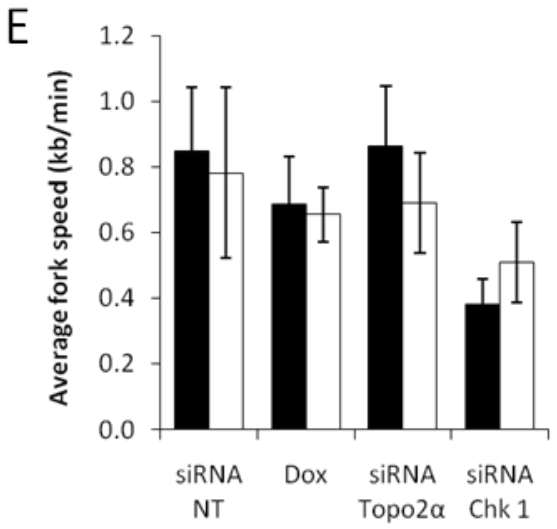

Figure 4.7 | Replication fork rate is unaffected by absence of Topo2α in HTETOP cells

A. Experimental design. Cells were treated as indicated for 72 hours after which they were pulse-labelled with 25 µM CldU (red) and 250 µM IdU (green) for 20 minutes respectively. They were then processed for DNA fibre spreads.

B. Representative images of DNA fibre tracks from samples treated 72 hours with 10 nM siRNA NT or 1 µg/ml doxycycline and 48 hours with 10 nM siRNA Chk1.

C. CldU track distribution of replication fork rates in samples treated 72 hours with 10 nM siRNA NT, siRNA and 1 µg/ml doxycycline or 10 nM siRNA Topo2α. Data bars are the means of at least three independent experiments. Error bars represent standard deviation from the mean.

D. CldU track distribution of replication fork rates in samples treated with 10 nM siRNA NT or siRNA Chk1. Samples were harvested 48 hours post transfection and processed for DNA fibre analysis.

E. Quantification of overall fork speed average. Black bars represent CldU tracks and white bars IdU tracks. Data bars are the means of at least three independent experiments. Error bars represent standard deviation from the mean.

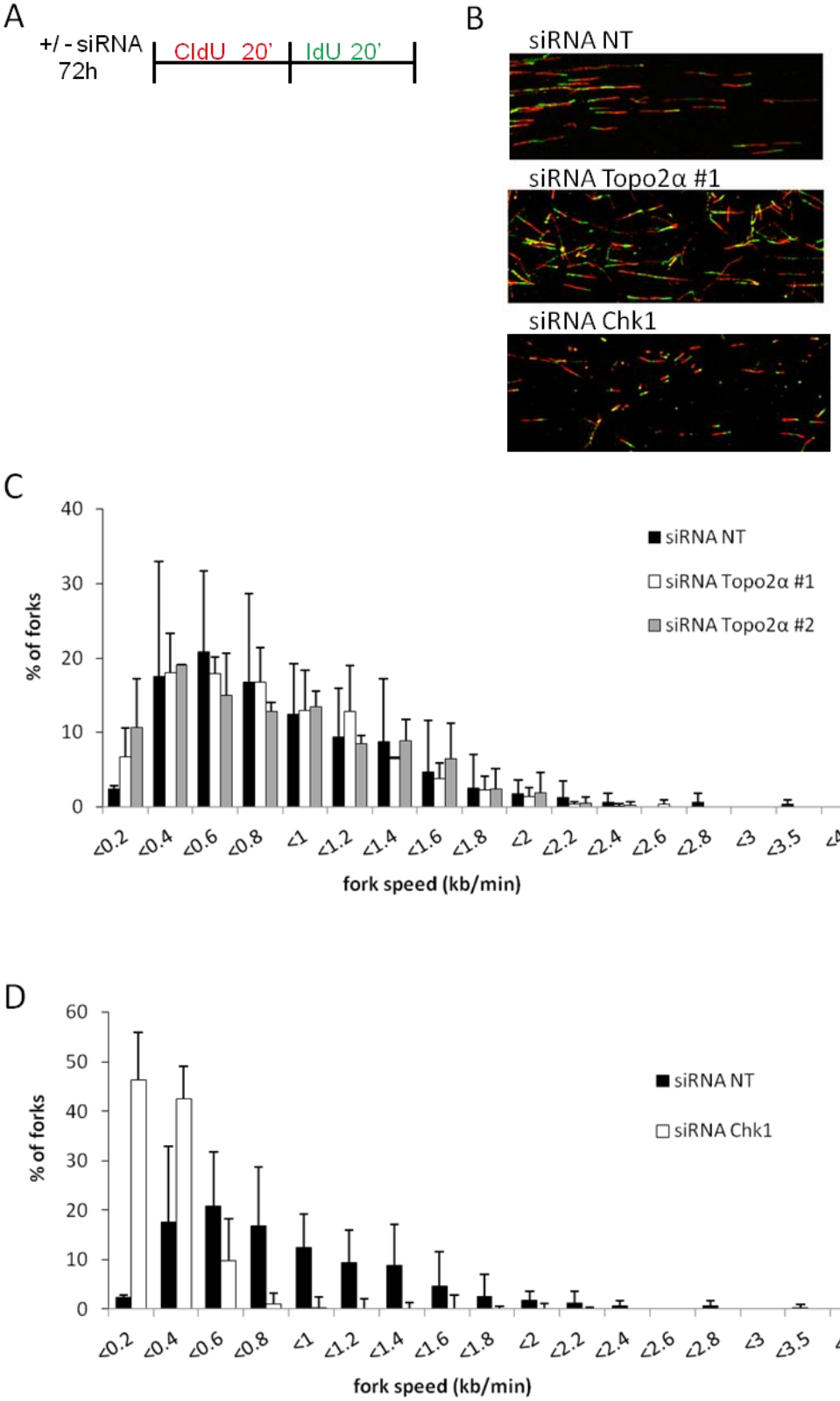
A
+/- siRNA
72h
CldU 20'
IdU 20'
B
siRNA NT
siRNA Topo2α #1
siRNA Chk1
C
% of forks
40
30
20
10
0
siRNA NT
siRNA Topo2α #1
siRNA Topo2α #2
<0.2
<0.4
<0.6
<0.8
<1
<1.2
<1.4
<1.6
<1.8
<2
<2.2
<2.4
<2.6
<2.8
<3
<3.5
<4
fork speed (kb/min)
D
% of forks
60
50
40
30
20
10
0
siRNA NT
siRNA Chk1
<0.2
<0.4
<0.6
<0.8
<1
<1.2
<1.4
<1.6
<1.8
<2
<2.2
<2.4
<2.6
<2.8
<3
<3.5
<4
fork speed (kb/min)

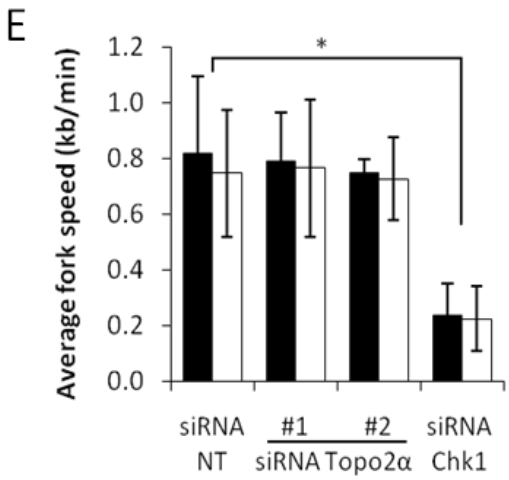

Figure 4.8 | Replication fork rate is unaffected by absence of Topo2α in U2OS cells

A. Experimental design. Cells were treated as indicated for 72 hours after which they were pulse-labelled with 25 µM CldU (red) and 250 µM IdU (green) for 20 minutes respectively. They were then processed for DNA fibre spreads.

B. Representative images of DNA fibre tracks from samples treated 72 hours with 10 nM siRNA NT or siRNA Topo2α #1 and for 48 hours with siRNA Chk1.

C. CldU track distribution of replication fork rates in samples treated for 72 hours with 10 nM siRNA NT or two different siRNA Topo2α sequences. Data bars are the means of at least three independent experiments. Error bars represent standard deviation from the mean.

D. CldU track distribution of replication fork rates in samples treated with 10 nM siRNA NT or siRNA Chk1. Samples were harvested 48 hours post transfection and processed for DNA fibre analysis.

E. Quantification of overall fork speed average. Black bars represent CldU tracks and white bars IdU tracks. Data bars are the means of at least three independent experiments. Error bars represent standard deviation from the mean. Statistical significance (p-value < 0.05) in Student's *t*-test is indicated by one star.

4.3.4 Analysis of DNA replication elongation in Topo2α depleted cells using the DNA fibre assay

In order to assess whether Topo2α is required to maintain fork progression during an unperturbed S phase, untreated cells and cells depleted of Topo2α were labelled sequentially with 25 μM CldU and 250 μM IdU for 20 minutes respectively (Figure 4.7 A and Figure 4.8A). An excess of IdU was used to minimize any incorporation of CldU that might be left inside the cells. In U2OS cells Topo2α was depleted with two different siRNA sequences in separate samples. HTETOP cells were depleted by doxycycline or by transfecting a single Topo2α siRNA sequence. All samples were assayed 72 hours post transfection or addition of doxycycline. Cells were harvested and processed for DNA fibre analysis as described in Material and Methods. Depletion of Chk1 by siRNA served as a positive control. Chk1 has previously been shown to maintain normal replication rate and in its absence, global extension rates were reduced up to half of those of undepleted samples [156]. The used siRNA Chk1 sequence was shown to work efficiently, but a Western blot analysis in these cells is required to complete this experiment.

The fibres were quantified manually and the rate of nucleotide incorporation was calculated using the extension factor of 2.59 kb / μm [154]. The frequency distribution of fork rates was plotted and average speed was calculated.

Figure 4.7 B and Figure 4.8 B show representative images of DNA fibres in both cell lines. Absence of Topo2α did not have an effect on fork rate progression in either of the cell lines (Figure 4.7 C and 4.8 C). Depletion of Topo2α with either siRNA sequence in U2OS cells rendered the average fork speed the same as with non-targeting siRNA (NT) (Figure 4.8 E), between 0.7 kb/min and 0.8 kb/min.

As in the case of U2OS cells, HTETOP cells depleted of Topo2α with doxycycline or siRNA Topo2α did not show affected fork rates as compared to non-treated HTETOP cells.

Fork speeds progressed at an average speed between 0.7 kb/min and 0.9 kb/min, independent of Topo2α status (Figure 4.7 E).

As expected, Chk1 depletion reduced the fork rates, as can be seen by the notable left shift in the distribution graph (Figure 4.7 D and 4.8 D). The average fork speed in Chk1 depleted cells was reduced to 0.2 kb/min in U2OS cells and 0.4 kb/min for CldU and 0.5 kb/min for IdU in HTETOP cells.

As expected, the average rate for CldU and IdU label did not differ. This is important to note as it indicates that the labels themselves did not alter the rate of replication, even with the 10-fold increase in IdU concentration.

4.3.5 Analysis of DNA replication and S phase kinetics in Topo2β depleted cells

Topo2β is mechanistically highly identical to Topo2α and prefers similar substrates [157, 158]. It is also able to compliment the loss of the single Topo2 in yeast. Therefore it was interesting to investigate if there was a replication phenotype associated with its knockdown. To understand if Topo2β has a role in propagating DNA synthesis, similar cell cycle and DNA fibre analyses as for elucidation of the role of Topo2α were performed. Both U2OS and HTETOP cells were depleted of Topo2β by siRNA treatment, and samples were analysed 72 hours post transfection (Figure 4.1 A and B).

Analysis of DNA fibres revealed an average fork speed of around 0.7 kb/min for both CldU and IdU tracks in Topo2β depleted HTETOP cells (Figure 4.9 A and B). This was not significantly different from cells treated with siRNA NT. In U2OS cells Topo2β depletion lowered the average fork speed from 0.8 kb/min to 0.6 kb/min for CldU tracks and from 0.7 kb/min to 0.5 kb/min for IdU tracks (Figure 4.10 B). However, this change was not statistically significant, suggesting Topo2β is not involved in maintaining the fork speed in either cell line.

To confirm that there was no change in the overall DNA replication kinetics and S phase progression, IdU pulse-labelled U2OS cells treated with siRNA Topo2β were harvested between 0 and 9 hours for a cell cycle analysis by FACS. At 0 hours, 72 hours after transfection, there was a slight accumulation of cells in S phase from 18% in siRNA NT samples to 25% in siRNA Topo2β (Figure 4.10 C). Nevertheless, the cells that had taken up IdU progressed through S phase at the same rate regardless of Topo2β status (Figure 4.9 D). This data indicates that Topo2β is not needed to maintain proper DNA replication and S phase progression.

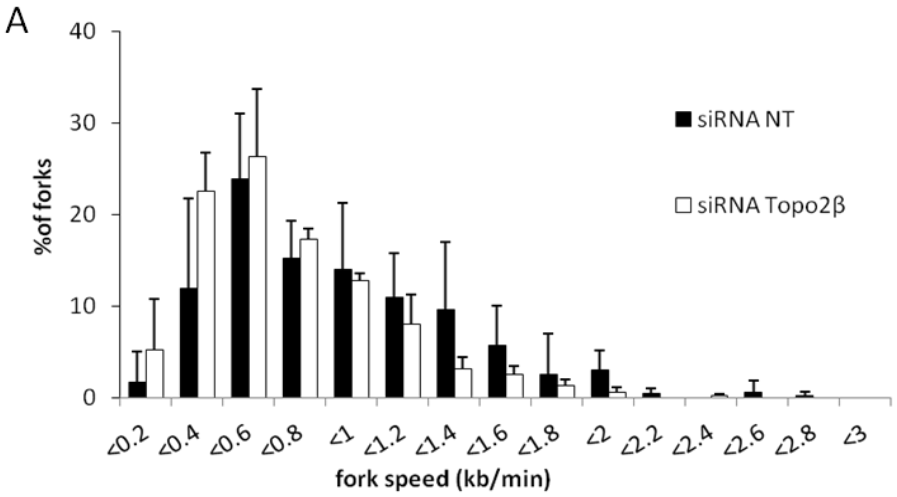

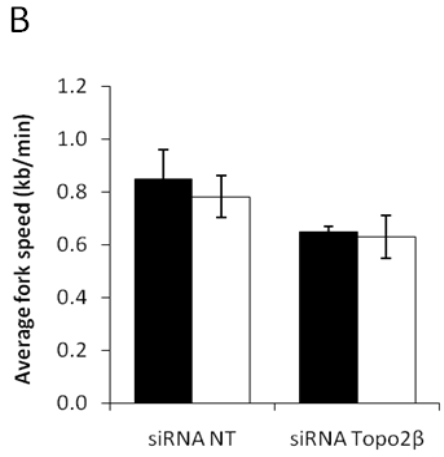

Figure 4.9 | Replication fork rate is unaffected by absence of Topo2β in HTETOP cells

A. CldU track distribution of replication fork rates in samples treated with 10 nM siRNA NT or siRNA Topo2β. Samples were harvested 72 hours post transfection and processed for DNA fibre analysis.

B. Quantification of overall fork speed average. Black bars represent CldU tracks and white bars IdU tracks. Data bars are the means of at least three independent experiments. Error bars represent standard deviation from the mean.

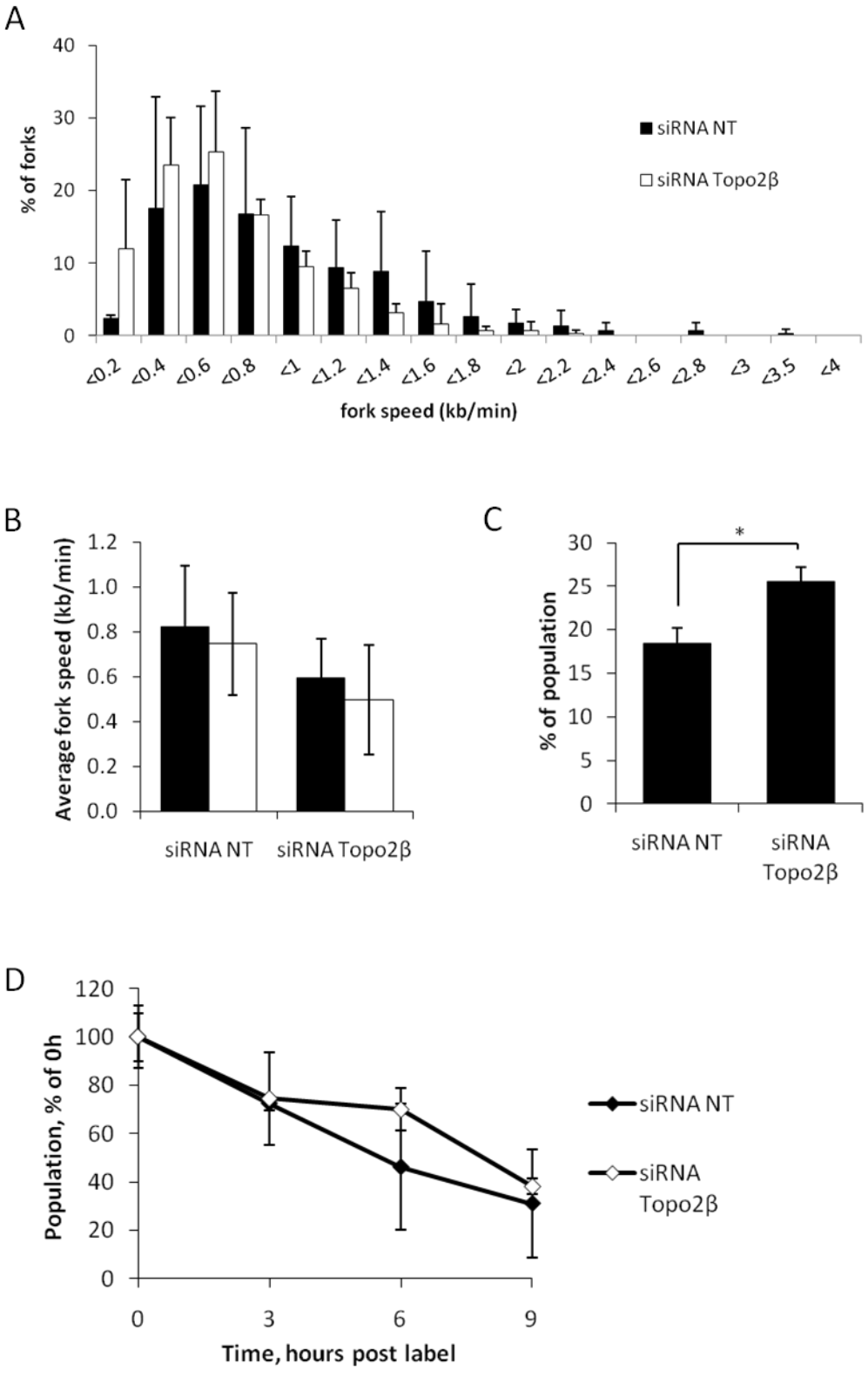
A
40
30
20
10
0
% of forks
siRNA NT
siRNA Topo2β
<0.2
<0.4
<0.6
<0.8
<1
<1.2
<1.4
<1.6
<1.8
<2
<2.2
<2.4
<2.6
<2.8
<3
<3.5
<4
fork speed (kb/min)
B
1.2
1.0
0.8
0.6
0.4
0.2
0.0
Average fork speed (kb/min)
siRNA NT
siRNA Topo2β
C
*
30
25
20
15
10
5
0
% of population
siRNA NT
siRNA Topo2β
D
120
100
80
60
40
20
0
Population, % of 0h
0
3
6
9
Time, hours post label
siRNA NT
siRNA Topo2β

Figure 4.10 | Replication fork rate and cell cycle progression is unaffected by absence of Topo2β in U2OS cells

A. CldU track distribution of replication fork rates in samples treated with 10 nM siRNA NT or siRNA Topo2β. Samples were harvested 72 hours post transfection and processed for DNA fibre analysis.

B. Quantification of overall fork speed average. Black bars represent CldU tracks and white bars IdU tracks. Data bars are the means of at least three independent experiments. Error bars represent standard deviation from the mean.

C. Proportion of cells in early-mid S phase at 0 hours. Quantification was done on samples treated with 10 nM siRNA Topo2β for 72 hours, and pulse-labelled with 25 μM IdU for 20 minutes, after which they were processed for analysis of IdU and DNA content (PI) by FACS analysis. Data bars are the means of at least three independent experiments. Error bars represent standard deviation from the mean. Statistical significance (p-value < 0.05) in Student's *t*-test is indicated by one star.

D. Cell progression though early-mid S phase 0, 3, 6, and 9 hours after 72 hours treatment with 10 nM Topo2β and IdU pulse-label. Cells were fixated in ethanol then processed and stained for DNA content (PI) and IdU incorporation. The proportion of cells in early-mid S and late S phase was calculated by gating, as illustrated previously. Data points are the means of at least three independent experiments. Error bars represent standard deviation from the mean.

4.3.6 Analysis of DNA replication and S phase kinetics in Topo2α/β depleted cells

To investigate if Topo2α and Topo2β compensate for each other during DNA replication, both isoforms were depleted in HTETOP and U2OS cells. After 72 hours Topo2α and Topo2β were efficiently knocked down (Figure 4.1 C) with the same siRNA as previous, and cells were processed for fibre analysis and cell cycle analysis as previously described.

Fibre analysis indicated that removal of both proteins did not affect DNA replication rate as evident by similar fork rate distribution (Figure 4.11 A and Figure 4.12 A) and unaltered average fork speeds in both cell lines (Figure 4.11 B and Figure 4.12 B). This conclusion is reinforced by an unaffected rate of S phase progression. Cells depleted of both Topo2 isoforms seemed to have a slight delay at early time points, but completed the early-mid S phase in a timely fashion (Figure 4.12 C).

In conclusion, depletion of both isoforms of Topo2 does not disrupt DNA replication as measured by the speed of the replication fork and the progression through early and mid S phase.

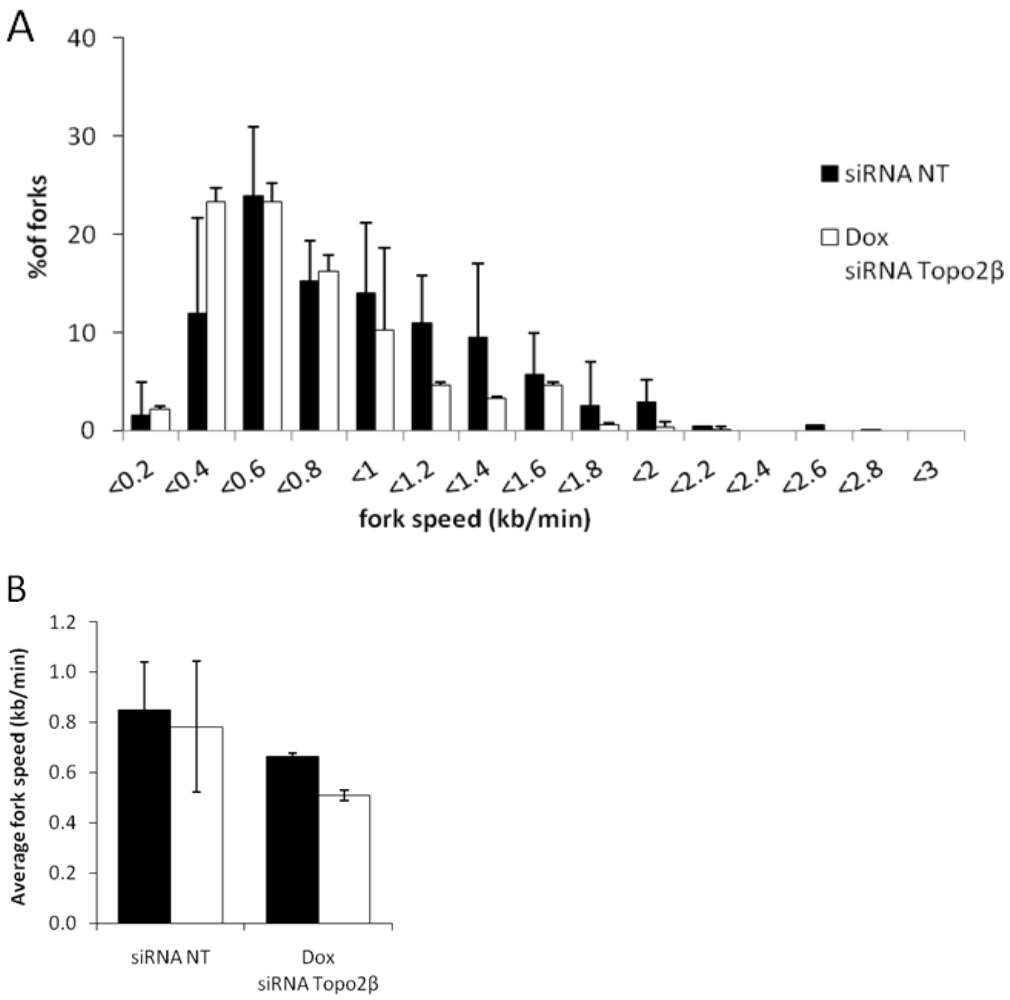

Figure 4.11 | Replication fork rate is unaffected by simultaneous absence of Topo2α and Topo2β in HTETOP cells

A. CldU track distribution of replication fork rates from DNA fibre spreads in samples treated with 10 nM siRNA NT or 1 µg/ml doxycycline and siRNA Topo2β. Samples were harvested 72 hours post transfection and processed for DNA fibre analysis.

B. Quantification of overall fork speed average. Black bars represent CldU tracks and white bars IdU tracks. Data bars are the means of at least three independent experiments. Error bars represent standard deviation from the mean

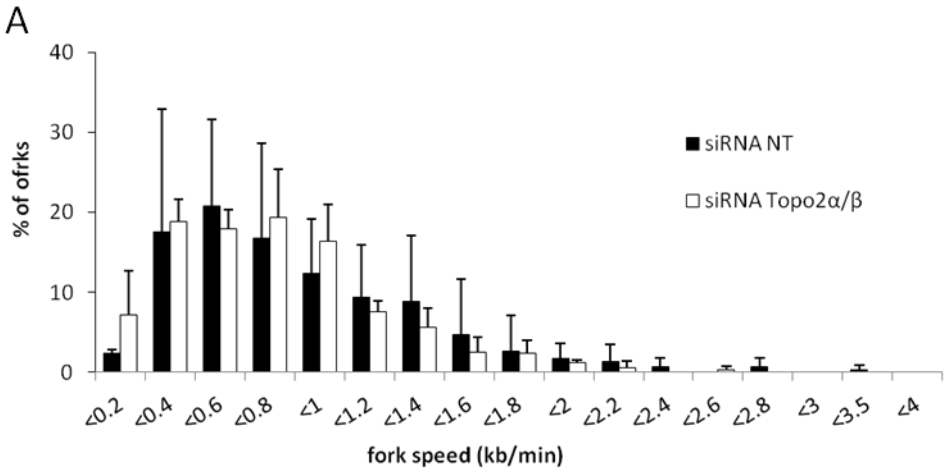
A
40
30
20
10
0
% of ofrks
siRNA NT
siRNA Topo2α/β
<0.2
<0.4
<0.6
<0.8
<1
<1.2
<1.4
<1.6
<1.8
<2
<2.2
<2.4
<2.6
<2.8
<3
<3.5
<4
fork speed (kb/min)

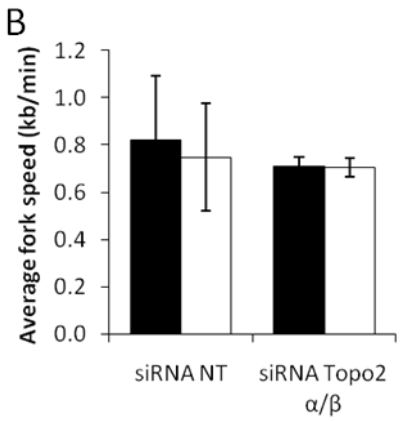
B
1.2
1.0
0.8
0.6
0.4
0.2
0.0
Average fork speed (kb/min)
siRNA NT
siRNA Topo2 α/β

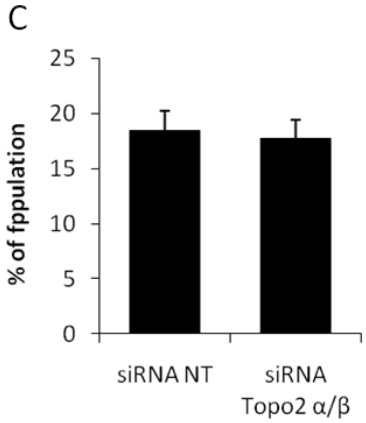
C
25
20
15
10
5
0
% of fppulation
siRNA NT
siRNA Topo2 α/β

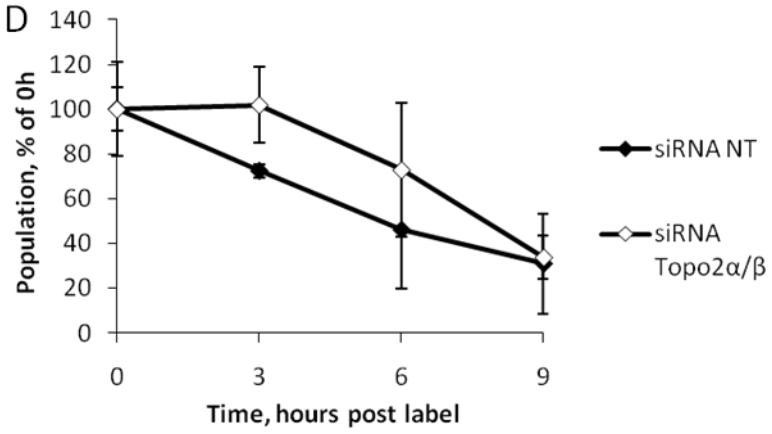
D
140
120
100
80
60
40
20
0
Population, % of 0h
0
3
6
9
Time, hours post label
siRNA NT
siRNA Topo2α/β

Figure 4.12 | Replication fork rate and cell cycle progression is unaffected by simultaneous absence of Topo2α and Topo2β in U2OS cells

A. CldU track distribution of replication fork rates from DNA fibre spreads in samples treated with 10 nM siRNA NT or siRNA Topo2α and Topo2β simultaneously. Samples were harvested 72 hours post transfection and processed DNA fibre analysis.

B. Quantification of overall fork speed average. Black bars represent CldU tracks and white bars IdU tracks. Data bars are the means of at least three independent experiments. Error bars represent standard deviation from the mean.

C. Proportion of cells in early-mid S phase at 0 hours. Quantification was done on samples treated with 10 nM siRNA NT or siRNA Topo2α and Topo2β simultaneously for 72 hours, and pulse-labelled with 25 μM IdU for 20 minutes, after which they were processed for analysis of IdU and DNA content (PI) by FACS analysis. Data bars are the means of at least three independent experiments. Error bars represent standard deviation from the mean.

D. Cell progression though early-mid S phase 0, 3, 6, and 9 hours after 72 hours treatment with 10 nM Topo2β and pulse-label with IdU. Cells were fixated in ethanol then processed and stained for DNA content (PI) and IdU incorporation. The proportion of cells in early-mid S and late S phase was calculated by gating, as illustrated previously. Data points are the means of at least three independent experiments. Error bars represent standard deviation from the mean.

4.4 Topo2 inhibition on replication progression

The function of Topo2α has predominantly been elucidated by using pharmacological inhibitors. The most common inhibitor, ICRF-193, acts by stabilizing the closed-clamp form of Topo2 on non-concovalently bound target DNA [68]. Treatment with the inhibitor causes a strong G2 arrest, termed decatenation checkpoint which is assumed to be separate from the damage G2 checkpoint [53]. However, depletion of Topo2α has not revealed the same stable G2 arrest. Moreover, the effects on replication differ in yeast cells depleted of Topo2 in comparison to those same cells with an enzymatically inactive protein . To clarify if inhibition and depletion of Topo2α differ in my experimental setting for replication elongation, the same replication assays were employed as in the previous section.

4.4.1 Inhibition efficiency of ICRF-193

To optimise the concentration of ICRF-193 an initial range between 1μM and 20 μM was determined by looking in the existing literature. Treatment with ICRF-193 inhibits Topo2 function and results in a G2 phase cell cycle arrest prohibiting cells from entering mitosis [14, 53, 68]. Consequently, cell accumulation in G2 phase, determined by FACS analysis was used to set the right dose of ICRF-193. HTETOP cells were treated in a dose dependent manner for 24 hours and DNA content was analysed by FACS analysis (Figure 4.13 A).

5 μM ICRF-193 caused a stronger G2 arrest than 1 μM, but the arrest was equally strong as with higher doses. Continuous treatment with ICRF-193 indicated that 5 μM reduced viability to same extent as 10 μM and 20 μM. These experiments suggested that 5 μM was the lowest efficient dose to inhibit Topo2.

It is widely assumed and shown in several publications that ICRF-193 treatment does not cause DNA damage [53]. However, a few studies have detected damage, particularly DSBs, following treatment with ICRF-193. Therefore to investigate damage status in

HTETOP cells, they were treated with ICRF-193 and DSB induction was determined by pulse-field gel electrophoresis (PFGE). Here, cells are moulded into a plug and then lysed. DNA is stripped of proteins by proteinase K treatment and the plugs are imbedded in an agarose gel. Intact DNA is too large to run into the gel and is contained in the plug. Conversely, DSBs fragment DNA into shorter pieces that are released into the gel by the current. PFGE is not as sensitive as other methods such as γH2AX foci labelling, but it is a direct method of detecting DSBs, unlike the other techniques. Because 1 μM did not show a strong G2 arrest, only the 5 μM, 10 μM, and 20 μM were investigated for induction of DBS.

On normal exposure, adjusted to the positive control, no DSBs were visible after ICRF-193 treatment (Figure 4.13 C). However, overexposure shows a clear dose dependent DSB induction after one hour of treatment. As the lowest concentration that induced a G2 phase accumulation, 5 μM ICRF-193 was used to assess time dependent damage accumulation. The overexposure shows an increase of DSBs over time. The 15 Gy dose represents 300 DBS per cell .

In conclusion, 5 μM, 10 μM, and 20 μM ICRF-193 are the tested doses that arrested cells in G2 phase. They also reduced viability at the same rate (Figure 4.13 B). However, ICRF-193 causes damage in HTETOP cells, so to reduce off-target effects and avoid undesirable DSB accumulation, 5 μM, the lowest does that had an effect, was used for all future experiments.

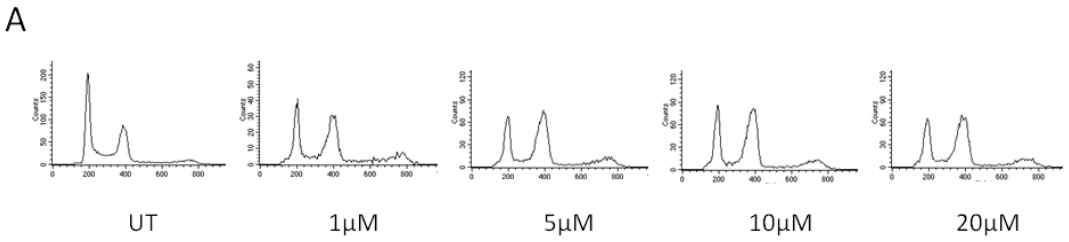
A
UT
1μM
5μM
10μM
20μM

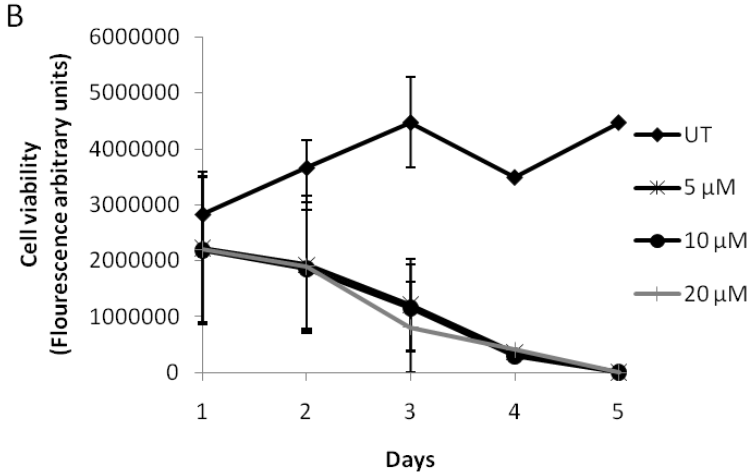
B
Cell viability
(Flourescence arbitrary units)
6000000
5000000
4000000
3000000
2000000
1000000
0
1
2
3
4
5
Days
UT
5 μM
10 μM
20 μM

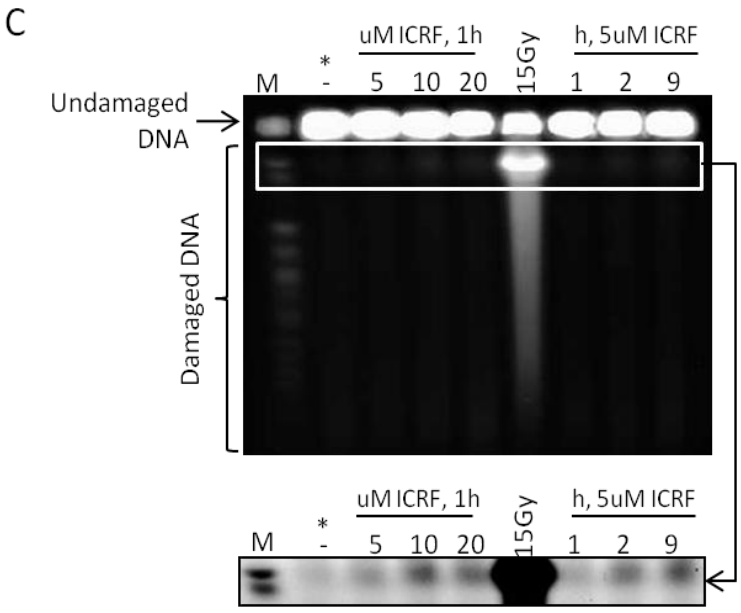
C
M
*
-
5
10
20
uM ICRF, 1h
15Gy
1
2
9
h, 5uM ICRF
Undamaged
DNA
Damaged DNA

Figure 4.13 | Topo2 inhibition causes G2 cell cycle arrest in HTETOP cells

A. Representative DNA content FACS plots of HTETOP cells. Cells were treated with 5 μM ICRF-193 as indicated or left untreated, UT, for 24 hours. Samples were harvested and fixed in ethanol and stained with PI for analysis.

B. Cell viability was measured by resazurin assay during continuous treatment with indicated doses of ICRF-193. Measurements were performed on the same samples each day, with the first measurement one day after treatment initiation. Data points are the means of at least three independent experiments. Error bars represent standard deviation from the mean.

C. PFGE gel stained with ethidium bromide. Cells were treated as indicated and then moulded into the plugs, except for IR treated cells that were irradiated in the plug. The exert shows overexposure.

4.4.2 Cell cycle analysis in the presence of Topo2 inhibitor ICRF-193

In order to establish if inhibiting Topo2α would disrupt replication, both HTETOP and U2OS cells were treated with 5 μM ICRF-193 and samples were prepared for fibre analysis and cell cycle analysis.

First, to investigate the overall progression of the S phase, cells were pulse-labelled with IdU and released into media with ICRF-193 to be sampled throughout the following 24 hours. To assess the cell cycle progression, DNA content and IdU incorporation were measured by FACS analysis as previously described (Figure 4.14 A).

Figure 4.14 B shows a series of representative images of HTETOP cells. The bottom panels show cells treated with ICRF-193. As compared to untreated cells in the top panel, there is no quantifiable difference in progression rate in early-mid S phase from 0 to 9 hours with ICRF-193 treatment (Figure 4.14 C). The same was noted for U2OS cells. This indicates that inhibition by ICRF-193 does not prevent timely progression through S phase and that inhibition is not different from depletion of Topo2α in this instance.

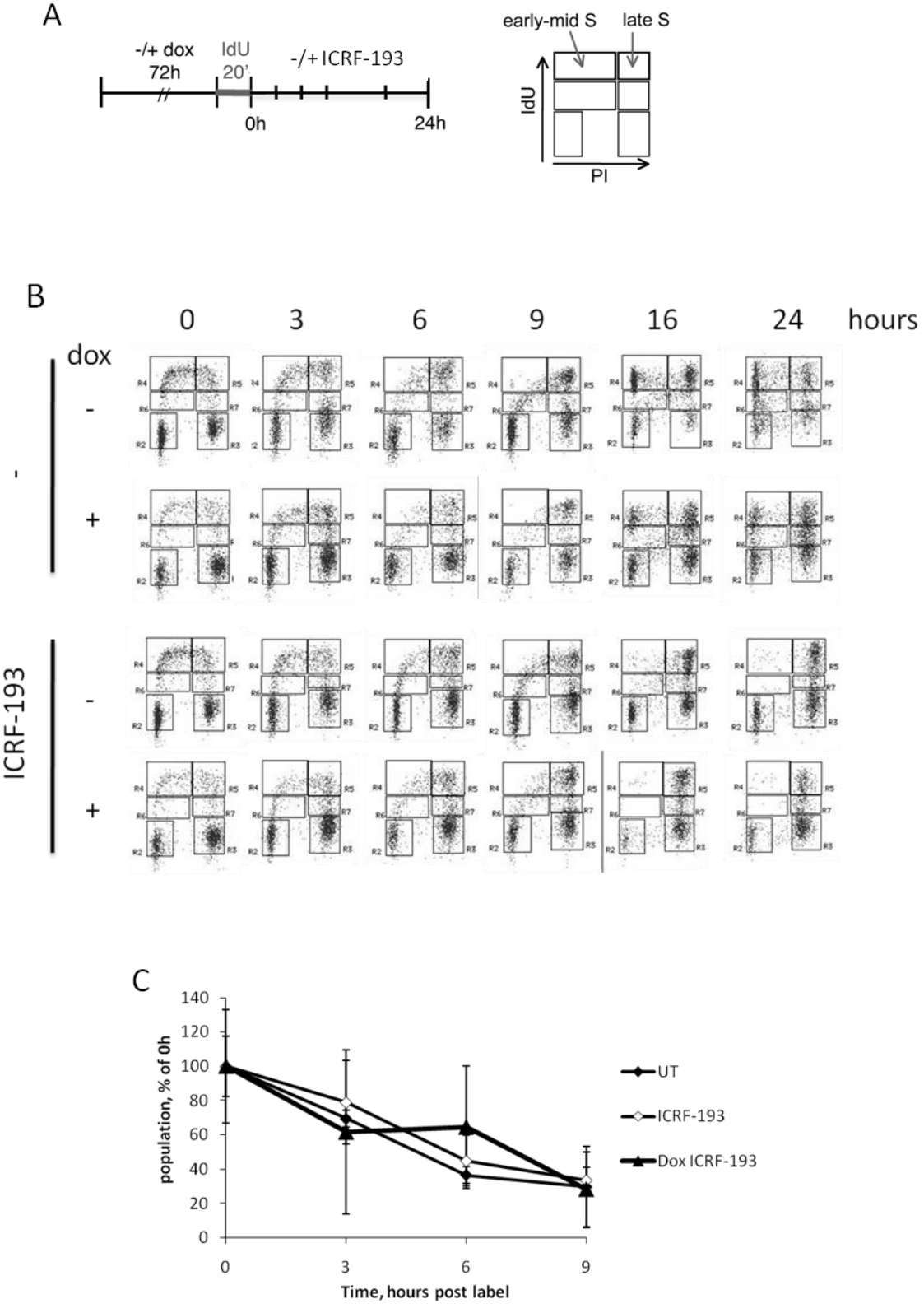
A
-/+ dox
72h
IdU
20'
-/+ ICRF-193
0h
24h
early-mid S
late S
IdU
PI
B
0
3
6
9
16
24
hours
dox
-
+
ICRF-193
-
+
C
population, % of 0h
140
120
100
80
60
40
20
0
0
3
6
9
Time, hours post label
UT
ICRF-193
Dox ICRF-193

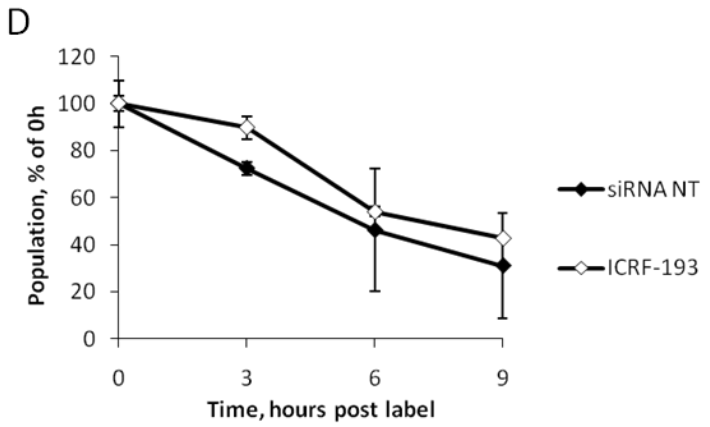

Figure 4.14 | S phase progression is unaffected by ICRF-193 inhibition in both U2OS and HTETOP cells

A. Experimental design. IdU was added to the last 20 minutes of the 72 hours doxycycline treatment. Cells were washed and released into media containing 5 µM ICRF-193 to be harvested at indicated time points.

B. Representative FACS plots of HTETOP cell samples collected at 0 – 24 hours after 72 hours treatment with 1 µg/ml doxycycline or untreated. Samples in the upper panels were released into fresh media and samples in the lower panels into media containing 5 µM ICRF-193. Cells were fixed in ethanol then processed and stained for DNA content (PI) and IdU incorporation. The proportion of cells in early-mid S and late S phase was calculated by gating, as illustrated.

C. Quantification of data represented in top two panels and the bottom panel. Data is plotted as percentage of time point 0 hours. Data points are the means of at least three independent experiments. Error bars represent standard deviation from the mean.

D. U2OS cell progression though early-mid S phase after 20 minute IdU pulse-label and consequent release into fresh media or 5 µM ICRF-193 media. Data was quantified in the same way as for HTETOP cells and is plotted as percentage of time point 0 hours. Data points are the means of at least three independent experiments. Error bars represent standard deviation from the mean.

As expected, ICRF-193 induced a G2 block. At 16 and 24 hour time point cells were arrested in 4N state (Figure 4.14 B, lower panels). It is interesting to note that the block is a result of a G2 arrest, but also a delay in late S phase as indicate by slow progression from

late S to G2. This is seen in the individual panels as the straight smear of cells from the top, late S gate, to the bottom, G2 gate.

As a control for ICRF-193 specificity, separate samples were also treated with both the inhibitor and doxycycline to remove the target protein Topo2α. The very bottom panels show the double treated samples, and as expected there is no difference in the progression rate from 0 to 9 hours in early and mid S phase. Interestingly, marked effect of ICRF-193 on G2 arrest was still observed when cells had been depleted of Topo2α by treatment with doxycycline. This would exclude an inhibitory ICRF-193 effect on Topo2α in cell cycle arrest.

A


CldU
IdU
1h
20'
20'
ICRF-193

B

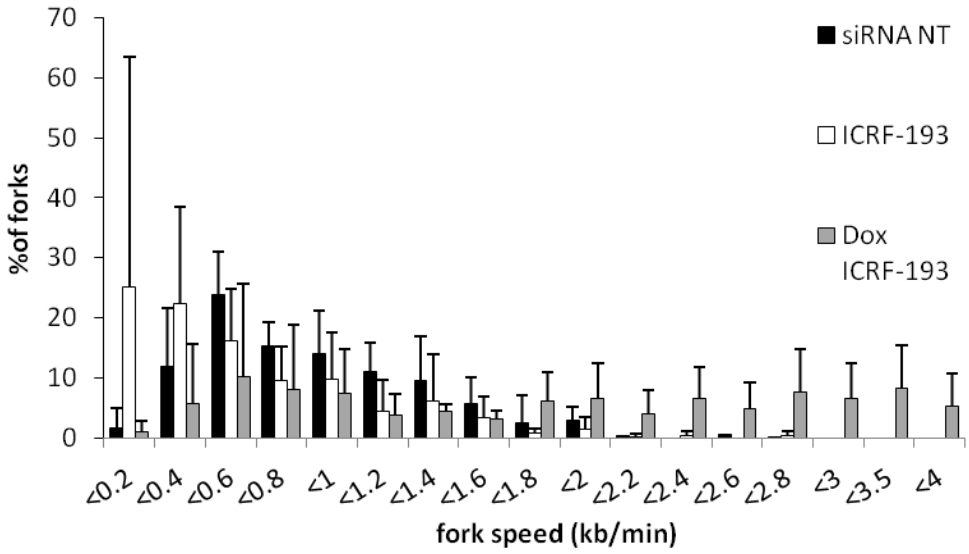
70
60
50
40
30
20
10
0
%of forks
siRNA NT
ICRF-193
Dox
ICRF-193
<0.2
<0.4
<0.6
<0.8
<1
<1.2
<1.4
<1.6
<1.8
<2
<2.2
<2.4
<2.6
<2.8
<3
<3.5
<4
fork speed (kb/min)

C

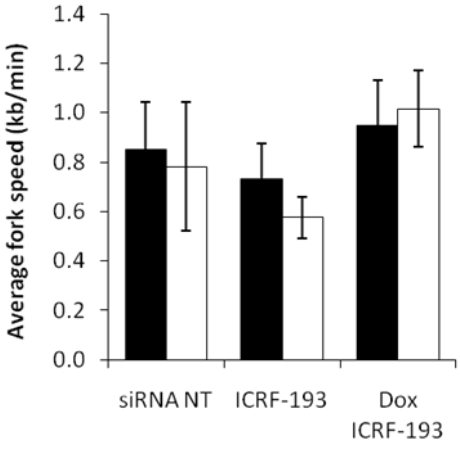
1.4
1.2
1.0
0.8
0.6
0.4
0.2
0.0
Average fork speed (kb/min)
siRNA NT
ICRF-193
Dox
ICRF-193

D

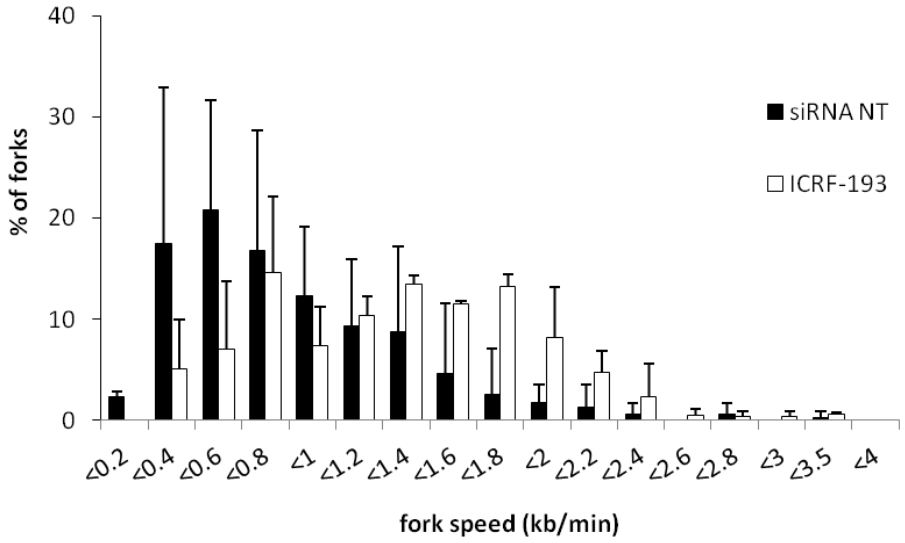
40
30
20
10
0
% of forks
siRNA NT
ICRF-193
<0.2
<0.4
<0.6
<0.8
<1
<1.2
<1.4
<1.6
<1.8
<2
<2.2
<2.4
<2.6
<2.8
<3
<3.5
<4
fork speed (kb/min)

E

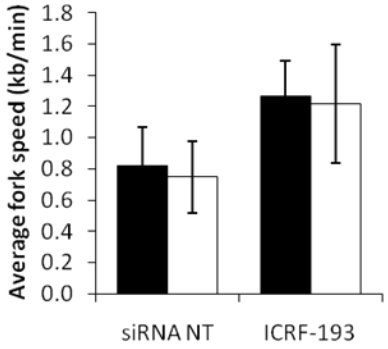
1.8
1.6
1.4
1.2
1.0
0.8
0.6
0.4
0.2
0.0
Average fork speed (kb/min)
siRNA NT
ICRF-193

F

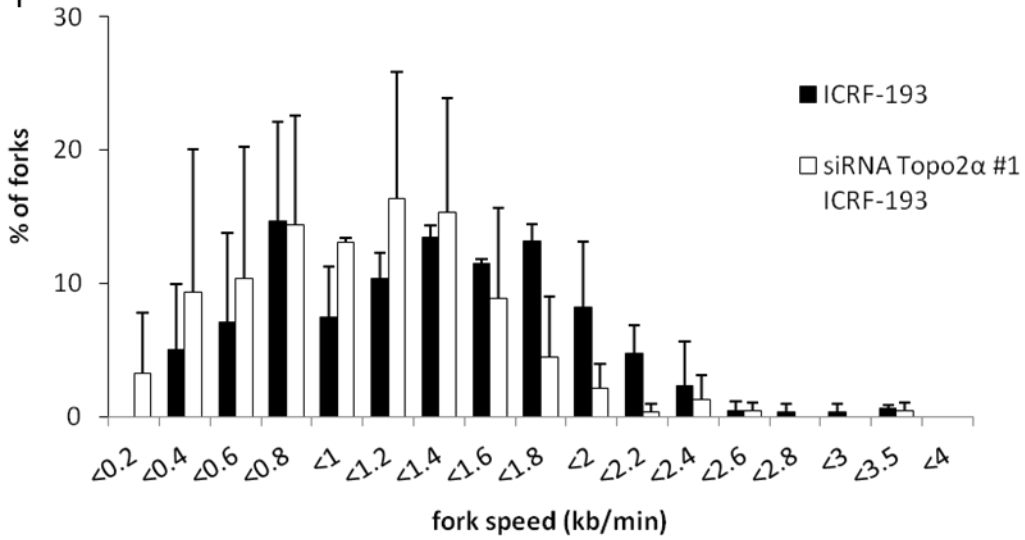
30
20
10
0
% of forks
ICRF-193
siRNA Topo2α #1
ICRF-193
<0.2
<0.4
<0.6
<0.8
<1
<1.2
<1.4
<1.6
<1.8
<2
<2.2
<2.4
<2.6
<2.8
<3
<3.5
<4
fork speed (kb/min)

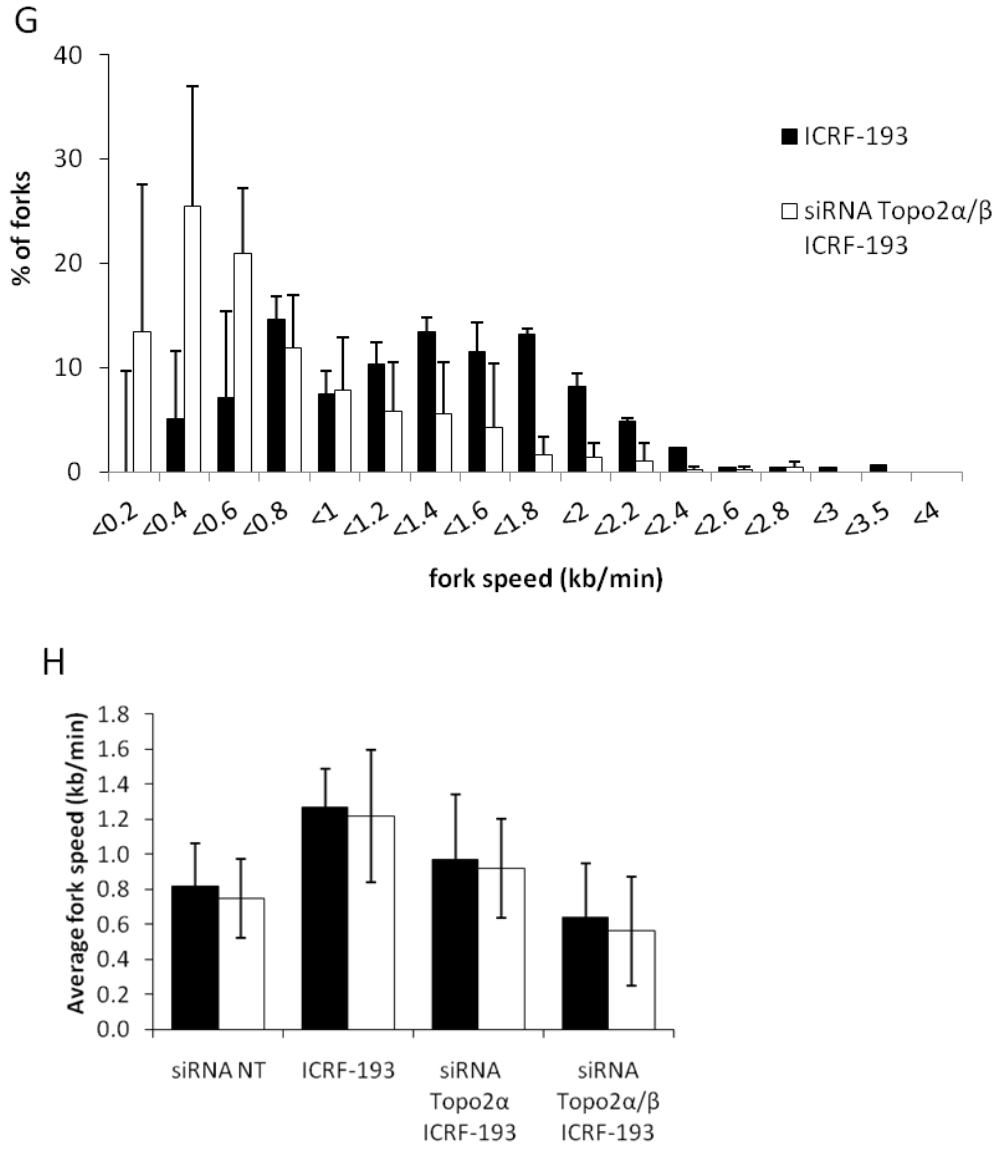

Figure 4.15 | Replication fork rate is unaffected by inhibition of Topo2α in HTETOP and U2OS cells

A. Experimental design. Cells were treated as indicated for 72 hours after which they were pulse-labelled with 25 µM CldU (red) and 250 µM IdU (green) for 20 minutes respectively. They were then processed for DNA fibre analysis.

B. CldU track distribution of replication fork rates in HTETOP cells. Samples are treated 72 hours either with 10 nM siRNA NT or 1 µg/ml doxycycline and 5 µM ICRF-193 was added for the last hour. Data bars are the means of at least three independent experiments. Error bars represent standard deviation from the mean**.**

C. Quantification of overall fork speed average. Black bars represent CldU tracks and white bars IdU tracks. Data bars are the means of at least three independent experiments. Error bars represent standard deviation from the mean.

D. CldU track distribution of replication fork rates in U2OS cells. Samples treated with 10 nM siRNA NT or 5 μM ICRF-193 for 1 hour.

E. Quantification of overall fork speed average. Black bars represent CldU tracks and white bars IdU tracks. Data bars are the means of at least three independent experiments. Error bars represent standard deviation from the mean.

F. CldU track distribution of replication fork rates in U2OS cells. Samples treated with 10 nM siRNA Topo2α for 72 hours or and 5 μM ICRF-193 was added for the last one hour**.**

G. CldU track distribution of replication fork rates in U2OS cells. Samples treated with 10 nM siRNA Topo2α and Topo2β simultaneously for 72 hours and 5 μM ICRF-193 was added for the last one hour.

H. Quantification of overall fork speed average. Black bars represent CldU tracks and white bars IdU tracks. Data bars are the means of at least three independent experiments. Error bars represent standard deviation from the mean.

4.4.3 DNA fibre analysis in the presence of Topo2 inhibitor ICRF-193

To prepare cells for fibre analysis, they were pre-treated with ICRF-193 for one hour prior to incubation with 25 μM CldU and 250 μM IdU for 20 minutes respectively (Figure 4.15 A). Cells were harvested and prepared as previously described.

When the distribution of fork rates was quantified and plotted, it showed no marked difference in ICRF-193 treated samples. The average fork speed after treatment did not change in HTETOP cells (Figure 4.15 B and C). Although not statistically significant, ICRF-193 increased the average fork speed in HTETOP cells when cells were simultaneously treated with doxycycline to remove Topo2α.

In U2OS cells ICRF-193 treatment increased fork speed from 0.8 k b/min, to 1.3 kb/min for CldU and 1.4 kb/min for IdU tracks (Figure 4.15 D and E) although this was not statistically different. Simultaneous depletion and inhibition of Topo2α reduced the increasing trend (Figure 4.15 F and H) and reduced the average speed to 1.0 kb/min.

One possible explanation that could account for why ICRF-193 treatment creates a trend of increased fork speed in both proficient and those cells depleted of Topo2α is that inhibitor exerts its effect by acting on Topo2β as well. To investigate if ICRF-193 affects both isoforms of Topo2, Topo2α and Topo2β were depleted in U2OS cells and then ICRF-193 was added. The trend of the increased fork speed was further reduced compared to single Topo2α siRNA knock-down, bringing the fork speed down to levels of untreated cells (Figure 4.15 G and H). These results could indicate that in U2OS cells ICRF-193 affects both Topo2 isoforms and that the trend of increased fork speed is potentially due to inhibition of both Topo2α and Topo2β.

4.4.4 Merbarone

The Topo2α inhibitor Merbarone inhibits the protein in the early stages in the catalytic cycle, preventing cleavage of the G-segment. Therefore, unlike with ICRF-193, where the T-segment has passed through and the break has been relegated, Merbarone traps the catenated substrate. To investigate if Merbarone treatment would affect individual replication forks, HTETOP cells were treated with increasing doses from 50 μM to 300 μM for one hour after which they were prepared for fibre analysis. There was no change after Merbarone treatment, independent of dose (Figure 4.16). These results indicate that Merbarone does not affect replication. It also suggests that the function of Topo2α is completely indispensable for replication, as it does not matter what intermediates are trapped.

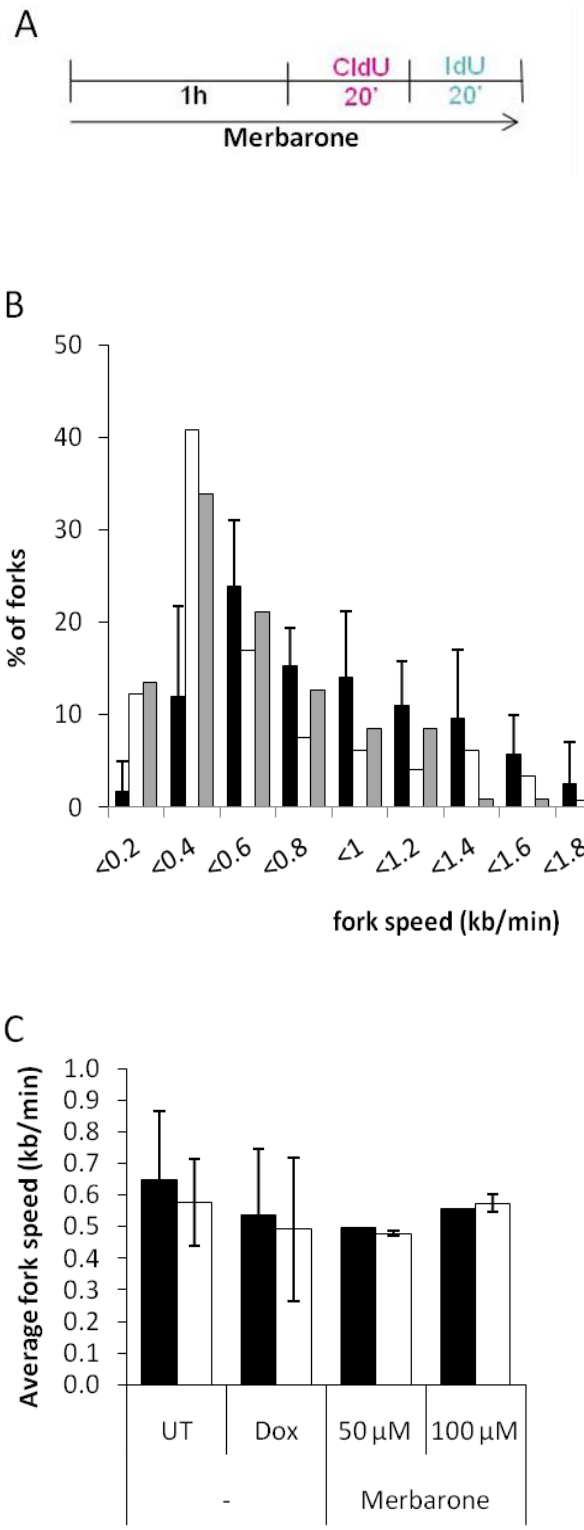
A
CldU
IdU
1h
20'
20'
Merbarone
B
50
40
30
20
10
0
% of forks
siRNA NT
100 µM
50 µM
<0.2
<0.4
<0.6
<0.8
<1
<1.2
<1.4
<1.6
<1.8
<2
<2.2
<2.4
<2.6
fork speed (kb/min)
C
Average fork speed (kb/min)
1.0
0.9
0.8
0.7
0.6
0.5
0.4
0.3
0.2
0.1
0.0
UT
Dox
50 µM
100 µM
-
Merbarone

Figure 4.16 | Merbarone inhibition of Topo2α does not affect replication rate

A. Experimental design. Cells were treated as indicated for 1 hour after which they were pulse-labelled with 25 μM CldU (red) and 250 μM IdU (green) for 20 minutes respectively. They were then processed for DNA fibre spreads.

B. CldU track distribution of replication fork rates for one experiment, except for siRNA NT samples. Error bars represent standard deviation from the mean.

C. Quantification of overall fork speed average. Black bars represent CldU tracks and white bars IdU tracks. Data bars are the means of at least three independent experiments. Error bars represent standard deviation from the mean.

4.5 Discussion

The work in this chapter describes the investigation of the role of Topo2α and Topo2β in S phase progression and replication elongation. Collectively, the data presented here leads to the conclusion that Topo2α is not needed for bulk DNA synthesis in early-mid S phase and that the individual replication forks are not perturbed. This conclusion is reinforced by the observation that neither depletion nor inhibition of Topo2 affect S phase. The data also suggests that Topo2β does not underpin replication on its own, nor by acting as a back-up to Topo2α.

At the time this research was undertaken the division of labour between Topo1 and Topo2 in replication was still debated. It was assumed that the positive supercoiling ahead of the replication fork is relaxed by type I topoisomerases, because of their efficiency to relax those substrates on naked DNA. However, there was only indirect evidence and the exact roles for Topo1 and Topo2α in propagating DNA replication still remained to be determined in a direct manner. It has been shown that yeast Topo2 is found in the proximity of the

replication fork and there are indications that Topo2 can contribute to proper replication [14, 44]. First, in *S. cerevisiae*, Topo2 is able to compensate for Topo1 while loss of both proteins leads to halted DNA replication [44, 144, 145]. Second, biochemical evidence suggest that Topo2α relaxes positive supercoiled plasmids faster than the negatively supercoiled ones [146]. Positive supercoils are generated by helical unwinding ahead of the replication fork and to deal faster with what can become a replication barrier, torsional stress can be transferred behind the replication machinery, forming precatenanes [7]. Although both Topo1 and Topo2 can remove positive supercoils, only Topo2 is able to resolve precatenanes. Yet another evidence for Topo2's involvement in replication is shown in previous studies that have used Topo2 poisons to study collapsed replication forks. This would certainly assume Topo2 to be active during replication and perhaps ahead of the fork. Namely, concurrent treatment with etoposide and aphidicolin, a Polα inhibitor which blocks replication, reduced etoposide induced toxicity [159]. An alternative explanation to Topo2α's role in replication is that sister chromatid unlinking takes place concurrently with replication. This hypothesis would assume that Topo2 is active during replication, but would place it behind the replication fork dealing only with the resolution of precatenates.

Although there is emerging evidence that Topo2α might be involved in the late stages of replication [46, 160] previous studies using siRNA have been unsuccessful in showing an indispensable role for Topo2α in replication elongation [14, 17]. It was therefore vital to minimise sources of false negative results, such as off-target effects of siRNA, or a specific genetic background that can potentially mask an effect. For this reason two well established cell lines and two non tumorous cells were used. For Topo2α knock-down two different siRNA sequences were used in addition to HTETOP cells.

In response to DNA replication block, the intra-S phase checkpoint is activated and cells accumulate in S phase to allow for repair. To this end, HU treatment has been used and

it was shown that total rate of DNA replication is reduced and late-origin firing is inhibited [14, 44, 153, 161]. Hence, if Topo2α depletion disrupted replication through accumulation of torsional stress and therefore stalling forks or even generating DNA damage, it is likely that those lesions would activate the S phase checkpoint and lead to accumulation of S phase cells.

Figure 4.2 and 4.3 show that the progression of early-mid S phase is unperturbed in absence of Topo2α independent of knock-down method or cell line. MRC5 and GM01604 cell lines also do not show evidence of activated checkpoint arrest, removing the doubt that genetic instability of tumorigenic background is masking a phenotype. Interestingly, Li *et al* performed the same experiment in HeLa cells where Topo2α was depleted using vector-based RNAi and found a strong cell cycle arrest in S phase [45].

It would have been useful to run a Western blot on MRC5 and GM01604 cells to confirm the knock-down, however time restrain limited the opportunity.

Checkpoint activation in response to slowed growth and replication can prevent S phase progression, but it can also activate dormant origins to rescue under-replicated regions. Inhibitions of ATM, ATR and Chk1 have all been associated with increased origin firing [43, 162-165]. To investigate if, by looking at bulk DNA synthesis by FACS analysis, other replication defects were masked, it was useful to look directly at individual replication forks. DNA fibre labelling revealed that the DNA replication rate was unaltered after Topo2α depletion reaffirming the conclusion that Topo2α is dispensable for replication propagation.

Topo2β is over 70% similar to Topo2α in the amino acid sequence, and the two enzymes have similar enzymological characteristics but, the two isoforms have different expression patterns [5]. Namely Topo2α protein levels are cell cycle regulated and the protein is associated with proliferating cells while the β isoform is independent of

proliferation status and has been implicated in transcription and neural development in mice [1]. It is known that Topo2β cannot compensate for Topo2α in mammalian cells and Topo2α is an essential protein, while cells can survive without Topo2β [42, 166] In yeast however both isoforms are able to compliment the loss of Topo2, which would suggest that Topo2β is enzymatically capable of catalysing the same reactions as Topo2α [42, 167, 168].

Accumulating evidence implicates Topo2β in transcription regulation, but for the purpose of thoroughness of this thesis it was interesting to test both isoforms in the experimental system. Notably, Topo2β experiments would have served as a formidable negative control if Topo2α depletion had generated a phenotype. Concluding from the obtained results, DNA replication rate is unaffected in both U2OS and HTETOP cell lines and in U2OS cells the S phase progression is left unaltered after Topo2β depletion. By depleting both isoforms it can be concluded that the isoforms do not compensate for each other and do not potentially mask a replication defect of a single knock-down.

Elucidation of Topo2 function in mammalian cells has relied mainly on usage of pharmacological inhibitors, which can be divided into two groups. Topo2 "poison" and catalytic inhibitors, of which ICRF-193 is the most potent. However, inhibition of a protein is not equivalent to complete depletion of it. And one recent example is that loss of PARP1 does not result in the same outcome as treatment with the PARP inhibitor [169]. In brief, treatment-induced SSBs accumulated after PARP1 inhibition, but not in cells treated with PARP1 siRNA. There are potentially several ways to explain this observation. First, treatment with the inhibitor traps the protein together with its substrate. In a scenario where another protein is able to compensate and perform the same enzymatic reaction, the substrate is left inaccessible to it. Secondly, if the inhibited protein has other functions, such as being part of a signalling cascade, that function might still be intact when the protein's enzymatic activity is inhibited. In case of depletion this would not be possible. Topo2α was recently

shown to be involved in decatenation checkpoint signalling [51, 67], and although it is too early to say if the inhibition leaves the signalling function intact, the possibility exists.

In the case of replication elongation and S phase progression there was no difference between siRNA depletion and ICRF-193 inhibition suggesting that Topo2α is not involved in these processes. However, there are other differences between the two treatments. The G2 block is more prevalent in ICRF-193 treated samples compared to Topo2α depleted cells (Figure 4.14 B). This can also be seen in Figure 4.5, where ICRF-193 treatment reduced proportion of cells in S phase whereas the siRNA treatment did not. Interestingly, Carpenter and Porter noticed a similar discrepancy in HTETOP cells when looking at chromosome condensation [52] concluding that ICRF-193 generated a more marked effect as compared to Topo2α depletion. In addition to the presented explanation that inhibitors can block back-up pathways, an alternative interpretation is that ICRF-193 is not Topo2α specific and elicits a G2 arrest through an alternative mechanism. Equally, it is possible that siRNA depletion is not complete and the few residual Topo2α molecules are able to catalyse the reaction, while ICRF-193 treatment would inhibit all molecules. From the cell cycle experiment in Figure 4.14 B, where both doxycycline and ICRF-193 were added and the G2 arrest is evident independent of doxycycline addition, it is hard to discern whether it is the unspecificity or inhibition of few remaining molecules that lead to those results. In conclusion, further studies are required to elucidate why ICRF-193 inhibition results in a different phenotype from depletion and what the mechanical basis for the phenotypes is.

Chapter 5

Results

5 Topo2α dependent polyploidization

5.1 Introduction

FACS analysis described in the previous chapter indicated that doxycycline treated HTETOP cells depleted of Topo2α accumulated a polyploid fraction. In this chapter I wanted to investigate further the molecular mechanism explaining this phenotype.

5.1.1 Cell cycle progression

The cell cycle is characterized by two main processes; DNA synthesis, and cell division. Proliferating mammalian cells go through four different cell cycle phases, G1, S, G2 and M phase, which are necessary to generate an identical copy of the original cell.

DNA is replicated during S phase to generate sister chromatids. The duplicated genome is then segregated in M phase (mitosis and cytokinesis), which is divided into several stages – prophase, prometaphase, metaphase, anaphase and telophase. During prophase the chromosomes condense following which the nuclear envelope breaks down in the prometaphase. This is followed by attachment of the microtubule to the kinetochores and alignment of the chromosomes to the metaphase plate in the metaphase stage. The two sets of chromosomes are separated in anaphase, the onset of which is thought to be delayed by the mitotic spindle checkpoint (MSC) until all kinetochores are attached to a set of microtubules. Telophase is the final stage of chromosome segregation when the nuclear envelope reforms and the chromatin decondenses.

Cell cycle progression is driven by cyclins and cyclin dependent kinases (Cdks). There are several cyclins (A, B, D, and E), which form complexes with either Cdk1, Cdk2 or Cdk4/6 to promote cell cycle progression. Protein levels of Cdks remain relatively stable, but the kinase activity is modulated by the cyclins, whose protein levels are cell phase dependent

(Figure 5.1) . Low levels of Cdk1 activity in G1 and S phase of the cell cycle allow for licensing. In S phase cells Cdk2 (in complex with primarily cyclin E) is required for origin firing and events in S-phase. Subsequently, mitosis is initiated through increased Cdk1 activity in complex with cyclin B, which simultaneously inhibits replication initiation. Exit from mitosis leads to degradation of Cdk1 by the anaphase-promoting complex (APC/C) complex and the low activity level allows for licencing, which is required for another round of replication. Disruption of this finely tuned cyclic system, can lead to disassociation of replication from cell cycle division and result in endoreduplication and polyploidy [52].

5.1.2 Cell cycle regulation

Progression through the cell cycle is controlled by checkpoints, which monitor accurate completion of each phase before progression into the next, thus ensuring fidelity of cell division and genetic stability (Figure 5.1). Prokaryotes have a robust and reliable DNA replication and repair system, but the radical addition in number of proteins and mechanisms increases the complexity in eukaryotes and calls for an augmentation of organization and coordination. To achieve this, the eukaryotic cell has superimposed an extra level of regulation with the checkpoint pathways. This network serves to interconnect replication, repair and cell cycle progression in a very fine-tuned manner.

Checkpoints exist in all phases of the cell cycle and are viewed as a signal cascade which recruits and activates the repair machinery and promotes cell-cycle delay to allow time for repair. If the damage is too extensive, the response is directed toward apoptosis. While most checkpoint responses are investigated after exogenous DNA damage, these mechanisms also function in response to endogenous damage.

The checkpoint response is dependent on two central protein kinase transducers ATM and ATR, which belong to the phosphatidylinositol 3-kinase-like kinase (PIKK) that also includes DNA dependent protein kinase (DNA-PK). In brief, DNA-PK and ATM respond to

DSB, while ATR mainly relays signals from UV damage and stalled replication forks. These apical kinases relay and amplify the DNA damage signal and exert an effect on the downstream Cdk activity to block cell cycle progression

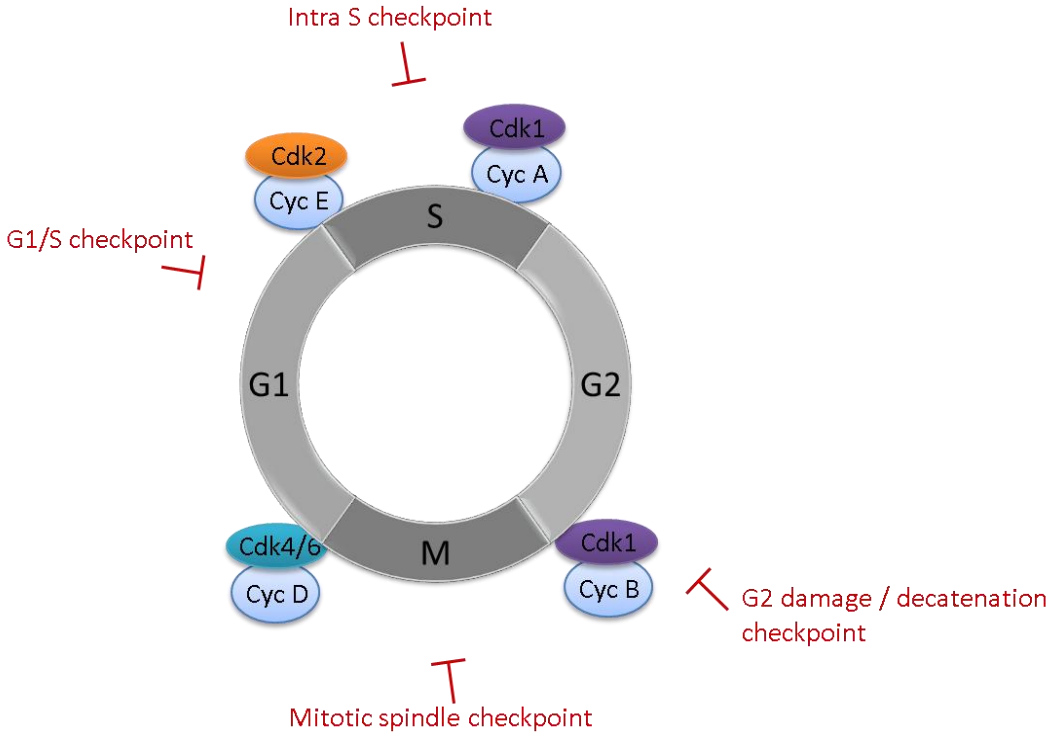

Figure 5.1 | Cell cycle regulation

The cell cycle progression is regulated by Cdk activity, which is modulated by forming a complex with different cyclins (Cyc). The checkpoints (indicated in red) monitor proper progression and genome integrity. They are activated by different substrates, dependent on the cell cycle stage, and their activation recruits repair machinery to damage and delays the cell cycle to allow for repair. To delay the cell cycle the checkpoints regulated the activity of Cdks.

5.1.3 Mechanisms of polyploidy

Polyploidy is a frequent phenomenon in nature and means that the cell has more than two sets of homologous chromosomes, i.e. it has diverged from the normal diploid state by a

whole set of chromosomes. This state is tolerated in human tissue in some cases, such as in the liver, but mainly polyploidy is undesirable. Mounting evidence suggests that tetraploidy is the initial step towards aneuploidy (irregular number of chromosomes), a hallmark of solid human cancers [170]. Human tetraploid cells, with the few exceptions, are genetically unstable and have higher rate of chromosome missegregation, perhaps because they are able to form multipolar spindles [171].

Polyploidy can arise through several mechanisms and the distinction between them can be hard to make as they can arise interdependently (Figure 5.2). Polyploid cells in a diploid organism can arise through three general mechanisms: endoreduplication, problems at cytokinesis, sometimes termed abortive cell cycle, and fusion. The latter mechanism will not be discussed here as it is outside the scope of this research.

Endoreduplication where DNA synthesis and origin firing become uncoupled from cell division is one way (Figure 5.2 D) [172]. Endoreduplication can result from re-firing of one origin several times during one S phase. Alternatively, origins may fire only once, as intended, but the S phase is not succeeded by mitosis, and a second round of replication is initiated without cell division. One mechanism to bypass mitosis is through a persistent DDR in G2, which blocks mitosis entry, but eventually results in resetting in a state resembling G1 without cell division (Figure 5.2 D). Prolonged inhibition of the cyclin B/Cdk1 complex results in low Cdk activity, which is permissive for origin relicensing, and cells can initiate another round of replication without having gone through cell division [172, 173]. Endoreduplication upon prolonged DDR and inhibition of mitosis has been shown in both *S. pombe* and human cells [174-178].

A failed cytokinesis is yet another mechanism to reach a polyploidy state. There are fundamentally two reasons why cytokinesis would not be properly executed, namely problems with the components directly involved in cytokinesis, such as those in the

midbody, or issues with the mitotic apparatus, which leads to inappropriate entry and a failed mitosis, also termed mitotic catastrophe (MC) (Figure 5.2 A and B) [178]. MC has been described as "delayed mitotic-linked cell death" or "reproductive death" denoting subsequent inability to proliferate and apoptosis or necrosis [178]. Causes for MC can include accumulated damage or problems with the mitotic machinery resulting in incorrect execution of events such as chromosome condensation, decatenation or mitotic spindle formation [171].

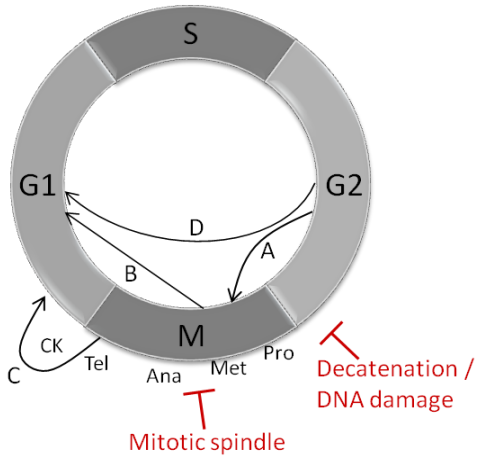

Figure 5.2 | **Pathways to polyploidy**

Cell cycle checkpoints strongly associated with preventing polyploidy are depicted in red.

A. G2 checkpoint abrogation adaptation can lead to entry into mitosis with damaged DNA prior to completion of DNA repair.

B. Mitotic slippage can lead to evasion of the mitotic spindle checkpoint and can lead to inappropriate commencement of anaphase. Problems with unsegregated or missegregated chromosomes can lead to problems with cytokinesis **C**.

D. Prolonged G2 checkpoint can result in bypass of mitosis and entry into G1 without chromosome segregation and cell division.

Prometaphase, Pro; Metaphase, Met; Anaphase, Ana; Telophase, Tel; Cytokinesis, CK. Adapted from [172].

Inappropriate entry into mitosis can result from an abrogated G2 checkpoint (Figure 5.2 A). The G2 damage checkpoint is activated by both SSBs and DSBs, and as few as 20 DSBs are enough for activation [179]. During normal conditions the onset of mitosis is initiated by kinase and phosphatase modifications of the cyclin B/Cdk1 complex. These modifications stabilize the protein complex and allow for nuclear import from the cytosol. The G2 checkpoint prevents these events and sequesters cyclin B in the cytoplasm until damage is repaired. Different defects in checkpoint machinery or checkpoint adaptation can result in illegitimate mitotic entry. Checkpoint adaptation describes cells that initiate a checkpoint arrest appropriately, but as a result of prolonged block start "leaking" into mitosis as the checkpoint is prematurely attenuated [178, 179].

Cells that attempt mitosis, but are not able to execute it effectively might arrest at the metaphase-anaphase transition by the MSC, mediated by the APC/C. Similar to checkpoint adaptation, premature exit from a prolonged mitotic arrest has been termed mitotic slippage. It is dependent on inappropriate degradation of cyclin B, which allows for entry into G1 phase without chromosome segregation and completion of mitosis (Figure 5.2 B). A problematic mitosis which is allowed to proceed might lead to failed cytokinesis (Figure 5.2 C). One widely accepted mechanism for how disrupted cytokinesis leads to polyploidy and aneuploidy is furrow (the groove made by the cell membrane, which is eventually cleaved as the cell completes cytokinesis) regression and subsequent reforming of the nuclear envelope around one or more clusters of missegregated chromosomes. There is evidence that the furrow regression leads to tetraploidy in the first cell cycle through nondisjunction of chromosomes [180]. Yet another model suggests that DNA bridges are broken by the cytokinetic furrow, leading to aneuploid cells, DSBs and DDR activation in G1 [181, 182].

Polyploidy is an undesirable state and can only take place once key tumour suppressor pathways have been disturbed, as illustrated by the general requirement of p53 loss in many cells [183, 184].

5.2 Aim

The aim of this chapter is to elucidate the mechanism by which Topo2α depleted cells become polyploid. Specifically, I wanted to distinguish between the several suggested pathways of polyploidization - bypassed mitosis, mitotic catastrophe or failure to complete cytokinesis. Additionally, we aimed to juxtapose the polyploidization caused by depletion of Topo2α to previous findings about ICRF-193 induced polyploidy.

5.3 Polyploidization after Topo2α depletion

To investigate polyploidization in HTETOP cells after Topo2α removal, doxycycline treated cells were followed for seven days. Longer incubation was not possible, as cells declined in viability and cell number (Figure 4.1 D). Samples were harvested and prepared for FACS analysis to investigate DNA content. As previously shown by Carpenter and Porter [52] incubation with doxycycline increased the polyploid cell fraction (defined as cells with a DNA content >4N, where N is the haploid chromosome number) (Figure 5.3 A and B) and a discrete 8N peak started to appear by day four, simultaneous with the broadening of the G2/M peak. Accumulation of 8N cells continued until day seven, but there was no increase in the overall percentage of cells in the 8N fraction (Figure 5.3). Interestingly, although the G2/M peak remained broad, there was no decrease of cells in G1 phase, suggesting that a fraction of cells were still in the diploid cell cycle (Figure 5.3 A).

To understand if the broadened G2/M peak constituted of cells arrested in G2 or M phase, samples from Figure 5.3 A were stained for phosphor-serine histone H3 (pSer-H3), a measurement of mitotic index (MI) [185]. Phosphorylation of this histone occurs in late G2

and spreads through condensed chromatin during M phase. Dephosphorylation begins in the anaphase and is completed in telophase. In normal cycling cells the percentage of pSer-H3 cells is typically around 1.5 % to 3 % and can drop down to as low as 0.2 % after damaging agents such as IR [186].

HTETOP cells had around 1 % mitotic cells and continued to enter mitosis after doxycycline addition (Figure 5.4 A and B) increasing even to 1.5 % in day two. Similarly to what was previously noted, it was only after day four of depletion that the mitotic index fell below the control value to around 0.8 % [52]. By day five cells seemed to have reduced mitotic entry. When treated with Nocodazole, a microtubule polymerization inhibitor which blocks cells in metaphase, doxycycline untreated cells accumulated in M phase, from the base level of 1 % to 11 % (Figure 5.5 A and B). Conversely, Topo2α depleted cells did not show this accumulation, indicating that by day five cells did not enter M phase and were therefore not affected by the inhibitor. Together this data indicates that depletion of Topo2α initially allows for cells to keep entering mitosis until day five, by which the mitotic entry declines, and accumulation of 8N cells rises.

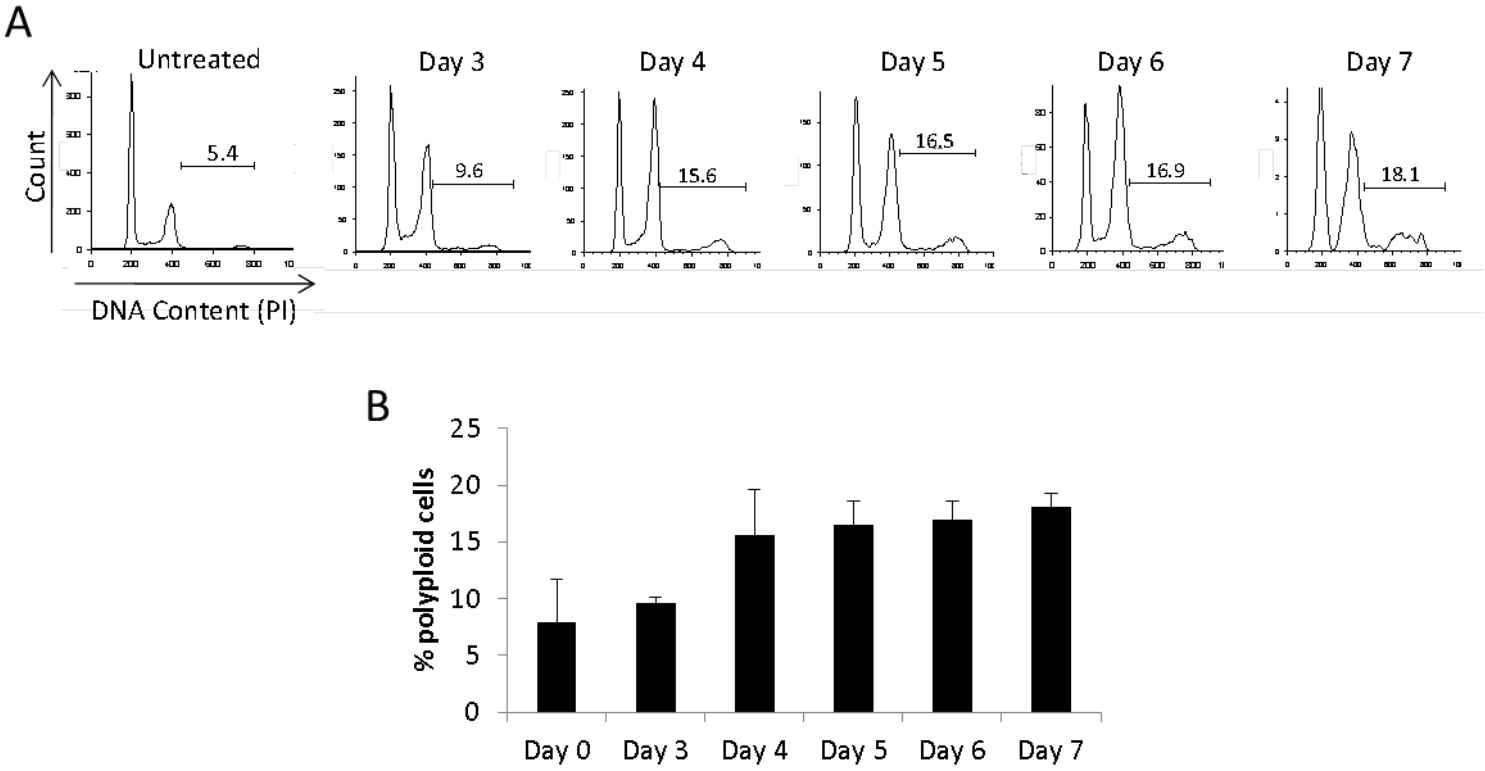

Figure 5.3 | Topo2α depletion increases polyploidization in HTETOP cells

HTETOP cells were grown in 1μM/ml doxycycline containing media and collected for analysis each day.

A. Representative FACS plots of cell samples prepared for DNA content analysis. The percentage of cells with >4N is depicted.

B. Quantification of cells with >4N represented in A. Error bars represent standard deviation from the mean.

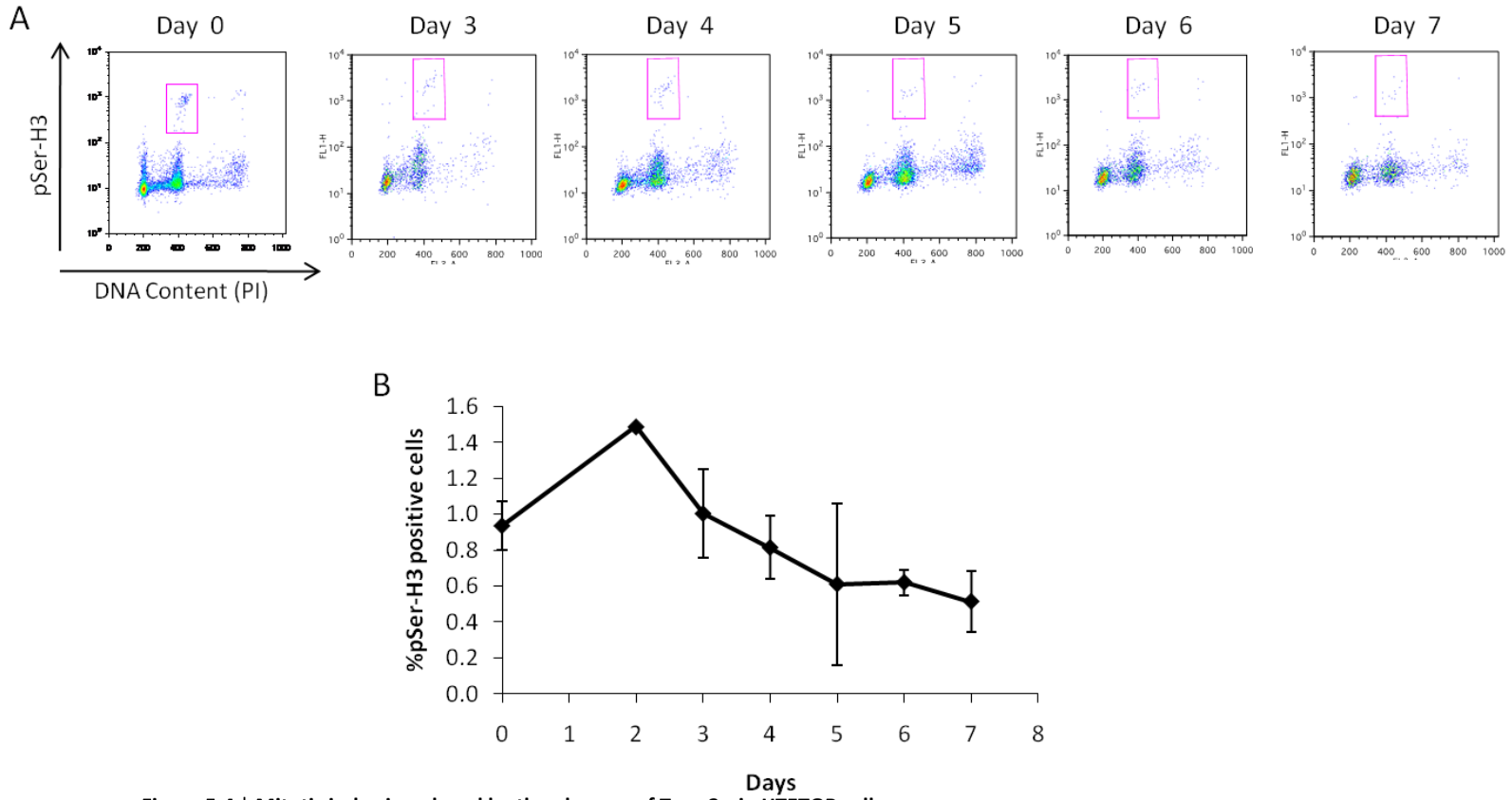

Figure 5.4 | Mitotic index is reduced by the absence of Topo2α in HTETOP cells

A. Representative FACS plots of cells stained for pSer-H3 and DNA content (PI). Cells were grown in the presence of 1 µM/ml doxycycline for indicated amount of days after which they were stained with pSer-H3 antibody and prepared for FACS analysis. The proportion of mitotic cells (mitotic index) was calculated by gating for pSer-H3 positive cells with 4N DNA content (squares).

B. Quantification of data represented in A. The MI (% pSer-H3 positive cells) at the indicated time points after treatment with one µM doxycycline is plotted. Data points are the means of at least three independent experiments. Error bars represent standard deviation from the mean.

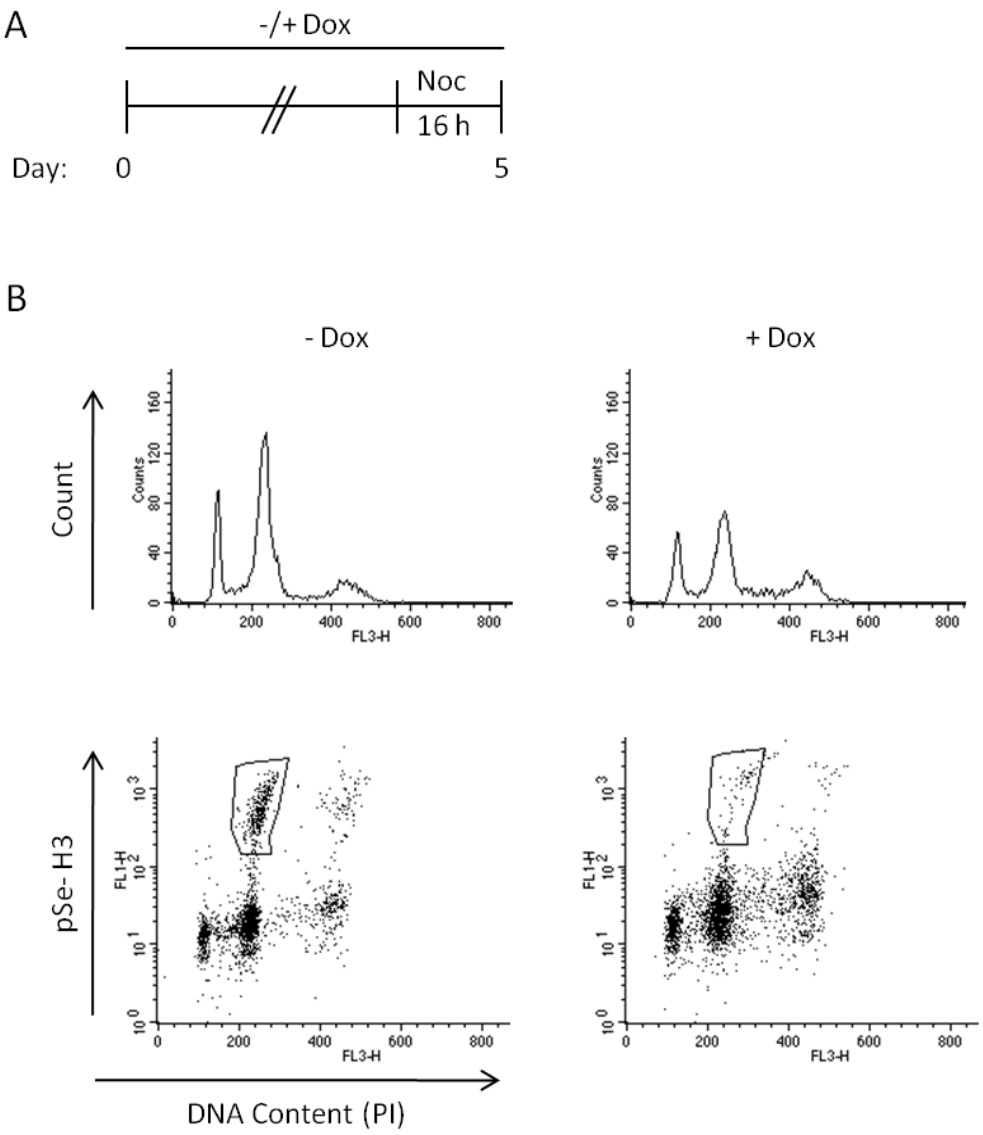

Figure 5.5 | Topo2α depleted HTETOP cells do not enter mitosis after five days

A. Experimental design. Cells were treated with 1 µM/ml doxycycline for five days and 50 nM Nocodazole was added during final 16 hours. They were stained with pSer-H3 antibody and prepared for FACS analysis.

B. The proportion of mitotic cells (mitotic index) was calculated by gating for pSer-H3 positive cells with 4N DNA content (gates).

5.4 Polyploidization after ICRF-193 treatment

To investigate if a similar polyploid phenotype arises when Topo2α is inhibited with ICRF-193, cells were continuously treated with 5 μM ICRF-193. This treatment completely reduced cell viability by day five and therefore analysis was only possible during the first four days (Figure 4.13). DNA content and pSer-H3 staining were measured using FACS analysis. As expected, cells were already blocked in G2/M after day one (Figure 5.6 A) accompanied by emptying of the G1 fraction. Interestingly, by day one the polyploid cell fraction increased from basal level of 5 % to 26 %, well above the levels in Topo2α depleted cells (Figure 5.6 B) and by day four 43 % of cells were in the polyploid fraction.

The broadened G2/M peak was not sustained by cells entering mitosis, as percentage of pSer-H3 positive cells dropped drastically to below 0.1 % by day two and remained there until day four (Figure 5.6 C and D). The delayed mitosis entry after ICRF-193 treatment is well established and is believed to be regulated by the G2 decatenation checkpoint [54].

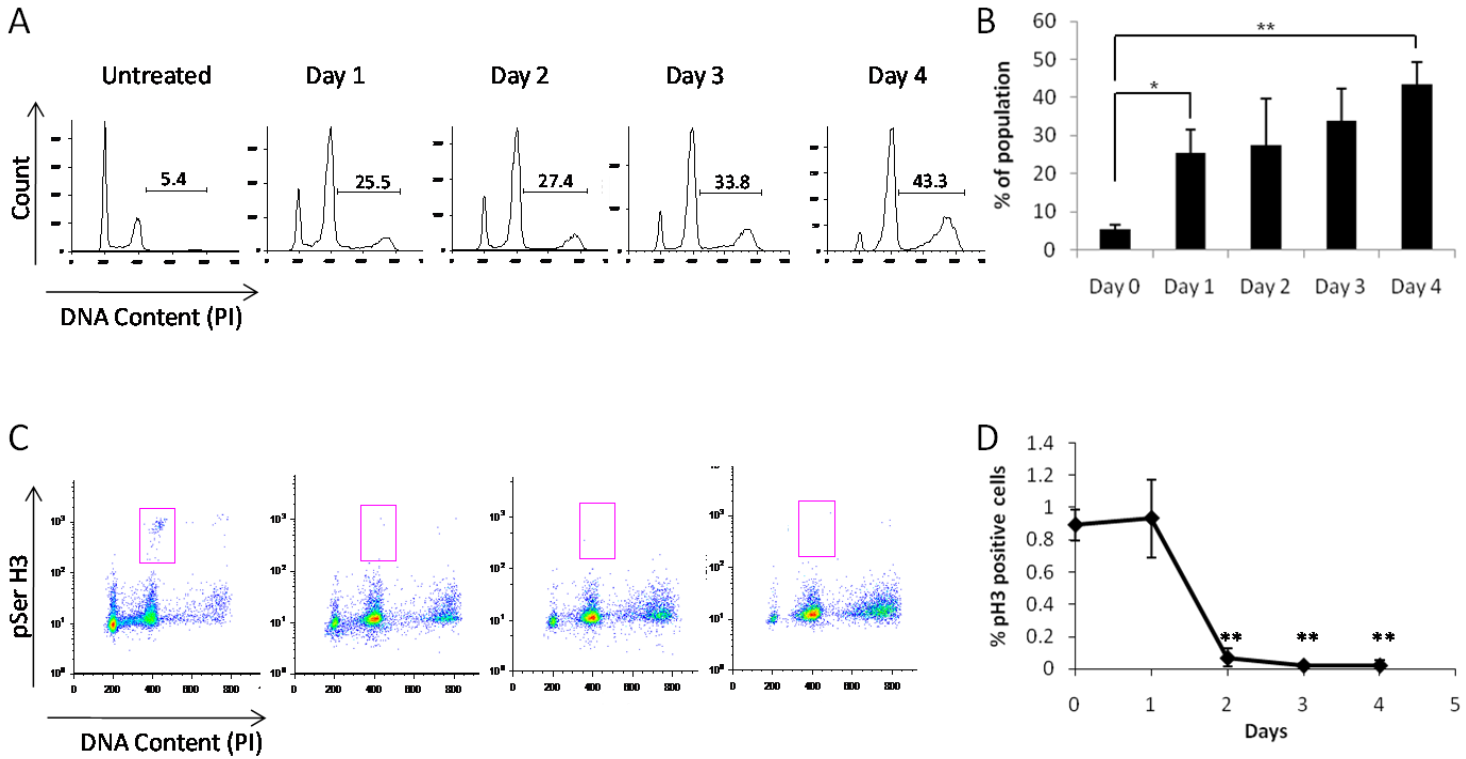

Figure 5.6 | ICRF-193 increases polyplodization and reduced mitotic index

HTETOP cells were grown in 5 ICRF-193 and collected for analysis each day.

A. Representative FACS plots of cell samples prepared for DNA content analysis. The percentage of cells with >4N is depicted.

B. Quantification of cells with >4N represented in A. Data points are the means of at least three independent experiments. Error bars represent standard deviation from the mean. Statistical significance in Student's *t*-test is indicated by two stars (p-value < 0.01) and one star (p-value < 0.05).

C. Representative FACS plots of cells stained for pSer-H3 and DNA content (PI).

D. Quantification of data represented in C. Data bars are the means of at least three independent experiments. Error bars represent standard deviation from the mean. Statistical significance (p-value < 0.01) in Student's *t*-test is indicated by two stars.

5.5 DNA damage after Topo2α depletion and inhibition

DNA damage is increasingly being recognized for its roles in promoting polyploidization. To investigate if damage is being generated during Topo2α depletion or ICRF-193 treatment cells were stained for p53 binding protein 1 (53BP1) foci. 53BP1 is used as a marker for DSB, as it is shown to relocalise to the sites of damage following IR treatment and is indicated in the early DSB repair response [10]. Cells that contained five or more large foci (defined as foci larger than 0.5 μm in diameter) were considered positive.

Depletion of Topo2α induced accumulation of 53BP1 foci by day four when close to 50 % of all cells were scored as positive (Figure 5.7 A and B). Additionally, the images show change in nuclei morphology. Large, irregular and bridged nuclei start to appear by day three, indicative of failed mitosis. Zeocin was used as a positive control as it has been shown to induce DSBs and also polyploidy through abrogated DDR [177].

ICRF-193 treated cells also accumulated 53BP1 foci albeit at much faster rate (Figure 5.8 A). After 24 hours almost 60 % of the cells had at least five large foci (Figure 5.8 B). This is consistent with the PFGE results that showed DSB induction, which was dose and time dependent (Figure 5.8 C). It has been shown that DSB repair inefficient CHO cells are sensitive to ICRF compounds. To investigate if this is consistent in human cells, glioblastoma MO59K and MO59J cells were treated with ICRF-193 for 24 hours and then released into fresh media. MO59K cells are wild type cells while MO59J completely lack DNA-PK_{CS}, a pivotal catalytic subunit in the NHEJ pathway, rendering the cells sensitive to IR and other DSB inducing agents [187]. Figure 5.8 D shows that MO50J reduced viability to a higher extent than MO59K cells after four to five days. These data shows that both depletion and inhibition of Topo2α lead to DNA damage. In the case of ICRF-193, the sensitivity of MO59J cells suggests that NHEJ is required to repair at least part of the damage and that if the damage is left unrepaired it leads to reduced viability.

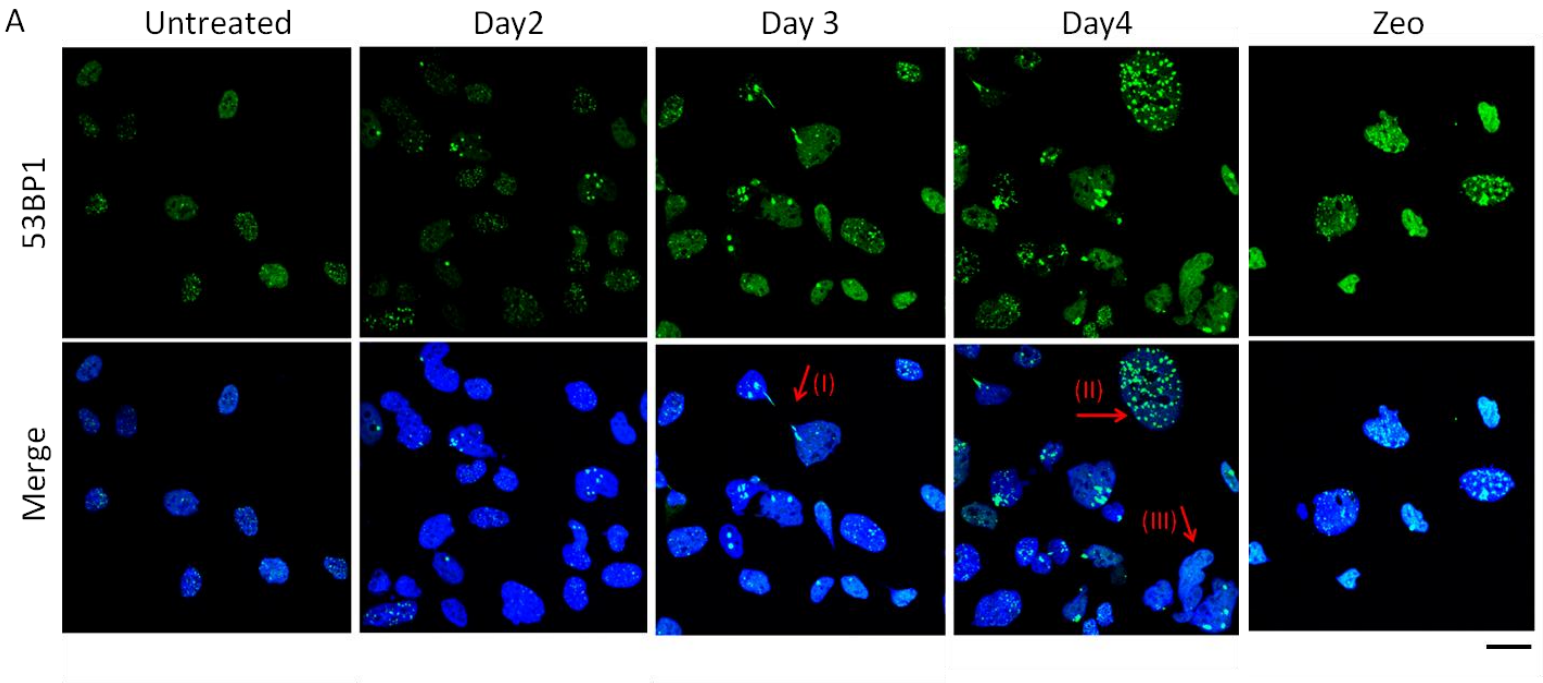

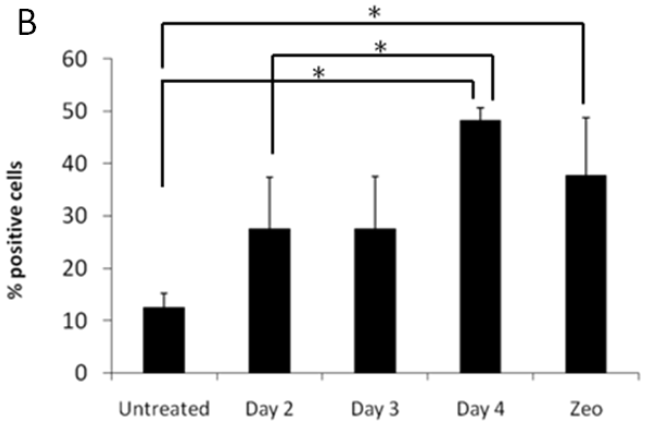

Figure 5.7 | 53BP1 foci are induced by the absence of Topo2α in HTETOP cells

A. Representative images of HTETOP cells treated with 1 µM/ml doxycycline for indicated amount of days. Cells treated with 100 µg/ml Zeocin for 48 hours served as a positive control Cells were stained for 53BP1 (green) and DNA (blue [To Pro]). Irregular nuclei structures are (I) DNA bridge (II) Large, regular nucleus (III) Large, irregular nucleus. Scale represents 10 µM.

B. Quantification of 53BP1 positive cells. Cells displaying five or more foci were regarded as positive (n > 200). Data bars are the means of at least three independent experiments. Error bars represent standard deviation from the mean. Statistical significance (p-value < 0.05) in Student's *t*-test is indicated by one star.

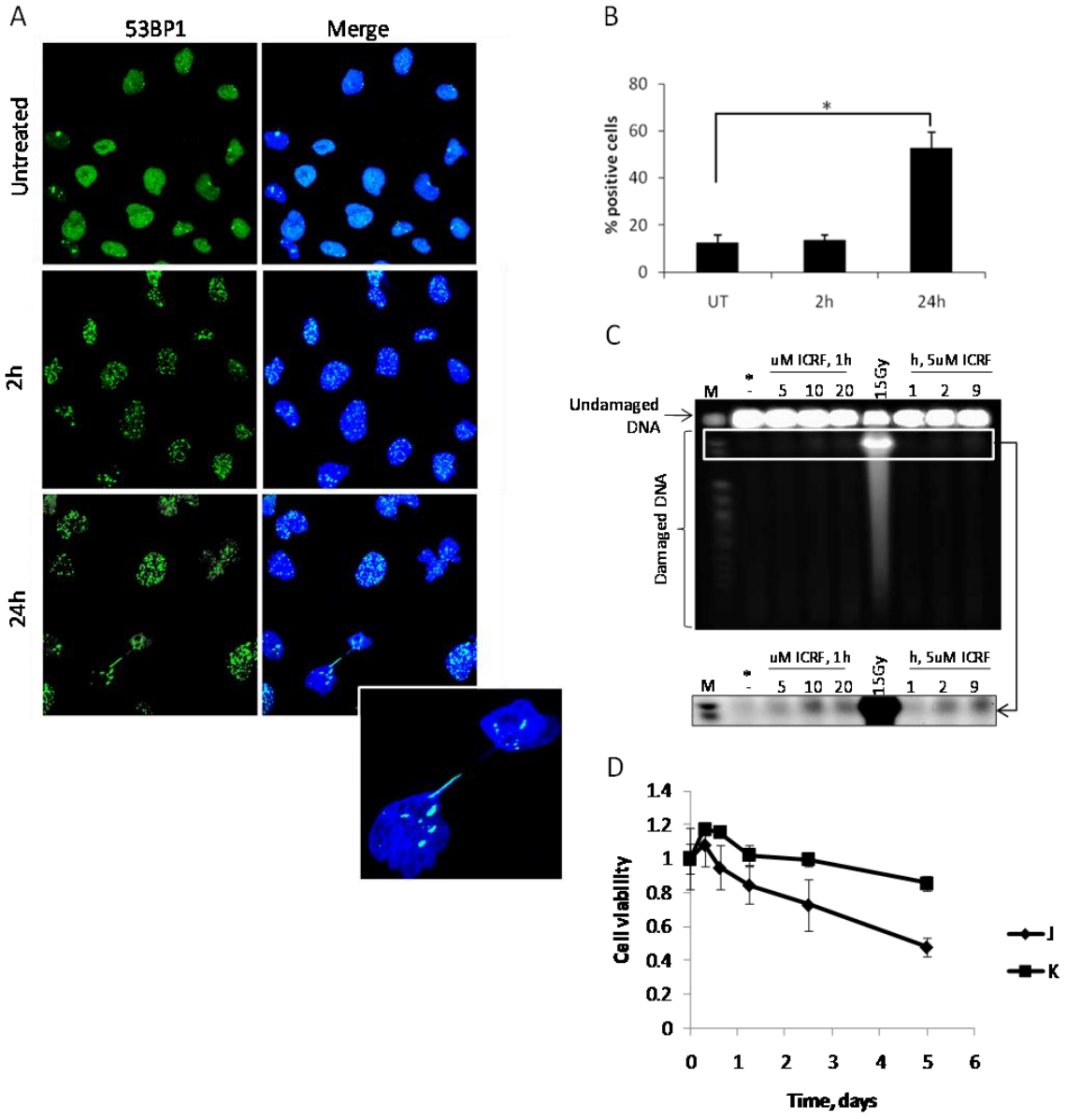

Figure 5.8 | ICRF-193 causes damage in HTETOP cells and sensitises NHEJ deficient cells

A. Representative images of HTETOP cells treated with 5 µM ICRF-193 for indicated times. Cells were stained for 53BP1 (green) and DNA (blue [To Pro]). Enlargement shows 53BP1 on the DNA bridge.

B. Quantification of 53BP1 positive cells. Cells displaying four or more foci were regarded as positive (n > 200). Data bars are the means of at least three independent experiments. Error bars represent standard deviation from the mean. Statistical significance (p-value < 0.05) in Student's *t*-test is indicated by one star. Marker, M.

C. PFGE gel stained with ethidium bromide. Cells were treated as indicated and then moulded into the plugs, except for IR treated cells that were irradiated in the plug. The exert shows overexposure.

D. Wild type MO59K (K) and DNA-PCcs deficient MO59J (J) cells were treated with 5 μM ICRF-193 for 24 hours and then released into fresh media for indicated amount of time. Cell viability was measured by resazurin assay. Measurements were performed on the same samples each day. X scale indicates days after release, with the first measurement at the time of release, after 24 hours of treatment. Data points are the (intra) mean from one experiment. Error bars represent standard deviation from the mean.

5.6 Discussion

The data represented in this chapter shows that both depletion and ICRF-193 inhibition of Topo2α leads to an accumulation of 8N cells, G2/M block, and a concurrent reduction of the MI. However, despite similar phenotype the two treatments differ in extent and kinetics – ICRF-193 treatment leads to an immediate cell cycle arrest in G2/M and a dramatic reduction of the MI. This is accompanied by a steady increase of polyploid cell fraction, which accumulates over 40% of the cells by day four of treatment. Depletion of Topo2α mimics the same trend, but the outcome never reaches the same intensity, even after seven days. It is reasonable to speculate that the initial response after doxycycline addition is delayed because of the time it takes to reach a full knock-down. According to Figure 4.1 C [52]and previous reports, the protein is reduced after 24 hours and not detectable after 48 hours [52]. However, the changes in phenotype following doxycycline addition measured here only appear after four days, suggesting there is a lag in the response.

5.6.1 ICRF-193 induced polyploidy

From this data it is only possible to speculate about which mechanism is responsible for the rise in polyploidy. Most research on Topo2α has been conducted using ICRF compounds and those reports have shed some light on the mechanisms of polyploidy induced by Topo2α inhibition [52, 188, 189]. Data suggests that the main pathway is through mitotic catastrophe and failed cytokinesis [52, 188, 189]. IF data in this chapter lends evidence to this hypothesis as can be seen in Figure 5.6 with appearance of DNA bridges and irregular nuclei. For these to appear, mitosis, and mainly anaphase, needs to have been attempted. Increase in DNA content without mitotic catastrophe, such as endoreduplication from S phase, leads to large, but regular nuclei. Therefore, FACS analysis can determine appearance of >4N cell fraction, while IF can be useful for availing the mechanism behind it. It would have been useful to have analysed the nuclei profile after longer ICRF-193 treatment to determine if there is an accumulation of irregular nuclei, although 24 hour treatment in Figure 5.7 A does already show appearance of these structures.

In case of ICRF-193, a possible hypothesis for polyploidy could be that the broadened G2/M peak seen in the FACS analysis is initially constituted by cells blocked in the G2 decatenation checkpoint. These cells eventually escape the checkpoint block and attempt mitosis in the first round of cell cycle, as can be seen in the unchanged mitotic index during day one. However, because segregation of chromosomes is unsuccessful, cells proceed through mitosis to an unsuccessful cytokinesis, and eventually forming the nuclear envelope around unsegregated, tetraploid chromosomes [188].

To follow the kinetics of appearance of cells in G1 state with 4N chromosomes ($G1_{tet}$) it is possible to stain for cyclin B protein followed by 2D FACS analysis. Although both $G1_{tet}$ and G2/M cells are in the 4N position, $G1_{tet}$ cells are negative for cyclin B staining

while G2/M cells have a positive cyclin B staining. Unfortunately this staining did not work in my hands.

The other possible way of polyploidy after ICRF-193 treatment is through bypass of M phase after G2 checkpoint activation (Figure 5.2 B) and a direct transition to $G1_{tet}$. It is possible that extended block in decatenation checkpoint, but also damage checkpoint in G2 could trigger this mechanism. Treatment of ICRF-193 was initially shown not to cause DNA damage [51, 53, 57] and the decatenation checkpoint activation after ICRF-193 was therefore believed to be distinct from the G2 damage checkpoint. The damage checkpoint relied on ATM activation, while ATR and BRCA1 were pivotal for the decatenation checkpoint [54]. However, several recent observations have challenged the view that ICRF-193 does not produce damage [70, 190-192], although the extent of the damage might be weaker as compared to topoisomerase II poisons. This issue remains controversial; however in this chapter I present evidence that HTETOP cells do accumulate damage after ICRF-193 treatment. The PFGE and damage foci analysis suggests that DSBs are accumulated in a time and dose dependent manner (Figure 5.8). Therefore it is conceivable that even G2 damage checkpoint is activated. Moreover, NHEJ deficient cells and HR deficient cells do show sensitivity towards ICRF-193 (Figure 5.8 D and [193-195]). These are the two major pathways for repairing DSB in a cell. Additionally, EM9 Chinese hamster ovary cell line, which is deficient in repair of both SSBs and DSBs due to a deficiency in the XRCC1 gene [196], was particularly sensitive to induction of polyploidy after ICRF-193 treatment as compared to the parental AA8 cell line [197]. More detailed analysis on where in the cell cycle damage occurs after ICRF-193 treatment is needed to determine the kinetics of the possible G2 damage checkpoint activation.

In conclusion there might be a mixture of mechanisms that lead to polyploidy after ICRF-193 treatment. Most data suggest that polyploidy arises through failed mitosis [54, 188], but Smith *et al.* do show that cells increase in size and DNA content while excluding cyclin B from the nucleus [189], indicating bypassed mitosis (Figure 5.9). Live cell imaging would be valuable to help unravel the mechanism of tetrapolidy on a single cell level as there might be different mechanisms that are masked by looking at a whole population. Imaging unlabelled cells would be useful as they can show attempted mitosis and furrow regression, but following labelled markers such as cyclin B kinetics with a cyclin B-GFP (Green Fluorescent Protein) plasmid could help extend understanding of the mechanism further. A recently developed live-cell imaging system, Fluorescent Ubiquitination-based Cell Cycle Indicator (FUCCI), would also be a valuable experimental system for following the cell cycle kinetics [198]. It is based on the alternating rise of geminin and Cdt1 levels throughout the cell cycle and visualising the two proteins by fluorescently tagged, but truncated protein forms [199]. In a normal cell the levels Cdt1 (red floroufor) rise in G1 to allow for licensing of replication origins. Geminin (green floroufor), an inhibitor of Cdt, starts accumulating in S, resulting in cells becoming yellow, before Cdt1 is degraded and only green geminin is visible in G2. Geminin is degraded during mitosis to allow for another Cdt1 peak in G1, ensuing a brief period of no fluorescence during mitosis. Cells that bypass mitosis would therefore lack the period without any marker. This system also allows for measuring the time spent in the different cell cycle phases. Unfortunately time constraints did not allow for finalisation of condition optimisation for this experiment.

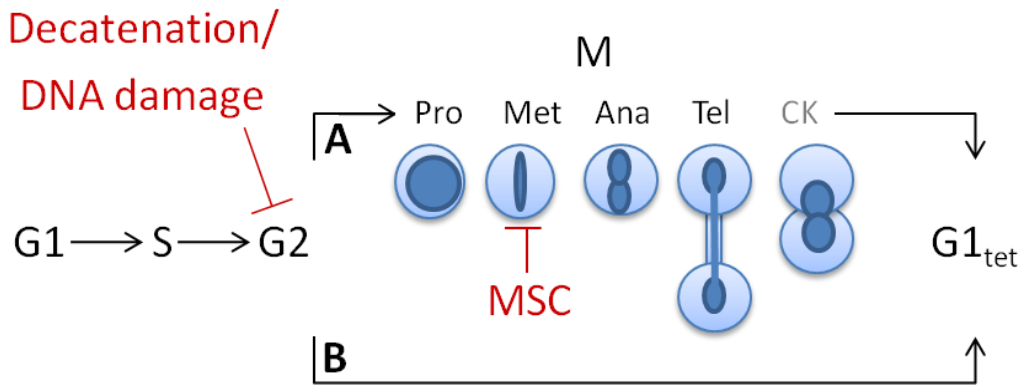

Figure 5.9 | Possible pathways to polyploidy after ICRF-193

Cell cycle checkpoints that are strong associated with preventing polyploidy are depicted in red.

A. Failed mitosis and evasion from checkpoints lead to a tetraploid G1 state.

B. Bypass of mitosis through checkpoint adaptation leads to G1 state with a tetraploid set of chromosomes that can lead to further polyploidization after consequent S phase.

G1 tetraploid cells, $G1_{tet}$; Mitotic Spindle Checkpoint, MSC; Prometaphase, Pro; Metaphase, Met; Anaphase, Ana; Telophase, Tel; Cytokinesis, CK.

5.6.2 *Topo2α depletion induced polyploidy*

The data represented in this chapter points towards a similar progression of events after Topo2α depletion as after ICRF-193 inhibition. However, there is a significant delay, even when time for the knock-down is accounted for, and a less significant effect on all parameters measured. A reasonable explanation for this discrepancy is that an inhibitor affects all the cells at the same time and therefore the effect is stronger and more evident. Alternatively, ICRF-193 could be unspecific. Previous publication and data presented in Chapter 4 would suggest that ICRF-193 does exert an effect even when cells have been pre-treated with doxycycline, depleting the target protein Topo2α [52].

An alternative interpretation of the discrepancy is that there is a true mechanistic difference between the two treatments. Few recent publications on the function of Topo2α have utilized knock-out or knock-down methods, but elucidation of Topo2α function has predominantly relied on usage of inhibitors, mainly ICRF derivatives. Mammalian cells were suggested to have a checkpoint sensitive to decatenation state, based on the observed G2 arrest after ICRF-193 treatment [53, 54]. Publications using mammalian cells where Topo2α was depleted noted instead that the mitotic entry was not blocked to the same extent or even unaffected [51, 52, 158]. Meanwhile, in yeast it was assumed that there is no decatenation checkpoint because yeast Topo2 depleted mutants do not arrest in G2, similar to a knock down in mammalian cells. In two recent reports however, authors generated new Topo2 yeast point mutants that render the protein catalytically inert. The mutant protein is capable of binding DNA but is unable to catalyse strand breakage, generating a similar structure as those generated after ICRF-193 treatment in mammalian cells. The mutant yeast strains were shown to undergo transient arrest in G2 which was Mec1 dependent (ATR yeast homologue), analogues to the phenotype of ICRF-193 treated mammalian cell [14, 200]. Therefore, it seems that even in yeast there is a difference between depletion and a catalytically inactive Topo2 protein with regards to the checkpoint activation. In conclusion, evidence from both yeast and mammalian cells indicate that a catalytically inactive protein, rather than catenated chromosomes, is sensed by the cell and required for activation of the decatenation point [51]. However it is difficult to imagine that the substrate for the decatenation checkpoint is an enzymatically inactive protein. This is especially problematic since ATR, which was described to be the apical kinase in the decatenation checkpoint, is activated by RPA coated ssDNA [107].

Lack of checkpoint activation after Topo2α depletion could be due to its direct involvement in checkpoint activation. In fact, this was recently shown in a publication in

which signalling by Topo2α was required for G2 decatenation checkpoint. Another putative scenario is that inhibition and depletion generate different DNA substrates, which affect the checkpoint differently. Namely, ICRF-193 inhibits Topo2α function by holding the enzyme as a closed clamp around the DNA substrate, which poses a physical barrier to any possible back-up protein that would be able to compensate for Topo2α. One scenario where a back-up pathway to a Topo2 mechanism might exist is during replication termination. Topo2 and Topo3 were suggested to act in two separate pathways when replication forks converge [16, 67] and there are currently evidence for both pathways [15, 46]. Therefore, if ICRF-193 blocked the replication termination substrate, not only would it be left unresolved, but also Topo3 as a back-up protein would not be able to access it. ssDNA would be generated by the replication helicase, flanking the ICRF-DNA substrate, which could serve to activate ATR. Conversely in case of depletion, the substrate would be left exposed for Topo3 to resolve the topological problems associated with converging replication forks.

The catalyticly inactive yeast Topo2 experiments lend evidence to this hypothesis. The inactive Topo2 strain accumulated incompletely replicated, gaped and nicked DNA molecules indicative of incomplete replication. Furthermore, the point mutant, similar to ICRF-193 treatment, activated the Mec1 checkpoint response at the end of S phase, comparable to the G2 decatenation checkpoint in mammalian cells. Depletion of Topo2 on the other hand did not activated Mec1 until after cytokinesis in the G1 phase of the second cell cycle, suggesting cells had to undergo cytokinesis to accumulate damage.

If the Topo3 pathway is able to compensate during replication termination, the model suggests that the fully replicated chromatids would not be catenated when mitosis begins (Figure 1.3). This is because the model suggests that each turn in the double-helix remaining between the two converging forks is first separated by the helicase, then nicked and

unwound by Topo3, and subsequently replicated by the polymerase to generate two decatenated strands. This questions the essential role of Topo2 during M phase in a Topo2 depleted cell. An explanation could be that Topo2 is indispensable for replication termination especially for sites which are hard to replicate, such as ribosomal DNA (rDNA) which is not resolved until mitosis, or centromeres [14, 201]. Alternatively the essential role of Topo2 in mitosis could also be partially due to suggested part of the midbody during cytokinesis [202]. This could be supported by the observation that in Topo2 depleted yeast cells, damage does not occur in anaphase but during cytokinesis [203]. Inevitably much additional work will have to be performed to better understand the exact mechanism and the proteins involved in replication termination.

While it has not been possible to provide definite answers to how polyploidy arises after Topo2α depletion the appearance of the IF images of doxycycline treated cells show appearance of irregular and bridged nuclei. Polyploidy is therefore seemingly a result of attempted mitosis and possibly MC, as opposed to bypassed mitosis. However, it is hard to assign an exact mechanism from the limited data presented here. Since Topo2α depletion leads to DNA damage after several days, there is a possibility that subsets of cells keep Cdk activity levels low after checkpoint activation and are able to accumulate $G1_{tet}$ cells without entering mitosis.

In conclusion more work is needed to firmly establish how cells become tetraploid after Topo2α depletion and how checkpoints are activated. It would be useful to follow DDR activation and the kinetic of it, including ATM and ATR activation, as well as downstream events such as cyclin B/Cdk1 activation.

Chapter 6

Conclusions

6 Conclusions and future perspectives

The initial aim of my thesis was to better understand the role of WRN protein, a RecQ helicase involved in several DNA metabolic pathways, mainly replication and repair. I performed an siRNA screen with a DNA repair and signalling library in WRN deficient cells with the aim to find SLIs with WRN and gain further understanding of its cellular function. WRN is reported to be epigentically silenced in 37% of colorectal cancers, which also correlates with a better prognosis after treatment with irinotecan (a CPT analogue), as silencing of WRN renders tumours more sensitive to irinotecan. Identifying SLIs can expand the understanding of a protein's function and can assist in defining its cellular mechanisms as well as providing opportunities for new treatment of cancer [85]. An SLI screen is a hypothesis forming experiment, where the relationship between the two genes needs to be explored in further detail to fully grasp the reason behind the synthetic lethality. The screen described in this thesis identified two proteins that, when depleted, resulted in increased lethality in WRN deficient cells: Chk1 and Topo2α. These proteins were thus used as a starting point for further hypothesis testing and are the basis for the rest the work in my thesis.

Chk1 acts as a pivotal mediator of the S phase checkpoint and is essential in promoting replication fork restart after stalling [204]. WRN protein is implicated in the recovery of stalled replication forks, where loss of WRN causes S phase defects and hypersensitivity to replication interfering agents . It is not unimaginable that these two proteins are somehow interdependent on each other during S phase. Indeed, a report published in 2010 by Ammazzalorso *et al.* [81, 205] showed that at stalled replication forks WRN and Chk1 act in compensatory ways to prevent fork collapse and DSB accumulation.

Loss of WRN resulted in fork collapse after stalling, which required Rad51-mediated recovery activated by Chk1.

The identification of Topo2α as synthetic lethal to WRN was an interesting result as it has been suggested that Topo2 interacts with a RecQ helicase for decatenation. In a paper published previous to the performed screen, it was indicated that Topo2α and WRN protein coimmunoprecipitate after treatment with topoisomerase inhibitor ICRF-193 and that the G2 decatenation checkpoint was abrogated in WRN cells, as indicated by lack of BRCA1 phosphorylation . Additionally, the authors demonstrate that while WRN deficient cells accumulated damage in the subsequent S phase, wild type cells did not, even when forced to enter S phase by overriding the G2 decatenation checkpoint by caffeine treatment.

Although the Topo2α results were promising and would have been interesting to follow up, I was unable to confirm the SLI between WRN and Topo2α in other cell lines. For this reason the focus of the thesis shifted towards characterising Topo2α and its role during replication.

Research on Topo2α is engaging for several reasons. To begin with, at the time the research was undertaken the division of labour between Topo1 and Topo2 during replication elongation was still unclear. A unique single-molecule analysis of DNA replication fork, the DNA fibre analysis, was available in the laboratory and could help test the hypothesis that Topo2α might be involved in alleviating topological stress during elongation. In fact, DNA fibre analysis was used in a recent publication by Tuduri *et al.* to identify Topo1 as the main topoisomerase in replication progression [43, 93, 205]. In the future it would be interesting to test if Topo2α can act as a back-up for Topo1 in mammalian cells as in yeast the double knock-out has a more severe phenotype as compared to individual mutants [44]. This research was attempted during the thesis, but knock-down of Topo1 was unsuccessful.

In addition to gaining a fundamental understanding of the role of topoisomerases in replication, this research may also have a clinical application. Topoisomerases 1 and 2 are the main targets for two large groups of front-line anticancer drugs. Although these treatments can be highly effective, many tumours do not respond to treatment or become resistant to it upon relapse. It is documented that sensitivity to these drugs depends on the expression levels of the respective proteins. In the case of Topo2α, deletion of *Topo2α* leads to primary chemoresistance in tumours. Equally, amplification of *Topo2α* results in a better response to Topo2 inhibitors [206]. Alterations in copy number of the *Topo2α* gene are frequent as its chromosomal location is close to the *HER-2* gene, one of the most frequently amplified oncogenes in breast cancer. An analogous situation has been indicated for Topo1 where protein expression is reduced as a response to Topo1 targeted treatment [58]. More interestingly, resistance to Topo1 inhibitors is often accompanied by concomitant upregulation of Topo2α levels and vice versa. This suggests that the two proteins can compensate for each other and that this is a potential caveat in an otherwise highly efficient treatment protocol. Understanding the mechanism behind Topo1 and Topo2α compensation could lead to better treatment of cancer. One such improvement could be to treat patients with Topo1 and Topo2 inhibitors concurrently.

The other interesting future direction of Topo2α research is to investigate its role in replication termination. Currently the mechanism of termination and the proteins involved is elusive. The topological problems when two forks converge were defined several years ago suggesting Topo2's involvement based on its biochemical properties . Evidence for this pathway is emerging, however, the methods available to study termination in mammalian cells are unreliable and at the moment the existing publications use prokaryotes, frog or yeast as experimental models [14-16, 46]. Experiments in U2OS and HTETOP cells showed that Topo2α depletion increased levels of ssDNA regions in mitotic cells and that these were

adjacent to newly replicated DNA. Topo2α activity was also required to remove PCNA from chromatid, suggesting that PCNA might be retained at sites of replication termination (H. Gad, personal communication). More extensive research as well as new experimental methods will be needed to understand how Topo2α is involved in replication termination in mammalian cells.

7 References

1. Pommier, Y., Leo, E., Zhang, H., and Marchand, C., *DNA Topoisomerases and Their Poisoning by Anticancer and Antibacterial Drugs.* Chemistry & biology, 2010. **17**(5): 421-433.
2. Schvartzman, J.B. and Stasiak, A., *A topological view of the replicon.* EMBO reports, 2004. **5**(3): 256-61.
3. Liu, L.F. and Wang, J.C., *Supercoiling of the DNA template during transcription.* Proc. Natl Acad. Sci. USA, 1987. **84**: 7024-7027.
4. Kanaar, R. and Cozzarelli, N.R., *Roles of supercoiled DNA structure in DNA transactions.* Current Opinion in Structural Biology, 1992. **2**(3): 369-379.
5. McClendon, A.K. and Osheroff, N., *DNA topoisomerase II, genotoxicity, and cancer.* Mutation Research/Fundamental and Molecular Mechanisms of Mutagenesis, 2007. **623**(1-2): 83-97.
6. Nelson, D.L., Cox, M., M., *Lehninger Principles of Biochemistry, 3rd edition*. 2001.
7. Wang, J.C., *Cellular roles of DNA topoisomerases: a molecular perspective.* Nat Rev Mol Cell Biol, 2002. **3**(6): 430-440.
8. Champoux, J. and Been, M., *Mechanistic Studies of DNA Replication and Genetic Recombination: ICN-UCLA Symposia on Molecular and Cellular Biology*. 1980, European Molecular Biology Organization. 809-815.
9. Peter, B.J., Ullsperger, C., Hiasa, H., Marians, K.J., and Cozzarelli, N.R., *The structure of supercoiled intermediates in DNA replication.* Cell, 1998. **94**: 819-827.
10. Wang, B., Matsuoka, S., Carpenter, P.B., and Elledge, S.J., *53BP1, a Mediator of the DNA Damage Checkpoint.* Science, 2002. **298**(5597): 1435-1438.
11. Gangloff, S., McDonald, J.P., Bendixen, C., Arthur, L., and Rothstein, R., *The yeast type I topoisomerase Top3 interacts with Sgs1, a DNA helicase homolog: a potential eukaryotic reverse gyrase.* Mol. Cell. Biol., 1994. **14**: 8391-8398.
12. Sundin, O. and Varshavsky, A., *Terminal stages of SV40 DNA replication proceed via multiply intertwined catenated dimers.* Cell, 1980. **21**: 103-114.
13. Sundin, O. and Varshavsky, A., *Arrest of segregation leads to accumulation of highly intertwined catenated dimers: Dissection of the final stages of SV40 DNA replication.* Cell, 1981. **25**(3): 659-669.
14. Baxter, J. and Diffley, J.F.X., *Topoisomerase II Inactivation Prevents the Completion of DNA Replication in Budding Yeast.* Molecular Cell, 2008. **30**(6): 790-802.
15. Suski, C. and Marians, K.J., *Resolution of Converging Replication Forks by RecQ and Topoisomerase III*. Molecular Cell, 2008. **30**(6): 779-789.
16. Wang, J.C., *DNA topoisomerases: why so many?* Journal of Biological Chemistry, 1991. **266**(11): 6659-6662.
17. Nitiss, J.L., *Targeting DNA topoisomerase II in cancer chemotherapy.* Nat Rev Cancer, 2009. **9**(5): 338-350.
18. Champoux, J.J., *DNA topoisomerases: structure, function, and mechanism.* Annu. Rev. Biochem., 2001. **70**: 369-413.
19. Corbett, K.D. and Berger, J.M., *Strucutre, molecular mechanisms, and evolutionary relationships in DNA topoisomerases.* Annual Review of Biophysics and Biomolecular Structure, 2004. **33**(1): 95-118.
20. Wang, J.C., *Interaction between DNA and an Escherichia coli protein omega.* J. Mol. Biol., 1971. **55**: 523-533.

21. Kirkegaard, K. and Wang, J.C., *Bacterial DNA topoisomerase I can relax positively supercoiled DNA containing a single-stranded loop.* J. Mol. Biol., 1985. **185**: 625-637.
22. Yang, J., Bachrati, C.Z., Ou, J., Hickson, I.D., and Brown, G.W., *Human Topoisomerase III alpha Is a Single-stranded DNA Decatenase That Is Stimulated by BLM and RMI1.* Journal of Biological Chemistry, 2010. **285**(28): 21426-21436.
23. Bergerat, A., *An atypical topoisomerase II from Archaea with implications for meiotic recombination.* Nature, 1997. **386**: 414-417.
24. Nichols, M.D., DeAngelis, K., Keck, J.L., and Berger, J.M., *Structure and function of an archaeal topoisomerase VI subunit with homology to the meiotic recombination factor Spo11.* EMBO J., 1999. **18**: 6177-6188.
25. Nitiss, J.L., *Investigating the biological functions of DNA topoisomerases in eukaryotic cells.* Biochim. biophys. Acta, 1998. **1400**: 63-81.
26. Forterre, P., *Genomics and early cellular evolution. The origin of the DNA world.* C. R. Acad. Sci. III, 2001. **324**: 1067-1076.
27. Lee, M.P., Brown, S.D., Chen, A., and Hsieh, T.S., *DNA topoisomerase I is essential in Drosophila melanogaster.* Proceedings of the National Academy of Sciences of the United States of America, 1993. **90**(14): 6656-60.
28. Goto, T., and Wang, J.C., *Cloning of yeast TOPI, the gene encoding DNA topoisomerase I, and construction of mutants defective in both DNA topoisomerase I and DNA topoisomerase II.* Proc. Nati. Acad. Sci. USA, 1985. **82**: 7178-7182.
29. Wallis, J.W., Chrebet, G., Brodsky, G., Rolfe, M., and Rothstein, R., *A hyper-recombination mutation in S. cerevisiae identifies a novel eukaryotic topoisomerase.* Cell, 1989. **58**: 409-419.
30. Morham, S.G., Kluckman, K.D., Voulomanos, N., and Smithies, O., *Targeted disruption of the mouse topoisomerase I gene by camptothecin selection.* Mol. Cell. Biol., 1996. **16**: 6804-6809.
31. Yang, X., Li, W., Prescott, E.D., Burden, S.J., and Wang, J.C., *DNA topoisomerase IIβ and neural development.* Science, 2000. **287**: 131-134.
32. St. Pierre, J., Wright, D.J., Rowe, T.C., and Wright, S.J., *DNA topoisomerase II is essential for preimplantation mouse development.* Molecular Reproduction and Development, 2002. **61**(3): 347-357.
33. Li, W. and Wang, J.C., *Mammalian DNA topoisomerase IIIα is essential in early embryogenesis.* Proc. Natl Acad. Sci. USA, 1998. **95**: 1010-1013.
34. Kwan, K.Y. and Wang, J.C., *Mice lacking DNA topoisomerase IIIβ develop to maturity but show a reduced mean lifespan.* Proc. Natl Acad. Sci. USA, 2001. **98**: 5717-5721.
35. Zhang, H., Meng, L.-H., and Pommier, Y., *Mitochondrial topoisomerases and alternative splicing of the human TOP1mt gene.* Biochimie, 2007. **89**(4): 474-481.
36. Kampranis, S.C., Bates, A.D., and Maxwell, A., *A model for the mechanism of strand passage by DNA gyrase.* Proc. Natl Acad. Sci. USA, 1999. **96**: 8414-8419.
37. Wang, J.C., *DNA topoisomerases.* Annu. Rev. Biochem., 1996. **65**: 635-692.
38. Berger, J.M., Gamblin, S.J., Harrison, S.C., and Wang, J.C., *Structure and mechanism of DNA topoisomerase II.* Nature, 1996. **379**: 225-232.
39. Classen, S., Olland, S., and Berger, J.M., *Structure of the topoisomerase II ATPase region and its mechanism of inhibition by the chemotherapeutic agent ICRF-187.* Proc. Natl Acad. Sci. USA, 2003. **100**: 10629-10634.
40. Deweese, J.E. and Osheroff, N., *The use of divalent metal ions by type II topoisomerases.* Metallomics, 2010. **2**(7): 450-459.
41. Nitiss, J.L., *DNA topoisomerase II and its growing repertoire of biological functions.* Nat Rev Cancer, 2009. **9**(5): 327-337.

42. Austin, C.A. and Marsh, K.L., *Eukaryotic DNA topoisomerase IIβ.* BioEssays, 1998. **20**(3): 215-226.
43. Tuduri, S., Crabbe, L., Conti, C., Tourriere, H., Holtgreve-Grez, H., Jauch, A., Pantesco, V., De Vos, J., Thomas, A., Theillet, C., Pommier, Y., Tazi, J., Coquelle, A., and Pasero, P., *Topoisomerase I suppresses genomic instability by preventing interference between replication and transcription.* Nat Cell Biol, 2009. **11**(11): 1315-1324.
44. Bermejo, R., Doksani, Y., Capra, T., Katou, Y.-M., Tanaka, H., Shirahige, K., and Foiani, M., *Top1- and Top2-mediated topological transitions at replication forks ensure fork progression and stability and prevent DNA damage checkpoint activation.* Genes & Development, 2007. **21**(15): 1921-1936.
45. Li, H., Wang, Y., and Liu, X., *Plk1-dependent Phosphorylation Regulates Functions of DNA Topoisomerase IIalpha in Cell Cycle Progression.* Journal of Biological Chemistry, 2008. **283**(10): 6209-6221.
46. Fachinetti, D., Bermejo, R., Cocito, A., Minardi, S., Katou, Y., Kanoh, Y., Shirahige, K., Azvolinsky, A., Zakian, V.A., and Foiani, M., *Replication Termination at Eukaryotic Chromosomes Is Mediated by Top2 and Occurs at Genomic Loci Containing Pausing Elements.* Molecular Cell, 2010. **39**(4): 595-605.
47. Storchova, Z. and Kuffer, C., *The consequences of tetraploidy and aneuploidy.* J Cell Sci, 2008. **121**(23): 3859-3866.
48. Holm, C., Covey, J.M., Kerrigan, D., and Pommier, Y., *Differential requirement of DNA replication for the cytotoxicity of DNA topoisomerase I and II inhibitors in Chinese hamster DC3F cells.* Cancer Res., 1989. **49**: 6365-6368.
49. Spell, R.M. and Holm, C., *Nature and distribution of chromosomal intertwinings in Saccharomyces cerevisiae.* Mol. Cell. Biol., 1994. **14**: 1465-1476.
50. Holm, C., Stearns, T., and Botstein, D., *DNA topoisomerase II must act at mitosis to prevent nondisjunction and chromosome breakage.* Mol. Cell. Biol., 1989. **9**: 159-168.
51. Bower, J.J., Karaca, G.F., Zhou, Y., Simpson, D.A., Cordeiro-Stone, M., and Kaufmann, W.K., *Topoisomerase IIα maintains genomic stability through decatenation G2 checkpoint signaling.* Oncogene, 2010. **29**(34): 4787-4799.
52. Carpenter, A.J. and Porter, A.C., *Construction, characterization, and complementation of a conditional-lethal DNA topoisomerase IIalpha mutant human cell line.* Mol. Biol. Cell, 2004. **15**: 5700-5711.
53. Downes, C.S., Clarke, D.J., Mullinger, A.M., Gimenez-Abian, J.F., Creighton, A.M., and Johnson, R.T., *A topoisomerase II-dependent G2 cycle checkpoint in mammalian cells.* Nature, 1994. **372**(6505): 467-470.
54. Deming, P.B., Cistulli, C.A., Zhao, H., Graves, P.R., Piwnica-Worms, H., Paules, R.S., Downes, C.S., and Kaufmann, W.K., *The human decatenation checkpoint.* Proceedings of the National Academy of Sciences of the United States of America, 2001. **98**(21): 12044-12049.
55. Chang, C.-J., Goulding, S., Earnshaw, W.C., and Carmena, M., *RNAi analysis reveals an unexpected role for topoisomerase II in chromosome arm congression to a metaphase plate.* J Cell Sci, 2003. **116**(23): 4715-4726.
56. Coelho, P.A., Queiroz-Machado, J., Carmo, A.M., Moutinho-Pereira, S., Maiato, H., and Sunkel, C.E., *Dual Role of Topoisomerase II in Centromere Resolution and Aurora B Activity.* PLoS Biol, 2008. **6**(8): e207.
57. Larsen, A.K., Escargueil, A.E., and Skladanowski, A., *Catalytic topoisomerase II inhibitors in cancer therapy.* Pharmacology & Therapeutics, 2003. **99**(2): 167-181.
58. Burgess, D.J., *Topoisomerase levels determine chemotherapy response in vitro and in vivo.* Proc. Natl Acad. Sci. USA, 2008. **105**: 9053-9058.

59. Bakkenist, C.J. and Kastan, M.B., *DNA damage activates ATM through intermolecular autophosphorylation and dimer dissociation.* Nature, 2003. **421**: 499-506.
60. Kaufmann, S.H., *Cell death induced by topoisomerase-targeted drugs: more questions than answers.* Biochim. Biophys. Acta, 1998. **1400**: 195-211.
61. Kaufmann, W.K., *Human topoisomerase II function, tyrosine phosphorylation and cell cycle checkpoints.* Proc. Soc. Exp. Biol. Med., 1998. **217**: 327-334.
62. Jensen, P.B. and Sehested, M., *DNA topoisomerase II rescue by catalytic inhibitors - a new strategy to improve the antitumor selectivity of etoposide.* Biochem. Pharmacol., 1997. **54**: 755-759.
63. Fortune, J.M. and Osheroff, N., *Merbarone inhibits the catalytic activity of human topoisomerase II[alpha] by blocking DNA cleavage.* J. Biol. Chem., 1998. **273**: 17643-17650.
64. Clifford, B., Beljin, M., Stark, G.R., and Taylor, W.R., *G2 arrest in response to topoisomerase II inhibitors: the role of p53.* Cancer Res., 2003. **63**: 4074-4081.
65. Nitiss, J.L., Pourquier, P., and Pommier, Y., *Aclacinomycin A stabilizes topoisomerase I covalent complexes.* Cancer Res., 1997. **57**: 4564-4569.
66. Perrin, D., van Hille, B., and Hill, B.T., *Differential sensitivities of recombinant human topoisomerase II[alpha] and [beta] to various classes of topoisomerase II-interacting agents.* Biochemical Pharmacology, 1998. **56**(4): 503-507.
67. Luo, K., Yuan, J., Chen, J., and Lou, Z., *Topoisomerase II alpha controls the decatenation checkpoint.* Nat Cell Biol, 2009. **11**(2): 204-210.
68. Skoufias, D.A., Lacroix, F.B., Andreassen, P.R., Wilson, L., and Margolis, R.L., *Inhibition of DNA Decatenation, but Not DNA Damage, Arrests Cells at Metaphase.* 2004. **15**(6): 977-990.
69. Wang, L. and Eastmond, D.A., *Catalytic inhibitors of topoisomerase II are DNA-damaging agents: induction of chromosomal damage by merbarone and ICRF-187.* Environ. Mol. Mutagen., 2002. **39**: 348-356.
70. Huang, K.C., *Topoisomerase II poisoning by ICRF-193.* J. Biol. Chem., 2001. **276**: 44488-44494.
71. Linka, R.M., *C-terminal regions of topoisomerase II alpha and II beta determine isoform-specific functioning of the enzymes in vivo.* Nucleic Acids Res., 2007. **35**: 3810-3822.
72. Lyu, Y.L. and Wang, J.C., *Aberrant lamination in the cerebral cortex of mouse embryos lacking DNA topoisomerase II[beta]*. Proc. Natl Acad. Sci. USA, 2003. **100**: 7123-7128.
73. Lyu, Y.L., Lin, C.-P., Azarova, A.M., Cai, L., Wang, J.C., and Liu, L.F., *Role of Topoisomerase II beta in the Expression of Developmentally Regulated Genes.* Mol. Cell. Biol., 2006. **26**(21): 7929-7941.
74. Ju, B.G., *A topoisomerase II[beta]-mediated dsDNA break required for regulated transcription.* Science, 2006. **312**: 1798-1802.
75. Ju, B.G. and Rosenfeld, M.G., *A breaking strategy for topoisomerase II[beta]/PARP-1-dependent regulated transcription.* Cell Cycle, 2006. **5**: 2557-2560.
76. Williamson, L.M. and Lees-Miller, S.P., *Estrogen receptor alpha-mediated transcription induces cell cycle-dependent DNA double strand breaks.* Carcinogenesis, 2010. **32**(3): 279-285.
77. Pedersen-Bjergaard, J., Andersen, M.K., Christiansen, D.H., and Nerlov, C., *Genetic pathways in therapy-related myelodysplasia and acute myeloid leukemia.* Blood, 2002. **99**(6): 1909-1912.
78. Azarova, A.M., *Roles of DNA topoisomerase II isozymes in chemotherapy and secondary malignancies.* Proc. Natl Acad. Sci. USA, 2007. **107**: 11014-11019.
79. Werner, O., *On cataract in conjunction with scleroderma*, in *Royal Ophthalmology Clinic*. 1904, Royal Christian Albrecht University of Kiel: Kiel.

80. Bennett, R.J. and Keck, J.L., *Structure and function of RecQ DNA helicases.* Crit Rev Biochem Mol Biol, 2004. **39**(2): 79-97.
81. Hickson, I.D., *RecQ helicases: caretakers of the genome.* Nat Rev Cancer, 2003. **3**(3): 169-178.
82. Hanada, K. and Hickson, I.D., *Molecular genetics of RecQ helicase disorders.* Cell Mol Life Sci, 2007. **64**(17): 2306-2322.
83. Yu, C.E., Oshima, J., Fu, Y.H., Wijsman, E.M., Hisama, F., Alisch, R., Matthews, S., Nakura, J., Miki, T., Ouais, S., Martin, G.M., Mulligan, J., and Schellenberg, G.D., *Positional cloning of the Werner's syndrome gene.* Science, 1996. **272**(5259): 258-62.
84. Cheng, W.H., Muftuoglu, M., and Bohr, V.A., *Werner syndrome protein: Functions in the response to DNA damage and replication stress in S-phase.* Exp Gerontol, 2007. **42**(9): 871-878.
85. Agrelo, R., Cheng, W.-H., Setien, F., Ropero, S., Espada, J., Fraga, M.F., Herranz, M., Paz, M.F., Sanchez-Cespedes, M., Artiga, M.J., Guerrero, D., Castells, A., von Kobbe, C., Bohr, V.A., and Esteller, M., *Epigenetic inactivation of the premature aging Werner syndrome gene in human cancer.* Proceedings of the National Academy of Sciences, 2006. **103**(23): 8822-8827.
86. Nakayama, H., Nakayama, K., Nakayama, R., Irino, N., Nakayama, Y., and Hanawalt, P.C., *Isolation and genetic characterization of a thymineless death-resistant mutant of Escherichia coli K12: identification of a new mutation (recQ1) that blocks the RecF recombination pathway.* Mol Gen Genet, 1984. **195**(3): 474-80.
87. Brosh, R.M., Jr., Orren, D.K., Nehlin, J.O., Ravn, P.H., Kenny, M.K., Machwe, A., and Bohr, V.A., *Functional and physical interaction between WRN helicase and human replication protein A.* J Biol Chem, 1999. **274**(26): 18341-50.
88. Shen, J.C., Gray, M.D., Oshima, J., and Loeb, L.A., *Characterization of Werner syndrome protein DNA helicase activity: directionality, substrate dependence and stimulation by replication protein A.* Nucleic Acids Res, 1998. **26**(12): 2879-85.
89. Constantinou, A., Tarsounas, M., Karow, J.K., Brosh, R.M., Bohr, V.A., Hickson, I.D., and West, S.C., *Werner's syndrome protein (WRN) migrates Holliday junctions and co-localizes with RPA upon replication arrest.* EMBO Rep, 2000. **1**(1): 80-4.
90. Shen, J. and Loeb, L.A., *Unwinding the molecular basis of the Werner syndrome.* Mech Ageing Dev, 2001. **122**(9): 921-44.
91. Poot, M., Hoehn, H., Runger, T.M., and Martin, G.M., *Impaired S-phase transit of Werner syndrome cells expressed in lymphoblastoid cell lines.* Exp Cell Res, 1992. **202**(2): 267-73.
92. Kunkel, T.A. and Burgers, P.M., *Dividing the workload at a eukaryotic replication fork.* Trends in Cell Biology, 2008. **18**(11): 521-527.
93. Franchitto, A., Oshima, J., and Pichierri, P., *The G2-phase Decatenation Checkpoint Is Defective in Werner Syndrome Cells.* Cancer Res, 2003. **63**(12): 3289-3295.
94. Kamath-Loeb, A.S., Loeb, L.A., Johansson, E., Burgers, P.M., and Fry, M., *Interactions between the Werner syndrome helicase and DNA polymerase delta specifically facilitate copying of tetraplex and hairpin structures of the d(CGG)n trinucleotide repeat sequence.* J Biol Chem, 2001. **276**(19): 16439-46.
95. Crabbe, L., Verdun, R.E., Haggblom, C.I., and Karlseder, J., *Defective telomere lagging strand synthesis in cells lacking WRN helicase activity.* Science, 2004. **306**(5703): 1951-3.
96. Crabbe, L., Jauch, A., Naeger, C.M., Holtgreve-Grez, H., and Karlseder, J., *Telomere dysfunction as a cause of genomic instability in Werner syndrome.* Proc Natl Acad Sci U S A, 2007. **104**(7): 2205-10.
97. Hisama, F.M., Bohr, V.A., and Oshima, J., *WRN's Tenth Anniversary.* Sci. Aging Knowl. Environ., 2006. **2006**(10): pe18-.

98. Rossi, M.L., Ghosh, A.K., and Bohr, V.A., *Roles of Werner syndrome protein in protection of genome integrity.* DNA Repair, 2010. **9**(3): 331-344.
99. Karmakar, P. and Bohr, V.A., *Cellular dynamics and modulation of WRN protein is DNA damage specific.* Mechanisms of Ageing and Development, 2005. **126**(11): 1146-1158.
100. Sung, P. and Klein, H., *Mechanism of homologous recombination: mediators and helicases take on regulatory functions.* Nat Rev Mol Cell Biol, 2006. **7**(10): 739-50.
101. Cheng, W.-H., Kusumoto, R., Opresko, P.L., Sui, X., Huang, S., Nicolette, M.L., Paull, T.T., Campisi, J., Seidman, M., and Bohr, V.A., *Collaboration of Werner syndrome protein and BRCA1 in cellular responses to DNA interstrand cross-links.* Nucleic Acids Research, 2006. **34**(9): 2751-2760.
102. Hinz, J.M., *Role of homologous recombination in DNA interstrand crosslink repair.* Environmental and Molecular Mutagenesis, 2010. **51**(6): 582-603.
103. Saintigny, Y., Makienko, K., Swanson, C., Emond, M.J., and Monnat, R.J., Jr., *Homologous recombination resolution defect in werner syndrome.* Mol Cell Biol, 2002. **22**(20): 6971-8.
104. Versini, G., Comet, I., Wu, M., Hoopes, L., Schwob, E., and Pasero, P., *The yeast Sgs1 helicase is differentially required for genomic and ribosomal DNA replication.* EMBO J, 2003. **22**(8): 1939-1949.
105. Rodriguez-Lopez, A.M., Whitby, M.C., Borer, C.M., Bachler, M.A., and Cox, L.S., *Correction of proliferation and drug sensitivity defects in the progeroid Werner's Syndrome by Holliday junction resolution.* Rejuvenation Res, 2007. **10**(1): 27-40.
106. Lavin, M.F. and Shiloh, Y., *The genetic defect in Ataxia-Telangiectasia.* Annual Review of Immunology, 1997. **15**(1): 177-202.
107. Cimprich, K.A. and Cortez, D., *ATR: an essential regulator of genome integrity.* Nat Rev Mol Cell Biol, 2008. **9**(8): 616-627.
108. Cheng, W.-H., Muftic, D., Muftuoglu, M., Dawut, L., Morris, C., Helleday, T., Shiloh, Y., and Bohr, V.A., *WRN Is Required for ATM Activation and the S-Phase Checkpoint in Response to Interstrand Cross-Link-Induced DNA Double-Strand Breaks.* Mol. Biol. Cell, 2008. **19**(9): 3923-3933.
109. Otterlei, M., Bruheim, P., Ahn, B., Bussen, W., Karmakar, P., Baynton, K., and Bohr, V.A., *Werner syndrome protein participates in a complex with RAD51, RAD54, RAD54B and ATR in response to ICL-induced replication arrest.* J Cell Sci, 2006. **119**(Pt 24): 5137-46.
110. Pichierri, P., Rosselli, F., and Franchitto, A., *Werner's syndrome protein is phosphorylated in an ATR//ATM-dependent manner following replication arrest and DNA damage induced during the S phase of the cell cycle.* Oncogene, 2003. **22**(10): 1491-1500.
111. Fire, A., Xu, S., Montgomery, M.K., Kostas, S.A., Driver, S.E., and Mello, C.C., *Potent and specific genetic interference by double-stranded RNA in Caenorhabditis elegans.* Nature, 1998. **391**(6669): 806-811.
112. Doi, N., Zenno, S., Ueda, R., Ohki-Hamazaki, H., Ui-Tei, K., and Saigo, K., *Short-Interfering-RNA-Mediated Gene Silencing in Mammalian Cells Requires Dicer and eIF2C Translation Initiation Factors.* Current Biology, 2003. **13**(1): 41-46.
113. Cerutti, H. and Casas-Mollano, J.A., *On the origin and functions of RNA-mediated silencing: from protists to man.* Curr. Genet., 2006. **50**(2): 81-99.
114. Tomari, Y. and Zamore, P.D., *Perspective: machines for RNAi.* Genes & Development, 2005. **19**(5): 517-529.
115. Gong, D. and Ferrell, J.J.E., *Picking a winner: new mechanistic insights into the design of effective siRNAs.* Trends in Biotechnology, 2004. **22**(9): 451-454.
116. Jackson, A.L. and Linsley, P.S., *Recognizing and avoiding siRNA off-target effects for target identification and therapeutic application.* Nat Rev Drug Discov, 2010. **9**(1): 57-67.
117. Jackson, A.L., Burchard, J., Leake, D., Reynolds, A., Schelter, J., Guo, J., Johnson, J.M., Lim, L., Karpilow, J., Nichols, K., Marshall, W., Khvorova, A., and Linsley, P.S., *Position-*

specific chemical modification of siRNAs reduces "off-target" transcript silencing. RNA-Publ. RNA Soc., 2006. **12**(7): 1197-1205.
118. Judge, A. and MacLachlan, I., *Overcoming the Innate Immune Response to Small Interfering RNA.* Human Gene Therapy, 2008. **19**(2): 111-124.
119. Lord, C.J., Martin, S.A., and Ashworth, A., *RNA interference screening demystified.* Journal of Clinical Pathology, 2009. **62**(3): 195-200.
120. Lucchesi, J.C., *Synthetic lethality and semi-lethality among functionally related mutants of Drosophila melanfgaster.* Genetics, 1968. **59**(1): 37-44.
121. Kaelin, W.G., *The Concept of Synthetic Lethality in the Context of Anticancer Therapy.* Nat Rev Cancer, 2005. **5**(9): 689-698.
122. Nijman, S.M.B., *Synthetic lethality: General principles, utility and detection using genetic screens in human cells.* FEBS letters, 2011. **585**(1): 1-6.
123. Dixon, S.J., Costanzo, M., Baryshnikova, A., Andrews, B., and Boone, C., *Systematic mapping of genetic interaction networks*, in *Annual Review of Genetics*. 2009. 601-625.
124. Iorns, E., Lord, C.J., Turner, N., and Ashworth, A., *Utilizing RNA interference to enhance cancer drug discovery.* Nat Rev Drug Discov, 2007. **6**(7): 556-568.
125. Mullen, J.R., Kaliraman, V., Ibrahim, S.S., and Brill, S.J., *Requirement for Three Novel Protein Complexes in the Absence of the Sgs1 DNA Helicase in Saccharomyces cerevisiae.* Genetics, 2001. **157**(1): 103-118.
126. Cox, L. and Faragher, R., *From old organisms to new molecules: integrative biology and therapeutic targets in accelerated human ageing.* Cellular and Molecular Life Sciences (CMLS), 2007. **64**(19): 2620-2641.
127. http://ccr.coriell.org.
128. Harrigan, J.A., Wilson, D.M., Prasad, R., Opresko, P.L., Beck, G., May, A., Wilson, S.H., and Bohr, V.A., *The Werner syndrome protein operates in base excision repair and cooperates with DNA polymerase beta.* Nucleic Acids Research, 2006. **34**(2): 745-754.
129. Gonzalez, R.J. and Tarloff, J.B., *Evaluation of hepatic subcellular fractions for Alamar blue and MTT reductase activity.* Toxicology in Vitro, 2001. **15**(3): 257-259.
130. Nociari, M.M., Shalev, A., Benias, P., and Russo, C., *A novel one-step, highly sensitive fluorometric assay to evaluate cell-mediated cytotoxicity.* Journal of Immunological Methods, 1998. **213**(2): 157-167.
131. Zhang, H.X., Du, G.H., Zhang, J.T., *Assay of mitochondrial functions by resazurin in vitro.* Acta Pharmacol Sin., 2004. **25**(3): 385-389.
132. Anoopkumar-Dukie, S., Carey, J.B., Conere, T., O'Sullivan, E., van Pelt, F.N., and Allshire, A., *Resazurin assay of radiation response in cultured cells.* Br J Radiol, 2005. **78**(934): 945-947.
133. Flygare, J., Armstrong, R.C., Wennborg, A., Orsan, S., and Hellgren, D., *Proteolytic cleavage of HsRad51 during apoptosis.* FEBS letters, 1998. **427**(2): 247-251.
134. Lord, C.J., McDonald, S., Swift, S., Turner, N.C., and Ashworth, A., *A high-throughput RNA interference screen for DNA repair determinants of PARP inhibitor sensitivity.* DNA Repair, 2008. **7**(12): 2010-2019.
135. Zhang, J.-H., Chung, T.D.Y., and Oldenburg, K.R., *A Simple Statistical Parameter for Use in Evaluation and Validation of High Throughput Screening Assays.* Journal of Biomolecular Screening, 1999. **4**(2): 67-73.
136. Echeverri, C.J., Beachy, P.A., Baum, B., Boutros, M., Buchholz, F., Chanda, S.K., Downward, J., Ellenberg, J., Fraser, A.G., Hacohen, N., Hahn, W.C., Jackson, A.L., Kiger, A., Linsley, P.S., Lum, L., Ma, Y., Mathey-Prevot, B., Root, D.E., Sabatini, D.M., Taipale, J., Perrimon, N., and Bernards, R., *Minimizing the risk of reporting false positives in large-scale RNAi screens.* Nat Meth, 2006. **3**(10): 777-779.

137. Watt, P.M., Louis, E.J., Borts, R.H., and Hickson, I.D., *Sgs1: A eukaryotic homolog of E. coil RecQ that interacts with topoisomerase II in vivo and is required for faithful chromosome segregation.* Cell, 1995. **81**(2): 253-260.
138. Boone, C., Bussey, H., and Andrews, B.J., *Exploring genetic interactions and networks with yeast.* Nat Rev Genet, 2007. **8**(6): 437-449.
139. Yamashita, M. and Emerman, M., *Retroviral infection of non-dividing cells: Old and new perspectives.* Virology, 2006. **344**(1): 88-93.
140. Hannon, G.J. and Rossi, J.J., *Unlocking the potential of the human genome with RNA interference.* Nature, 2004. **431**(7006): 371-378.
141. Mirzaei, H., Syed, S., Kennedy, J., and Schmidt, K.H., *Sgs1 Truncations Induce Genome Rearrangements but Suppress Detrimental Effects of BLM Overexpression in Saccharomyces cerevisiae.* Journal of Molecular Biology, 2011. **405**(4): 877-891.
142. Franchitto, A., Pirzio, L. M., Prosperi , E., Sapora , O., Bignami, M. and Pichierri, P., *Replication fork stalling in WRN-defi cient cells is overcome by prompt activation of a MUS81-dependent pathway.* JCB, 2008. **183**(2): 241-252.
143. Lucas, I., Germe, T., Chevrier-Miller, M., and Hyrien, O., *Topoisomerase II can unlink replicating DNA by precatenane removal.* EMBO J, 2001. **20**(22): 6509-6519.
144. Kim, R.A., Wang J.C., *Function of DNA topoisomerases as replication swivels in Saccharomyces cerevisiae.* J. Mol. Biol., 1989. **208**(2): 257-267.
145. Brill S.J., D., S., Voelkel-Meiman, K., Sternglanz, R., *Need for DNA topoisomerase activity as a swivel for DNA replication for transcription of ribosomal RNA.* Nature, 1987. **326**(6111): 414-416.
146. McClendon, A.K., Rodriguez, A.C., and Osheroff, N., *Human Topoisomerase II beta Rapidly Relaxes Positively Supercoiled DNA.* Journal of Biological Chemistry, 2005. **280**(47): 39337-39345.
147. Champoux, J.J. and Dulbecco, R., *An Activity from Mammalian Cells That Untwists Superhelical DNA-A Possible Swivel For DNA Replication.* Proceedings of the National Academy of Sciences of the United States of America, 1972. **69**(1): 143-146.
148. Chakalova, L., Debrand, E., Mitchell, J.A., Osborne, C.S., and Fraser, P., *Replication and transcription: shaping the landscape of the genome.* Nat Rev Genet, 2005. **6**(9): 669-77.
149. Garg, P. and Burgers, P.M., *DNA polymerases that propagate the eukaryotic DNA replication fork.* Crit Rev Biochem Mol Biol, 2005. **40**(2): 115-28.
150. Pacek, M., Tutter, A.V., Kubota, Y., Takisawa, H., and Walter, J.C., *Localization of MCM2-7, Cdc45, and GINS to the site of DNA unwinding during eukaryotic DNA replication.* Mol Cell, 2006. **21**(4): 581-7.
151. Walter, J. and Newport, J., *Initiation of eukaryotic DNA replication: origin unwinding and sequential chromatin association of Cdc45, RPA, and DNA polymerase alpha.* Mol Cell, 2000. **5**(4): 617-27.
152. Landers, J.E., Cassel, S.L., and George, D.L., *Translational Enhancement of mdm2 Oncogene Expression in Human Tumor Cells Containing a Stabilized Wild-Type p53 Protein.* Cancer Research, 1997. **57**(16): 3562-3568.
153. Boye, B.G.a.E., *The multiple facets of the intra-S checkpoint.* Cell Cycle, 2008. **7**(15): 2315 - 2320.
154. Jackson, D.A. and Pombo, A., *Replicon Clusters Are Stable Units of Chromosome Structure: Evidence That Nuclear Organization Contributes to the Efficient Activation and Propagation of S Phase in Human Cells.* The Journal of Cell Biology, 1998. **140**(6): 1285-1295.
155. Merrick, C.J., Jackson, D., and Diffley, J.F.X., *Visualization of Altered Replication Dynamics after DNA Damage in Human Cells.* Journal of Biological Chemistry, 2004. **279**(19): 20067-20075.

156. Petermann, E., Maya-Mendoza, A., Zachos, G., Gillespie, D.A.F., Jackson, D.A., and Caldecott, K.W., *Chk1 Requirement for High Global Rates of Replication Fork Progression during Normal Vertebrate S Phase.* Mol. Cell. Biol., 2006. **26**(8): 3319-3326.
157. Caroline, A.A. and Katherine, L.M., *Eukaryotic DNA topoisomerase II.* Bioessays, 1998. **20**(3): 215-226.
158. Sakaguchi, A. and Kikuchi, A., *Functional compatibility between isoform α and β of type II DNA topoisomerase.* J Cell Sci, 2004. **117**(7): 1047-1054.
159. Fan, J.R., *Cellular processing pathways contribute to the activation of etoposide-induced DNA damage responses.* DNA Repair, 2008. **7**: 452-463.
160. Cuvier, O., Stanojcic, S., Lemaitre, J.-M., and Mechali, M., *A topoisomerase II-dependent mechanism for resetting replicons at the S-M-phase transition.* Genes & Development, 2008. **22**(7): 860-865.
161. Bartek, J., Lukas, C., and Lukas, J., *Checking on DNA damage in S phase.* Nat Rev Mol Cell Biol, 2004. **5**(10): 792-804.
162. Anglana, M., Apiou, F., Bensimon, A., and Debatisse, M., *Dynamics of DNA replication in mammalian somatic cells: nucleotide pool modulates origin choice and interorigin spacing.* Cell, 2003. **114**: 385-394.
163. Courbet, S., *Replication fork movement drives remodeling of chromatin loops and origin choice in mammalian cells.* Nature, 2008. **455**: 557-560.
164. Gilbert, D.M., *Replication origin plasticity, taylor-made: inhibition vs recruitment of origins under conditions of replication stress.* Chromosoma, 2007. **116**: 341-347.
165. Ibarra, A., Schwob, E., and Méndez , J., *Excess MCM proteins protect human cells from replicative stress by licensing backup origins of replication.* Proceedings of the National Academy of Sciences, 2008. **105**(26): 8956-8961.
166. Grue, P., Grasser, A., Sehested, M., Jensen, P.B., Uhse, A., Straub, T., Ness, W., and Boege, F., *Essential Mitotic Functions of DNA Topoisomerase II alpha Are Not Adopted by Topoisomerase II beta in Human H69 Cells.* Journal of Biological Chemistry, 1998. **273**(50): 33660-33666.
167. Jensen S, R.C.S., Jenkins J.R., Andersen A.H., Hickson I.D., *Human DNA topoisomerases II alpha and II beta can functionally substitute for yeast TOP2 in chromosome segregation and recombination.* Mol Gen Genet., 1996. **252**(1-2): 79-86.
168. Wasserman, R.A., Austin, C.A., Fisher, L.M., and Wang, J.C., *Use of Yeast in the Study of Anticancer Drugs Targeting DNA Topoisomerases: Expression of a Functional Recombinant Human DNA Topoisomerase II alpha in Yeast.* Cancer Research, 1993. **53**(15): 3591-3596.
169. Ström, C.E., Johansson, F., Uhlen, M., Al-Khalili Szigyarto, C., Erixon, K., and Helleday, T., *Poly (ADP-ribose) polymerase (PARP) is not involved in base excision repair but PARP inhibition traps a single-strand intermediate.* Nucleic Acids Research, 2010: 1-10.
170. Storchova, Z. and Pellman, D., *From polyploidy to aneuploidy, genome instability and cancer.* Nat Rev Mol Cell Biol, 2004. **5**(1): 45-54.
171. Ganem, N.J., Storchova, Z., and Pellman, D., *Tetraploidy, aneuploidy and cancer.* Current Opinion in Genetics & Development, 2007. **17**(2): 157-162.
172. Porter, A., *Preventing DNA over-replication: a Cdk perspective.* Cell Division, 2008. **3**(1): 3.
173. Diffley, J.F.X., *Regulation of early events in chromosome replication.* Current Biology, 2004. **14**(18): R778-R786.
174. Kiang, L., Heichinger, C., Watt, S., Bähler, J., and Nurse, P., *Cyclin-dependent kinase inhibits reinitiation of a normal S-phase program during G2 in fission yeast.* Molecular and Cellular Biology, 2009. **29**(15): 4025-4032.
175. Itzhaki, J.E., Gilbert, C.S., and Porter, A.C., *Construction by gene targeting in human cells of a "conditional' CDC2 mutant that rereplicates its DNA.* Nat Genet, 1997. **15**: 258 - 265.

176. Waldman, T., Lengauer, C., Kinzler, K.W., and Vogelstein, B., *Uncoupling of S phase and mitosis induced by anticancer agents in cells lacking p21.* Nature, 1996. **381**(6584): 713-716.
177. Davoli, T., Denchi, E.L., and de Lange, T., *Persistent Telomere Damage Induces Bypass of Mitosis and Tetraploidy.* Cell, 2010. **141**(1): 81-93.
178. Vakifahmetoglu, H., Olsson, M., and Zhivotovsky, B., *Death through a tragedy: mitotic catastrophe.* Cell Death Differ, 2008. **15**(7): 1153-1162.
179. Lobrich, M. and Jeggo, P.A., *The impact of a negligent G2/M checkpoint on genomic instability and cancer induction.* Nat Rev Cancer, 2007. **7**(11): 861-869.
180. Shi, Q. and King, R.W., *Chromosome nondisjunction yields tetraploid rather than aneuploid cells in human cell lines.* Nature, 2005. **437**(4061): 1038-1042.
181. Weaver, B.A.A., Silk, A.D., and Cleveland, D.W., *Cell biology: Nondisjunction, aneuploidy and tetraploidy.* Nature, 2006. **442**(7104): E9-E10.
182. Mullins, J. and Biesele, J.J., *Terminal phase of cytokinesis in D-98S cells.* The Journal of Cell Biology, 1977. **73**(3): 672-684.
183. Erenpreisa J, I.A., Wheatley SP, Kosmacek EA, Ianzini F, Anisimov AP, Mackey M, Davis PJ, Plakhins G, Illidge TM., *Endopolyploidy in irradiated p53-deficient tumour cell lines: Persistence of cell division activity in giant cells expressing Aurora B- kinase.* Cell Biol Int, 2008. **24**: 621-633.
184. Castedo, M., Perfettini, J.-L., Roumier, T., Andreau, K., Medema, R., and Kroemer, G., *Cell death by mitotic catastrophe: a molecular definition.* Oncogene, 2004. **23**(16): 2825-2837.
185. Hendzel, M.J., Wei, Y., Mancini, M.A., Van Hooser, A., Ranalli, T., Brinkley, B.R., Bazett-Jones, D.P., and Allis, C.D., *Mitosis-specific phosphorylation of histone H3 initiates primarily within pericentromeric heterochromatin during G2 and spreads in an ordered fashion coincident with mitotic chromosome condensation.* Chromosoma, 1997. **106**(6): 348-360.
186. Xu, B., Kim, S.-t., and Kastan, M.B., *Involvement of Brca1 in S-Phase and G2-Phase Checkpoints after Ionizing Irradiation.* Mol. Cell. Biol., 2001. **21**(10): 3445-3450.
187. Allalunis-Turner, M.J., Barron, G.M., Day, R.S. 3rd, Dobler, K.D., Mirzayans, R., *Isolation of two cell lines from a human malignant glioma specimen differing in sensitivity to radiation and chemotherapeutic drugs.* Radiat Res., 1993. **134**(3): 349-54.
188. Ishida, R., Sato, M., Narita, T., Utsumi, K.R., Nishimoto, T., Morita, T., Nagata, H., and Andoh, T., *Inhibition of DNA topoisomerase II by ICRF-193 induces polyploidization by uncoupling chromosome dynamics from other cell cycle events.* The Journal of Cell Biology, 1994. **126**(6): 1341-1351.
189. Smith, P., Marquez, N., Wilthsire, M, *Mitotic bypass via an occult cell cycle phase following DNA topoisomerase II inhibition in p53 functional human tumor cells.* Cell Cycle, 2007. **6**(16): 2071-2081.
190. Park, I. and Avraham, H.K., *Cell cycle-dependent DNA damage signaling induced by ICRF-193 involves ATM, ATR, CHK2, and BRCA1*. Experimental Cell Research, 2006. **312**(11): 1996-2008.
191. Hajji, N., Pastor, N., Mateos, S., Domínguez, I., and Cortés, F., *DNA strand breaks induced by the anti-topoisomerase II bis-dioxopiperazine ICRF-193.* Mutation Research/Fundamental and Molecular Mechanisms of Mutagenesis, 2003. **530**(1-2): 35-46.
192. Jensen, L.H., *A novel mechanism of cell killing by anti-topoisomerase II bisdioxopiperazines.* J. Biol. Chem., 2000. **275**: 2137-2146.
193. Jensen, L., Dejligbjerg, M., Hansen, L., Grauslund, M., Jensen, P., and Sehested, M., *Characterisation of cytotoxicity and DNA damage induced by the topoisomerase II-directed bisdioxopiperazine anti-cancer agent ICRF-187 (dexrazoxane) in yeast and mammalian cells.* BMC Pharmacology, 2004. **4**(1): 31.

194. Purificación, M., Fabienne, B., Jacques, P., *Ku antigen is required to relieve G2 arrest caused by inhibition of DNA topoisomerase II activity by the bisdioxopiperazine ICRF-193.* 2001. **20**(16): 1990-1999.
195. Pastor, N., José Flores, M., Domínguez, I., Mateos, S., and Cortés, F., *High yield of endoreduplication induced by ICRF-193: a topoisomerase II catalytic inhibitor.* Mutation Research/Genetic Toxicology and Environmental Mutagenesis, 2002. **516**(1-2): 113-120.
196. Thompson, L.H., Brookman, K.W., Jones, N.J., Allen, S.A., and Carrano, A.V., *Molecular cloning of the human XRCC1 gene, which corrects defective DNA strand break repair and sister chromatid exchange.* Mol. Cell. Biol., 1990. **10**(12): 6160-6171.
197. Cortés, F., Pinero, J., and Palitti, F., *Cytogenetic effects of inhibition of topoisomerase I or II activities in the CHO mutant EM9 and its parental line AA8.* Mutation Research/Fundamental and Molecular Mechanisms of Mutagenesis, 1993. **288**(2): 281-289.
198. Sakaue-Sawano, A., Kurokawa, H., Morimura, T., Hanyu, A., Hama, H., Osawa, H., Kashiwagi, S., Fukami, K., Miyata, T., Miyoshi, H., Imamura, T., Ogawa, M., Masai, H., and Miyawaki, A., *Visualizing Spatiotemporal Dynamics of Multicellular Cell-Cycle Progression.* Cell, 2008. **132**(3): 487-498.
199. Blow, J.J. and Dutta, A., *Preventing re-replication of chromosomal DNA.* Nat Rev Mol Cell Biol, 2005. **6**(6): 476-486.
200. Andrews, C.A., Vas, A.C., Meier, B., Gimenez-Abien, J.F., Diaz-Martinez, L.A., Green, J., Erickson, S.L., VanderWaal, K.E., Hsu, W.-S., and Clarke, D.J., *A mitotic topoisomerase II checkpoint in budding yeast is required for genome stability but acts independently of Pds1/securin.* Genes & Development, 2006. **20**(9): 1162-1174.
201. Sullivan, M., Higuchi, T., Katis, V.L., and Uhlmann, F., *Cdc14 Phosphatase Induces rDNA Condensation and Resolves Cohesin-Independent Cohesion during Budding Yeast Anaphase.* Cell, 2004. **117**(4): 471-482.
202. Skop, A.R., Liu, H., Yates, J., Meyer, B.J., and Heald, R., *Dissection of the Mammalian Midbody Proteome Reveals Conserved Cytokinesis Mechanisms.* Science, 2004. **305**(5680): 61-66.
203. Houchmandzadeh, B., Marko, J.F., Chatenay, D., and Libchaber, A., *Elasticity and Structure of Eukaryote Chromosomes Studied by Micromanipulation and Micropipette Aspiration.* The Journal of Cell Biology, 1997. **139**(1): 1-12.
204. Petermann, E. and Caldecott, K.W., *Evidence that the ATR/Chk1 pathway maintains normal replication fork progression during unperturbed S phase.* Cell Cycle, 2006. **5**(19): 2203-9.
205. Ammazzalorso, F., Pirzio, L.M., Bignami, M., Franchitto, A., and Pichierri, P., *ATR and ATM differently regulate WRN to prevent DSBs at stalled replication forks and promote replication fork recovery.* EMBO J, 2010. **29**(18): 3156-3169.
206. Järvinen, T.A.H. and Liu, E.T., *Topoisomerase IIα gene (TOP2A) amplification and deletion in cancer – more common than anticipated.* Cytopathology, 2003. **14**(6): 309-313.

8 Appendix 1

Table 8.1 | Complete data set from the siRNA screen

SD, Standard Deviation

Z-score calculated using average and SD

Viability (% of siRNA NT)					AG03141 viability (% of GM01604)			
	Average		SD					
siRNA SMARTpool	GM01604	AG03141	GM01604	AG03141	siRNA SMARTpool	Average	SD	Z-score
AKT1	84.1	84.1	3.2	18.0	AKT1	103.4	22.1	0.44
AKT2	65.9	46.4	9.6	17.9	AKT2	70.4	27.1	-1.50
APEX1	85.0	91.7	7.3	27.9	APEX1	107.8	32.8	0.70
APEX2	96.8	89.0	14.7	21.1	APEX2	91.9	21.8	-0.24
ATM	94.5	79.5	21.0	10.4	ATM	84.2	11.0	-0.69
ATR	78.1	97.9	5.6	15.3	ATR	125.3	19.6	1.72
BLM	112.8	103.8	22.2	12.8	BLM	92.0	11.3	-0.23
BRCA1	75.3	53.1	12.0	8.0	BRCA1	70.5	10.6	-1.49
BRCA2	85.6	68.6	6.3	15.3	BRCA2	80.2	17.8	-0.92
BRIP1	64.5	74.5	2.8	19.1	BRIP1	115.6	29.6	1.16
C17orf41	134.0	82.6	5.7	23.7	C17orf41	61.6	17.7	-2.01
C9ORF76	71.9	99.9	24.2	19.9	C9ORF76	138.8	27.7	2.52
CCNA1	120.3	74.8	9.5	15.3	CCNA1	62.2	12.7	-1.98
CCNA2	60.5	25.4	12.2	11.5	CCNA2	42.0	19.0	-3.16
CCNB1	71.5	63.5	18.1	30.2	CCNB1	88.8	42.2	-0.41
CCNB2	81.5	60.7	9.5	20.0	CCNB2	74.5	24.6	-1.25
CCNB3	69.3	72.9	13.0	26.4	CCNB3	105.3	38.1	0.55
CCND1	71.3	66.2	14.1	15.9	CCND1	92.8	22.3	-0.18
CCND2	84.4	60.3	22.4	27.2	CCND2	71.5	32.2	-1.43
CCND3	47.2	61.1	5.6	21.9	CCND3	129.4	46.5	1.97
CCNE1	106.5	51.0	18.0	11.6	CCNE1	47.8	10.9	-2.82
CCNE2	73.8	74.8	3.1	21.7	CCNE2	101.3	29.4	0.32
CDC2	74.9	37.6	5.6	12.2	CDC2	50.1	16.3	-2.68
CDK2	151.3	89.2	22.6	18.1	CDK2	59.0	11.9	-2.17
CDK4	89.7	81.2	10.5	27.2	CDK4	90.6	30.4	-0.31
CDK6	77.0	43.7	6.0	20.1	CDK6	56.8	26.1	-2.29
CETN2	84.8	50.6	8.6	20.1	CETN2	59.7	23.7	-2.12
CFDP1	82.5	57.3	2.5	9.3	CFDP1	69.4	11.3	-1.56
CHEK1	55.8	13.2	19.9	5.8	CHEK1	23.7	10.4	-4.24
CHEK2	77.8	66.2	23.9	20.8	CHEK2	85.1	26.8	-0.63
CHTF18	98.0	81.2	16.8	18.8	CHTF18	82.9	19.2	-0.76
CKN1	112.6	78.8	17.3	28.5	CKN1	70.0	25.3	-1.52
CLSPN	35.5	62.2	3.7	40.4	CLSPN	174.9	113.6	4.63
CUL4A	86.1	90.6	7.7	21.8	CUL4A	105.3	25.3	0.55
CUL4B	79.0	73.9	6.3	32.9	CUL4B	93.6	41.7	-0.14
DCLRE1A	98.0	89.9	27.3	37.6	DCLRE1A	91.8	38.4	-0.24
DCLRE1B	51.5	86.7	25.0	16.6	DCLRE1B	168.4	32.3	4.26
DCLRE1C	108.4	87.1	25.7	23.1	DCLRE1C	80.3	21.3	-0.91
DDB1	89.9	58.6	12.6	26.7	DDB1	65.2	29.6	-1.80
DDB2	118.3	76.9	34.1	18.8	DDB2	65.1	15.9	-1.81
DEPC-1	124.5	69.0	8.9	7.4	DEPC-1	55.4	5.9	-2.38
DNMT1	97.1	72.7	10.4	30.0	DNMT1	74.8	30.8	-1.24
DUT	77.4	60.3	20.1	21.2	DUT	77.9	27.4	-1.05
EGFR	135.0	91.5	25.3	14.8	EGFR	67.7	11.0	-1.65
EME1	71.1	78.0	14.2	12.6	EME1	109.7	17.7	0.81
EME2	87.8	90.1	10.9	24.0	EME2	102.6	27.4	0.39
ERCC1	67.5	62.8	16.6	26.2	ERCC1	93.1	38.9	-0.16
ERCC2	84.5	123.3	7.2	16.8	ERCC2	146.0	19.9	2.94
ERCC4	88.2	82.9	16.7	17.8	ERCC4	94.0	20.2	-0.11
ERCC5	60.7	113.1	6.7	23.0	ERCC5	186.4	37.9	5.31
ERCC6	65.2	51.0	2.2	26.9	ERCC6	78.1	41.2	-1.04
EXO1	156.0	121.5	25.5	16.8	EXO1	77.9	10.8	-1.06
FANCA	77.9	62.5	6.0	35.7	FANCA	80.2	45.8	-0.92
FANCB	60.8	62.0	10.2	36.9	FANCB	102.0	60.7	0.36
FANCC	66.2	78.2	17.1	31.6	FANCC	118.0	47.7	1.30
FANCD2	106.3	73.4	18.5	20.3	FANCD2	69.0	19.1	-1.58

Z-score calculated using average and SD

Viability (% of siRNA NT)					AG03141 viability (% of GM01604)			
	Average		SD					
siRNA SMARTpool	GM01604	AG03141	GM01604	AG03141	siRNA SMARTpool	Average	SD	Z-score
FANCE	81.0	45.6	13.1	37.1	FANCE	56.3	45.8	-2.33
FANCF	128.0	87.9	34.9	17.1	FANCF	68.6	13.4	-1.60
FANCG	97.3	105.9	12.4	21.9	FANCG	108.9	22.5	0.76
FANCL	149.6	108.6	26.7	54.8	FANCL	72.6	36.6	-1.37
FBXO18	97.2	46.5	15.5	40.4	FBXO18	47.9	41.5	-2.82
FEN1	90.9	86.8	24.8	32.0	FEN1	95.5	35.2	-0.02
FLJ10719	94.5	134.7	13.3	33.2	FLJ10719	142.6	35.1	2.74
FLJ12610	123.7	131.5	1.9	27.2	FLJ12610	106.3	22.0	0.61
FLJ21816	56.2	63.7	21.9	37.8	FLJ21816	113.4	67.3	1.03
FLJ35220	92.2	107.1	20.0	32.7	FLJ35220	116.1	35.5	1.19
G22P1	75.9	59.7	6.4	8.0	G22P1	78.6	10.6	-1.02
GTF2H2	73.6	67.5	15.8	35.8	GTF2H2	91.8	48.6	-0.24
H2AFX	92.6	131.1	59.8	78.0	H2AFX	141.5	84.2	2.68
HUS1	120.2	101.2	21.6	16.7	HUS1	84.2	13.9	-0.69
IGF1	127.3	139.2	17.5	52.1	IGF1	109.3	40.9	0.79
IGF1R	93.5	119.0	12.3	2.7	IGF1R	127.2	2.9	1.84
IGF2	109.8	52.1	15.7	45.2	IGF2	47.5	41.1	-2.84
INCENP	59.0	13.1	5.8	7.7	INCENP	22.1	13.0	-4.33
INSR	69.8	49.6	20.8	20.8	INSR	71.0	29.8	-1.46
IRS1	85.9	88.3	54.8	40.8	IRS1	102.7	47.5	0.40
KIAA1596	77.1	51.9	3.3	31.7	KIAA1596	67.3	41.1	-1.68
LGP2	62.8	60.1	9.3	14.2	LGP2	95.8	22.6	-0.01
LIG3	115.0	116.4	20.7	19.0	LIG3	101.2	16.6	0.31
LIG4	62.1	73.0	12.1	17.0	LIG4	117.6	27.4	1.27
MAD2L2	67.3	59.8	16.7	10.4	MAD2L2	89.0	15.5	-0.41
MAP2K2	104.2	149.8	9.3	43.2	MAP2K2	143.8	41.5	2.81
MAPK1	41.1	50.9	13.5	27.4	MAPK1	123.7	66.6	1.63
MDC1	70.6	71.2	10.1	19.2	MDC1	100.9	27.2	0.29
MEN1	77.5	69.8	14.9	23.3	MEN1	90.1	30.0	-0.34
MGC5178	86.9	87.8	31.5	18.6	MGC5178	101.1	21.4	0.30
MGC5528	129.7	93.7	13.9	11.2	MGC5528	72.3	8.6	-1.38
MGMT	135.9	108.1	40.1	21.7	MGMT	79.6	16.0	-0.96
MLH1	131.5	138.4	14.4	14.9	MLH1	105.2	11.3	0.55
MMS19L	96.5	108.2	18.3	22.5	MMS19L	112.2	23.3	0.96
MNAT1	69.3	104.9	8.0	24.9	MNAT1	151.3	35.9	3.25
MPG	75.7	79.6	1.2	26.9	MPG	105.2	35.5	0.54
MRC1	146.3	103.5	49.9	16.6	MRC1	70.8	11.4	-1.48
MRE11A	98.1	134.2	21.6	25.5	MRE11A	136.7	26.0	2.40
MSH2	95.6	106.9	26.8	16.1	MSH2	111.8	16.9	0.93
MSH3	64.1	103.5	21.3	19.5	MSH3	161.5	30.4	3.85
MSH6	108.3	105.1	25.7	24.1	MSH6	97.0	22.2	0.07
MUS81	101.7	95.8	28.9	13.0	MUS81	94.2	12.8	-0.10
MUTYH	104.3	106.4	18.4	23.6	MUTYH	102.0	22.6	0.36
NBS1	101.6	95.5	18.2	10.4	NBS1	93.9	10.3	-0.12
NEIL1	107.2	106.1	25.3	19.0	NEIL1	99.0	17.7	0.18
NEIL2	77.4	111.5	15.3	23.1	NEIL2	144.1	29.8	2.83
NEIL3	116.1	104.7	37.0	27.5	NEIL3	90.1	23.7	-0.34
NEK2	55.0	60.2	14.5	15.8	NEK2	109.5	28.7	0.80
NTHL1	77.9	100.5	34.0	17.5	NTHL1	129.1	22.4	1.95
NUDT1	84.8	76.2	25.7	33.7	NUDT1	89.8	39.7	-0.36
PARP1	99.3	91.2	16.1	8.0	PARP1	91.9	8.1	-0.24
PARP2	82.9	120.4	14.8	25.9	PARP2	145.3	31.3	2.90
PHB	107.9	88.1	24.6	28.1	PHB	81.7	26.1	-0.83
PIR51	108.7	102.0	27.5	25.9	PIR51	93.8	23.8	-0.12
PLK	0.0	0.0	0.0	0.0	PLK	57.5	48.4	-2.25
PLK2	85.9	90.9	7.8	20.5	PLK2	105.9	23.9	0.59

Z-score calculated using average and SD

Viability (% of siRNA NT)					AG03141 viability (% of GM01604)			
	Average		SD					
siRNA SMARTpool	GM01604	AG03141	GM01604	AG03141	siRNA SMARTpool	Average	SD	Z-score
PLK3	88.5	123.1	8.6	21.9	PLK3	139.1	24.8	2.54
PMS1	126.3	92.0	50.8	32.8	PMS1	72.8	26.0	-1.35
PMS2	86.7	79.9	43.7	38.3	PMS2	92.2	44.2	-0.22
PNKP	82.5	82.5	28.3	34.9	PNKP	100.0	42.3	0.24
POLB	47.5	100.7	18.2	36.1	POLB	212.2	76.0	6.82
POLD1	76.2	79.6	39.0	23.6	POLD1	104.4	30.9	0.50
POLE	60.2	54.9	25.3	35.6	POLE	91.2	59.2	-0.28
POLE3	88.1	66.5	26.4	20.6	POLE3	75.5	23.3	-1.20
POLE4	143.4	70.4	85.9	19.8	POLE4	49.1	13.8	-2.75
POLG	117.4	123.0	21.0	29.0	POLG	104.8	24.7	0.52
POLH	120.5	89.4	39.2	42.2	POLH	74.1	35.0	-1.28
POLI	105.1	81.7	37.0	36.7	POLI	77.7	34.9	-1.07
POLK	37.8	51.8	11.7	32.3	POLK	137.2	85.5	2.42
POLL	115.7	88.6	53.1	34.7	POLL	76.6	30.0	-1.13
POLM	80.8	71.9	36.7	26.6	POLM	89.0	32.9	-0.40
POLN	68.3	88.8	27.3	26.7	POLN	130.1	39.2	2.01
POLQ	101.3	90.7	37.3	38.4	POLQ	89.5	38.0	-0.37
POT1	110.5	89.2	32.3	19.2	POT1	80.7	17.4	-0.89
PP3856	114.5	88.5	26.0	27.0	PP3856	77.3	23.5	-1.09
PRDX2	118.9	82.4	37.1	20.5	PRDX2	69.3	17.3	-1.56
PRKDC	52.0	92.6	6.4	26.5	PRKDC	178.0	51.0	4.82
PTCH	134.4	134.7	42.3	9.4	PTCH	100.2	7.0	0.25
PTEN	107.5	69.5	31.8	31.5	PTEN	64.6	29.3	-1.84
PTTG1	124.4	144.7	9.1	54.3	PTTG1	116.4	43.7	1.20
RAD1	104.9	79.2	36.9	27.5	RAD1	75.4	26.2	-1.20
RAD17	100.1	62.3	48.3	28.4	RAD17	62.2	28.3	-1.98
RAD18	143.0	108.6	48.5	22.8	RAD18	76.0	15.9	-1.17
RAD21	97.2	23.9	48.7	5.3	RAD21	24.6	5.5	-4.18
RAD23A	118.7	79.8	45.2	45.9	RAD23A	67.2	38.7	-1.68
RAD23B	86.0	74.8	25.6	26.9	RAD23B	87.0	31.3	-0.52
RAD50	110.4	71.1	32.4	24.0	RAD50	64.4	21.8	-1.85
Rad51	0.2	0.2	0.0	0.2	Rad51	158.4	100.2	3.67
RAD51C	126.4	130.4	32.3	17.3	RAD51C	103.1	13.6	0.43
RAD51L1	149.5	142.9	38.4	5.2	RAD51L1	95.5	3.5	-0.02
RAD51L3	106.0	110.6	28.9	14.4	RAD51L3	104.3	13.5	0.49
RAD52	51.2	69.4	7.6	43.8	RAD52	135.3	85.4	2.32
RAD54B	93.8	70.9	32.7	9.1	RAD54B	75.5	9.7	-1.20
RAD54L	87.2	119.5	22.3	17.8	RAD54L	137.1	20.4	2.42
RAD9A	83.8	118.3	20.7	21.3	RAD9A	141.2	25.5	2.66
RBBP8	85.7	49.7	25.9	10.2	RBBP8	58.0	11.9	-2.22
RECQL	137.0	123.6	48.6	33.0	RECQL	90.3	24.1	-0.33
RECQL4	108.1	101.1	34.4	25.3	RECQL4	93.6	23.4	-0.14
RECQL5	104.9	119.0	25.9	19.4	RECQL5	113.4	18.5	1.03
REV1L	95.0	175.6	6.1	20.4	REV1L	184.8	21.5	5.22
REV3L	103.1	119.5	4.9	18.6	REV3L	115.8	18.0	1.17
RFC1	111.3	77.1	10.6	5.9	RFC1	69.3	5.3	-1.56
RNF40	78.4	83.4	8.7	30.5	RNF40	106.3	38.9	0.61
RPA1	33.6	31.6	7.0	12.8	RPA1	93.9	38.1	-0.12
RUVBL2	75.0	49.3	2.1	25.2	RUVBL2	65.8	33.6	-1.77
SHPRH	122.0	126.5	23.3	23.7	SHPRH	103.7	19.5	0.46
SIRT1	99.6	111.1	23.4	20.9	SIRT1	111.6	21.0	0.92
SIRT6	112.7	98.7	13.6	38.3	SIRT6	87.6	34.0	-0.49
SMARCA1	84.8	79.3	14.9	19.1	SMARCA1	93.5	22.5	-0.14
SMARCA2	115.2	92.1	17.3	30.3	SMARCA2	79.9	26.3	-0.94
SMARCA3	136.1	101.2	21.9	27.2	SMARCA3	74.4	20.0	-1.26
SMARCA4	51.1	75.9	8.4	10.1	SMARCA4	148.4	19.7	3.08

Z-score calculated using average and SD

Viability (% of siRNA NT)					AG03141 viability (% of GM01604)			
	Average		SD					
siRNA SMARTpool	GM01604	AG03141	GM01604	AG03141	siRNA SMARTpool	Average	SD	Z-score
SMC5L1	70.2	71.0	12.9	5.9	SMC5L1	101.2	8.5	0.31
SMUG1	119.5	121.9	43.2	24.9	SMUG1	102.0	20.8	0.36
SOD1	174.6	110.1	1.5	37.3	SOD1	63.1	21.4	-1.93
STK11	123.3	66.8	19.4	17.3	STK11	54.2	14.1	-2.45
TDG	175.3	153.4	13.9	71.2	TDG	87.5	40.6	-0.49
TDP1	89.7	88.4	32.2	40.6	TDP1	98.5	45.3	0.16
TERF2IP	68.0	78.8	1.6	5.0	TERF2IP	115.8	7.3	1.17
TIMELESS	46.4	39.7	5.3	20.5	TIMELESS	85.5	44.1	-0.61
TNKS2	139.5	183.7	24.2	67.3	TNKS2	131.7	48.2	2.10
TOP1	121.2	119.6	14.8	28.6	TOP1	98.7	23.6	0.17
TOP2A	72.1	26.4	4.2	2.7	TOP2A	36.7	3.7	-3.48
TOP3A	122.2	108.4	7.0	32.0	TOP3A	88.7	26.2	-0.42
TOP3B	128.4	121.2	12.1	34.6	TOP3B	94.4	27.0	-0.09
TOPBP1	46.7	23.7	23.4	2.4	TOPBP1	50.7	5.2	-2.65
TP53BP1	141.5	123.2	28.6	26.3	TP53BP1	87.1	18.6	-0.52
TP73	66.3	64.4	24.9	17.5	TP73	97.1	26.4	0.07
TREX1	100.8	110.3	12.2	20.2	TREX1	109.5	20.0	2.01
TREX1	118.9	154.8	8.0	46.2	TREX1	130.2	38.9	0.80
TREX2	82.6	136.7	13.9	52.5	TREX2	165.4	63.5	4.08
UBE2A	122.2	140.3	0.8	25.1	UBE2A	114.8	20.5	1.11
UBE2B	154.4	180.0	3.1	42.1	UBE2B	116.5	27.3	1.21
UBE2I	69.1	76.6	7.3	28.6	UBE2I	110.8	41.4	0.87
UBE2N	102.5	94.2	5.9	41.5	UBE2N	91.9	40.5	-0.23
UBE2V2	136.1	126.1	22.9	27.9	UBE2V2	92.7	20.5	-0.19
UNG	107.5	138.9	14.8	71.2	UNG	129.2	66.2	1.95
WDHD1	48.4	36.5	12.7	11.7	WDHD1	75.4	24.2	-1.20
WRN	88.5	76.1	14.9	8.2	WRN	86.0	9.3	-0.58
XAB2	16.0	20.7	7.5	8.3	XAB2	128.8	51.9	1.93
XPC	134.6	157.1	12.6	33.4	XPC	116.7	24.8	1.22
XRCC1	85.3	103.6	13.6	36.2	XRCC1	121.5	42.4	1.50
XRCC2	66.2	47.6	8.3	7.2	XRCC2	71.9	10.9	-1.41
XRCC3	141.9	111.0	48.8	45.2	XRCC3	78.3	31.9	-1.03
XRCC4	140.1	108.9	17.2	32.0	XRCC4	77.7	22.8	-1.07
XRCC5	139.2	155.8	4.5	33.4	XRCC5	111.9	24.0	0.94